2022

Modulation of Prefrontal Cortex activity and sociability by local interneurons expressing corticotropi-releasing hormone

Michael Riad

MODULATION OF PREFRONTAL CORTEX ACTIVITY AND SOCIABILITY BY LOCAL INTERNEURONS EXPRESSING CORTICOTROPIN-RELEASING HORMONE

A Thesis Presented to the Faculty of
The Rockefeller University
in Partial Fulfillment of the Requirements for
the degree of Doctor of Philosophy

by
Michael Riad
June 2022

MODULATION OF PREFRONTAL CORTEX ACTIVITY AND SOCIABILITY BY LOCAL INTERNEURONS EXPRESSING CORTICOTROPIN-RELEASING HORMONE

Michael Riad, Ph.D.
The Rockefeller University 2022

The cerebral cortex is composed primarily of two neuronal cell types: excitatory pyramidal cells and inhibitory interneurons. Their neurochemical diversity and complex organization into interconnected laminar and columnar circuits imbues the cortex with countless computational and functional possibilities. At the behavioral level, changes in the molecular profile and electrophysiological activity of cortical neurons produce noticeable changes in perception, learning and memory, motor skills, and executive cognitive functions.

In the initial chapter of this thesis, I briefly cover the history and progress of cell type studies in cerebral cortex and provide frameworks for understanding and interrogating interneuron diversity. We next apply modern molecular tools to test the validity of a proposed circuit model for cortical serotonin receptor 3 (5-HT3$_A$R) interneurons enriched with corticotropin-releasing hormone (CRH), generated using these established frameworks. Molecular profiling using Translating Ribosome Affinity Purification (TRAP-seq) predicted an elegant, bimodal postsynaptic mechanism for CRH neuron modulation of both pyramidal cells and interneurons. In mouse prefrontal cortex (mPFC), we initiate a host of molecular, anatomical, and electrophysiological studies in this less understood subpopulation and validate that cortical CRH cells are interneurons (CrhINs). Further characterization revealed CrhINs express vasoactive intestinal peptide (VIP), a marker for the disinhibitory class of interneurons. These preliminary findings predict an elegant and multi-layered mechanism for CrhIN activation of prefrontal cortex, achieved through complementary GABAergic signaling and CRH release.

In chapter two, we use transgenic mouse lines, RNA sequencing, gene excision, cell type-specific viral approaches, and electrophysiological whole cell patch clamp recordings, in combination with optogenetics and pharmacology, to probe the validity of this proposed circuit. Oxytocin receptor interneurons (OxtR-INs), a subset of somatostatin interneurons first discovered and characterized by Drs. Miho Nakajima, Kun Li, Ines Ibañez-Tallon, and Nathaniel Heintz, were found to mediate prosocial and anxiolytic effects through the release of corticotropin-releasing hormone binding protein (CRHBP). CRHBP, the endogenous antagonist to CRH, sequesters unbound CRH and blocks CRH – CRHR1 signaling, ultimately reducing the excitability of CRHR1 L2/3 pyramidal cells. A critical insight revealed in these initial studies is the identification of CRH peptide expression in VIP interneurons and, in contrast, CRHBP expression in SST interneurons. To test the prediction that CRH/VIP interneurons both inhibit OxtR/SST/CRHBP interneurons and release CRH onto CRHR1 expressing neurons, we applied optogenetic stimulation at both low and high frequency, in parallel with pharmacology, to isolate dual cell type-specific GABA and CRH-mediated currents in mPFC.

Following this characterization, we employed an opposing strategy to determine the behavioral influence of prefrontal CrhINs. First, we conditionally deleted mPFC CRH mRNA and subsequently protein expression via FLOX excision. Second, we activated CrhINs via chemogenetics and the non-endogenous receptor hM3Dq to induce release of both CRH and of GABA. These complementary loss- and gain-of-function approaches reveal a sexually dimorphic and functionally distinct role for cortical CRH production from that of the well-established hypothalamus. Taken together, our results outline a novel, frequency-dependent cortical microcircuit dependent on release of both the neurotransmitter GABA and the neuropeptide CRH by mPFC CrhINs.

In Chapter three, we discuss the significance of these findings in the context of postsynaptic studies of cell type diversity and the frequency-dependent conditions required to evoke temporally precise and selective neurotransmitter and neuropeptide release *in vitro*. The sexually dimorphic patterns observed across experiments outlined a novel functional microcircuit in cortex whereby CrhINs modulate mPFC through both inhibition of interneurons and through local release of CRH. When analyzed at the molecular, electrophysiological, and behavioral levels, our findings reveal an elegant postsynaptic mechanism whereby CrhINs exert a net excitatory effect in mPFC through both GABAergic and CRH signaling that is more pronounced in males than in females. The distinct yet complementary modulation of OxtR-INs and L2/3 pyramidal cells by CrhINs offers new insights into the functional organization of mPFC microcircuits and the neuromodulatory impact of cortical CRH production.

ACKNOWLEDGMENTS

For those curious enough to follow the pursuit of expanding collective scientific knowledge, s*cientia pro bono humani generis*, they understand firsthand that the application of the scientific method is arduous and always full of risk and reward. Despite these perils, success is achievable provided a student commits to a collaborative effort that requires years of endless mentorship. It is in this context that I am forever grateful for the mentorship and opportunity given to me by Dr. Nathaniel Heintz and Dr. Ines Ibañez-Tallon at The Laboratory of Molecular Biology. Without their astonishing level of intellectual generosity, extensive experiences unraveling brain circuits, and their encyclopedic knowledge of every biological cell type, this work would never have been accomplished. Their mentorship shaped the course of experimentation and my greatest achievement overall– learning the methodical and relentless application of the scientific method. Greatest of all is my appreciation and acknowledgement of my wife, my sister, my brother-in-law, and my mother and my father. Their endless support and ability to motivate me allowed me to persevere and push back into what seemed like endless boundaries.

No boundary proved more daunting than achieving and maintaining a perfect whole cell recording configuration using a glass electrode with an aperture 1/75 the diameter of a human hair while simultaneously applying waves of potent pharmacological toxins. Patch clamp electrophysiology is truly a technique for the brave and it is in this light that I thank Drs. Tiago Branco, Cristoph Schmidt-Hieber, Ian Duguid, Annalisa Scimemi, and Nicolas Wanaverbecq. I am genuinely grateful that Cold Spring Harbor Laboratory and The Rockefeller University enable PhD students the once-in-a-lifetime

opportunity to learn advanced scientific techniques firsthand from field leaders. The entirety of electrophysiological studies conducted here would not have been possible without the foundational hands-on experiences I gained in *The Ion Channels in Synaptic and Neural Circuit Physiology* course at Cold Spring Harbor Laboratory. They mentored me, painstakingly I might add, in the complex techniques required to complete a large portion of these studies.

In equal light, I am forever indebted to The David Rockefeller Graduate Program and to those who support it. It is truly a remarkable scientific culture where a student is given unrestricted patience, resources, and encouragement. Here, a student can focus on science to the exclusion of all practicalities and worries and with the privilege to conduct wildly innovative experiments on a moment's notice. Also of great importance, the intellectual contributions and critiques from my committee chair, Dr. Winrich Freiwald, and my committee members Dr. Charles Gilbert and Dr. Gord Fishell, can never be understated. Very few graduate students have the privilege of having access to scientists with broad and yet also stunningly deep expertise of molecular biology, physiology, and all things related to cerebral cortex.

Last, but never least, I want to extend my sincerest appreciation to each and every member of the Heintz Laboratory who dedicates their day applying the scientific method in the pursuit of something new. I could not have asked for a more diverse, collaborative, and engaging environment. It has been an incredible experience and opportunity to work alongside Sylvia Lipford, Cuidong Wang, Meghana Rao, Benjamin Fait, Dr. Christina Pressl, Dr. Bianca Cotto, Dr. Elitsa Stoyanova, Dr. Laura Kus, Dr. Tatsuya Murakami, and Dr. Kun Li. I am grateful to each and every one of you for your help and for your friendship.

TABLE OF CONTENTS

LIST OF FIGURES

LIST OF TABLES

LIST OF ABBREVIATIONS

Abbreviation	Description
ACTH	adrenocorticotropic hormone
ChR2	channelrhodopsin-2
CNO	clozapine N-oxide
CRH	corticotropin-releasing hormone
CRHBP	corticotropin-releasing hormone binding protein
CrhINs	corticotropin-releasing hormone interneurons
CRHR1	corticotropin-releasing hormone receptor 1
cAMP	cyclic AMP
cc	current clamp
CNQX	cyanquixaline 6-cyano-7-nitroquinoxaline-2,3-dione
EPSC	excitatory postsynaptic current
GPCR	G protein coupled receptor
GDPβ-S	guanosine 5′-[β-thio]diphosphate trilithium salt
IHC	immunohistochemistry
ISH	*in situ* hybridization
IPSC	inhibitory postsynaptic current
INs	interneurons
L2/3	layer 2/3
L5	layer 5
mPFC	medial prefrontal cortex
OXT	oxytocin
OxtR-INs	oxytocin receptor interneurons
PVN	paraventricular nucleus of the hypothalamus
PVALB	parvalbumin
PTX	picrotoxin
PCs	pyramidal cells
5-HT	serotonin
5-HT3AR	serotonin receptor 3A
SST	somatostatin
TRAP	Translating Ribosome Affinity Purification
VIP	vasoactive intestinal peptide
Vc	voltage clamp
Vh	voltage hold
GABA	γ-Aminobutyric acid

CHAPTER 1. Introduction

1.1 Classification and organization of cell types in cerebral cortex

The most evolutionarily affected biological structure in advanced species like humans and nonhuman primates is the cerebral cortex. Its neurons form the most intricately connected structure in the brain that is host to a majority of our complex computational, sensory, and cognitive functions. Neurons produce a wide array of neurotransmitters, neuropeptides, and neuromodulatory substances that act on receptors in dispersed cell types to alter cortical circuit function. Cell type diversity is therefore inherent to the evolution of the cortex and key to delineating the dynamic relationship between brain activity and behavior. When looking back over the pioneering drawings of anatomist Santiago Ramón y Cajal, arguably the most striking feature is not the cells themselves but the diversity between them. Using the now classic Golgi silver stain allowed Ramón y Cajal to accurately redraw the elaborate but stereotyped morphology of neurons in visual cortex **(Figure 1.1A)**, cerebellum, and retina. These studies provided support for his neuron doctrine, enabling the first classification scheme for addressing diversity among cell types in the brain **(Cajal et al., 1888)**. The technique fully visualizes the entire arborization and strikingly reveals that cell type morphology is grossly conserved between human and murine cortex **(Džaja et al., 2014, Figure 1.1B)**.

Importantly, a requisite but often overlooked aspect is the density of cortical neurons that are not visible via Golgi stains. By technical limitation, Golgi stains are selective for an as-of-yet unknown factor and are estimated to label only 1% of all

neurons present **(Pasternak et al., 1975)**. An attempt to quantify the number of cells and synaptic connections in 1 cubic millimeter of mouse cortex begins to reveal its true scale. There exist on average 10 million cortical neurons and 2.5 miles of axons per 1 cubic millimeter of mouse cortex, however this figure is daunted by the number of synaptic connections between these cells, estimated at 10 billion **(Figure 1.1C)**.

1.2 Molecular determinants for cell type wiring in cortex

The organization and connectivity of the cerebral cortex gives rise to complex behavioral, sensory, and cognitive functions **(Das and Gilbert, 1995; Tsao et al., 2003)**. Within the four main subdivisions of cortex: the frontal, parietal, occipital, and temporal lobes, there exist general principles in structure and organization of the cortex. The cortex is typically organized in six layers spanning functionally repeated columns **(Hubel and Wiesel, 1959)** and is composed primarily of excitatory pyramidal cells and inhibitory interneurons. Pyramidal neurons project to and receive projections from subcortical structures, forming reciprocal feedforward and feedback connections. Within cortex, functional properties are arranged over a laminar and columnar organization enabling the formation and computational capabilities of complex local microcircuits **(Barbas, 2015)**.

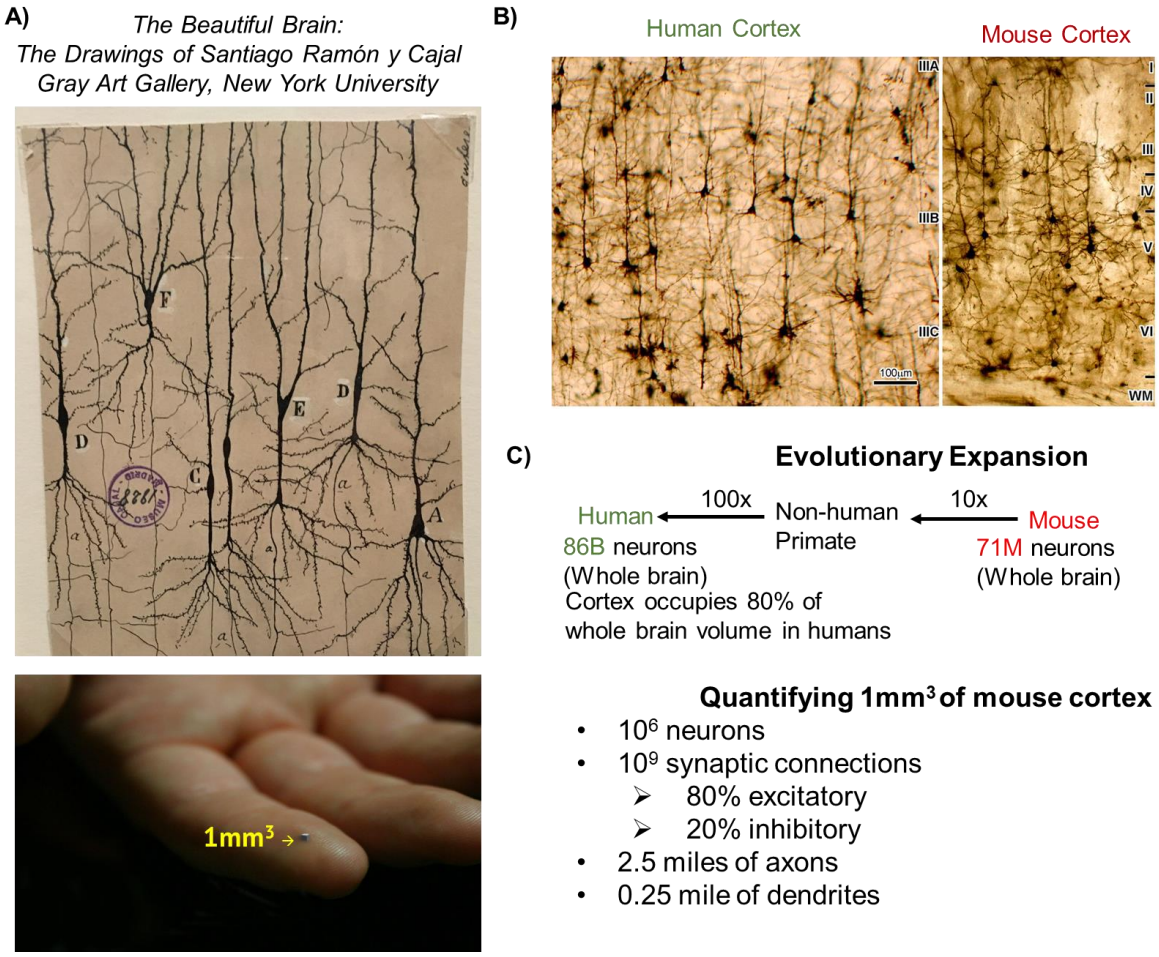

Figure 1.1. Principal pyramidal cells of cerebral cortex.

a) Hand-drawn reconstruction of neurons in visual cortex. From *The Beautiful Brain: The Drawings of Santiago Ramón y Cajal. Gray Art Gallery, New York University*
b) Golgi staining in cortex labeling pyramidal cells in both mouse and human cortex
c) Quantification of various neuronal measurements in 1 cubic millimeter of mouse cortex

Cortical pyramidal cells have diverse morphological and physiological properties **(van Aerde and Feldmeyer, 2015)** yet they all typically release the excitatory neurotransmitter glutamate, which binds to postsynaptic ionotropic glutamate receptors to allow influx of cations and cell depolarization. Based on their laminar positioning, pyramidal cells either project locally forming corticocortical connections, or to subcortical structures, such as the corticostriatal and corticothalamic projection pathways. Interneurons, in contrast to pyramidal cells, do not project to other anatomical structures and instead form local inhibitory microcircuits **(Feldmeyer et al., 2018)** through the synaptic release of the neurotransmitter γ-Aminobutyric acid (GABA), the major inhibitory signaling molecule in CNS neurons **(Florey and McLennan, 1959**, **Sigel et al., 2012**). Its functional analogue, glycine, is expressed in lieu of GABA in brain stem and spinal cord neurons. In CNS, stereotyped localization of GABA receptors at somata, nearby dendrites, and along the axon and axon initial segment, allows interneurons to spatially target and selectively shunt inputs to and outputs from individual pyramidal neurons, shaping all forms of action potential generation and synaptic communication in the brain. All action potentials and postsynaptic release of neurotransmitters and other molecules are the result of the spatial and temporal summation of hundreds to thousands of presynaptic inputs, both excitatory and inhibitory, summing to the firing threshold of a neuron **(Magee, 2000)**. Dynamic spatial modulation of electrical activity in CNS neurons is central to recurrent neural networks and logic gates for synaptic modeling and *in silico* computations **(Wynn et al., 2012; Mante et al., 2013)**.

Whereas pyramidal cells in cortex are subdivided based on their layer and patterns of connectivity **(Leone et al., 2008)**, cortical interneurons are instead classified

based on the neurochemical marker they express. Almost 99% percent of all cortical interneurons express one of the three following neurochemical markers: parvalbumin (PVALB), somatostatin (SST), or serotonin receptor 3A (5-$HT_{3A}R$) **(Kawaguchi and Kubota, 1996; Rudy et al., 2010)**.

Despite their shared developmental lineages **(Miyoshi et al., 2011, Lim et al., 2018)** and molecular profiles, interneurons are among the most neurochemically and morphologically diverse cell types in the CNS. Interneurons are typically subdivided into subclasses based on morphology, synaptic targeting patterns, firing properties, and molecular profiles **(Figure 1.2A)** (adapted from **Tremblay et al., 2016)**, stitching together a simple yet foundational framework to classify interneuron properties. To agree upon the extent of their complexity, leading researchers met in the birthplace of Santiago Ramón y Cajal in Navarra, Spain in 2005 and agreed upon the aptly named Petilla Terminology **(Yuste et al., 2005, Petilla Interneuron Nomenclature Group, 2008)**, an extensive framework to structure studies of interneuron subtype and function by morphological, molecular, and physiological features **(Table 1.1)**. As the field progressed, intersectional transgenic approaches gave access to molecularly distinct cell types **(Yang et al., 1997; Gong et al., 2007),** which when coupled with the pioneering application of light-gated ion channels **(Nagel et al., 2003, Boyden et al., 2005),** has enabled dual cell type specific synaptic studies in complex brain circuits **(He et al., 2016)**.

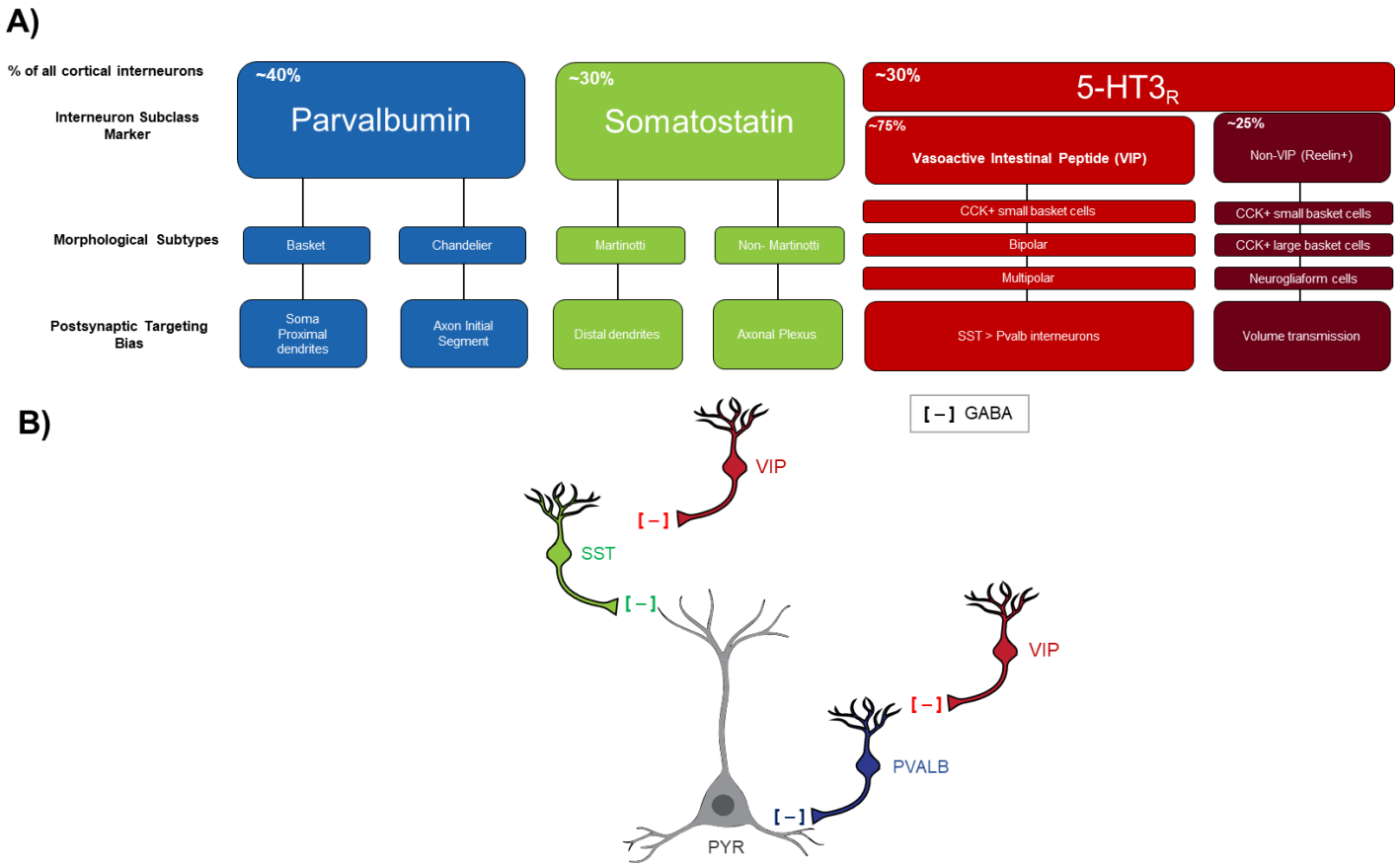

Figure 1.2. Three interneuron molecular subtypes account for 99% of all cortical interneurons.

a) Classification by main molecular marker, morphological pattern, and postsynaptic targeting bias
b) Interneuron wiring schematic across molecular subtypes in cortex

Table 1.1. *Petilla Terminology for studying interneuron diversity.*

1) Morphological features
• Soma: shape; size; orientation
• Dendrite: arborization polarity; branch metrics; fine structure; postsynaptic element
• Axon: initial segment; arbor trajectory; terminal shape; branch metrics; boutons; synaptic targets
• Connections: chemical and electrical; source; location and distribution
2) Molecular features
• Transcription factors
• Neurotransmitters or their synthesizing enzymes
• Neuropeptides
• Calcium-binding proteins
• Receptors: ionotropic; metabotropic
• Structural proteins
• Cell-surface markers
• Ion-channels
• Connexins
• Transporters: plasma membrane; vesicular
3) Physiological features
• Passive or subthreshold parameters: resting membrane potential; membrane time constants; input resistance; oscillation and resonance; rheobase and chronaxie; rectification
• Action potential (AP) measurements: amplitude; threshold; half-width; afterhyperpolarization; afterdepolarization; changes in AP waveform during train
• Dendritic backpropagation
• Depolarizing plateaus
• Firing pattern: oscillatory and resonant behavior
• Onset response to depolarizing step; steady-state response to depolarizing step
• Response to hyperpolarizing step: rectification; rebound
• Spiking recorded extracellularly: phase relationship to oscillations
• Functional response specificity; cross-correlation and other dynamics
• Postsynaptic responses: spontaneous and evoked
• Ratio of receptor subtypes; spatial and temporal summation
• Short- and long-term plasticity
• Gap junctions

Basket and chandelier PVALB interneurons block action potential initiation by targeting the spike initiation zone, most notably the soma, its nearest dendrites, and the axon initial segment, thereby filtering pyramidal cell output **(Fish et al., 2013)**. PVALB interneurons are marked by their ability to sustain fast AP firing rates exceeding 10hz **(Owen et al., 2018)** and as such are commonly referred to as Fast-Spiking Interneurons. In contrast, SST interneurons filter inputs to pyramidal cells by targeting dendrites. While non-Martinotti SST interneurons lack this axonal plexus in layer 1 and are not yet well characterized functionally, Martinotti SST interneurons display a stereotypic axonal plexus in layer 1 of cortex and target the dendritic tuft of pyramidal cells **(Pfeffer et al., 2013)**. Of important interest to this doctoral research is the OxtR-IN expressing subpopulation of SST interneurons, which release the endogenous CRH antagonist CRHBP.

5-HT_{3A} interneurons encompass a functionally diverse class of serotonin-responsive neurons. There are at least six morphologically and functionally distinct subtypes of 5-HT_{3A} interneurons **(Lee et al., 2010)**, however, they can be broadly subdivided into two classes based on their expression of either vasoactive intestinal peptide (VIP) or reelin **(Figure 1.2)**. Whereas most interneurons inhibit pyramidal cells, VIP interneurons primarily inhibit SST and PVALB interneurons. This dampens SST and PVALB-mediated inhibition of pyramidal cells, a transsynaptic process referred to as disinhibition **(Acsady et al., 1996; Letzkus et al., 2011).** Activation of VIP interneurons, mainly via glutamatergic inputs from nearby and long-range pyramidal cells and via neuromodulatory inputs from the raphe nuclei, evokes a robust increase in pyramidal

cell excitation that occurs after a brief delay, usually on the order of 100 msec **(Kepecs & Fishell 2014)**.

Monoamine inputs to VIP interneurons come from the serotonergic loci of the brain, the raphe nuclei, which project to most brain areas and interact across all receptor subtypes **(Vertes et al., 1999)**. 5-HT_{3A}, the sole ionotropic serotonin receptor, is permeable to both Na^+ and K^+ and resulting in cell depolarization after 5-HT binding activation **(Derkach et al., 1989)**. All other serotonin receptor subtypes are metabotropic and mediate signals through G-protein subunits, summarized in **Table 1.2** (adapted from **Hannon et al., 2008, Leiser et al., 2015)**.

While 5-HT_{3A} is known to be expressed exclusively in cortical interneurons **(Lee et al., 2010)** and functions to increase excitability through the inflow of cations, 5-HT_{1A} is expressed most notably in L2/3 pyramidal neurons projecting to limbic brain regions **(Palchaudhuri et al., 2005)** and functions primarily as an inhibitory auto receptor, providing negative feedback modulation of L2/3 excitability. In contrast, 5-HT_{2A} is expressed on both pyramidal cells **(Willins et al., 1997)** and PVALB **(Puig et al., 2010)** and SST interneurons **(de Filippo et al., 2021)** and its activation evokes high AP firing rates in both interneurons classes. 5-$HT5_A$ is expressed primarily in L5 cortical pyramidal cells **(Belgard et al., 2011)**, and has been shown to exert a net outward current and inhibitory effect, likely via downstream modulation of K+ ion channels **(Goodfellow et al., 2012)**,

Table 1.2 *Serotonin receptor coupling and expression in medial prefrontal cortex.*

5-HT Receptor Subtype	G protein subunit	Function	mPFC Expression
5-HT1A	G i/o	Inhibitory	+
5-HT1B	G i/o	Inhibitory	+
5-HT1D	G i/o	Inhibitory	–
5-HT1E	G i/o	Inhibitory	–
5-HT1F	G i/o	Inhibitory	–
5-HT2A	G q/11	Excitatory	+
5-HT2B	G q/11	Excitatory	–
5-HT2C	G q/11	Excitatory	+
5-HT3	N/A	Ionotropic	+
5-HT4 (murine only)	G s	Excitatory	+
5-HT5A	G i/o	Inhibitory	+
5-HT5B	N/A	Unknown	–
5-HT6	G s	Excitatory	+
5-HT7	G s	Excitatory	+

1.3 Neurotransmitters and neuropeptides in central nervous system neurons

Cortical neurons typically express either the neurotransmitter glutamate or GABA, and their postsynaptic modulation has been well characterized. While molecular profiling, mRNA and protein labeling reveal abundant neuropeptide ligand and receptor expression across cortex **(Vassilatis et al., 2003)**, far less is understood regarding their potential for postsynaptic modulation across diverse cell types. Circuit models are typically simplified according to Dale's Principle of "one neuron, one transmitter". However, multi-transmitter neurons **(Granger et al., 2016),** neurons which co-release multiple amino acid neurotransmitters (GABA, glutamate, glycine) and neuropeptides (orexin, vasopressin, dynorphin, etc.), exist and have been characterized across several brain regions. As early as 1976, neuropeptides, notably enkephalin, had been localized in the brain **(Hughes et al., 1975).** Initially labeled "unusual substances", pioneering studies began to characterize and reveal the functional implications regarding release of multiple molecules from the same cell type in invertebrates and mammalian smooth muscle **(Kupfermann, 1991).** More recently, multi-transmitter neurons have been found in orexin neurons of the hypothalamus, which release both glutamate and orexin **(Schöne et al., 2014)**, in cortical VIP-expressing interneurons that release both GABA and acetylcholine **(Tasic et al., 2018)**, in cortical SST-expressing interneurons that release GABA and CRHBP **(Nakajima et al., 2014, Li et al., 2016)**, and in midbrain dopaminergic neurons **(Tritsch et al., 2012)**. Most interneurons in the mammalian brain express both fast acting neurotransmitters and neuropeptides or other secreted modulatory proteins **(Smith et al., 2019),** demonstrating the complexity and diversity underlying neuropeptides and neurotransmitters in CNS cell type expression**.**

The conditions for neurotransmitter and neuropeptide release differ in their mechanisms of synthesis, transport, packaging, and release **(Muschol and Salzberg, 2000, Granger et al., 2016)**. In most instances, fast-acting neurotransmission occurs at a dedicated pre- and post-synapse, resulting in a time-locked evoked postsynaptic current in response to a single optogenetic pulse **(Arrigoni et al., 2014)**. It is well established that neurotransmitters are typically stored in clear synaptic vesicles docked adjacent to the synaptic cleft, thus single spike Ca^{2+} transients are sufficient for their vesicle fusion and release. In contrast, efficient release of neuropeptide containing dense core vesicles requires tetanic stimulation at higher frequencies. Postsynaptic waveforms indicating GPCR binding and signaling are, as-of-yet, difficult to ascribe **(Figure 1.3).**

A logical yet substantial technical achievement in the ability to selectively evoke neurotransmitter or neuropeptide release was demonstrated using ChR2-expressing orexin neurons of the lateral hypothalamus and 470nm LED frequency stimulation. These studies revealed that at low frequency LED photo stimulation, ChR2-expression orexin neurons release glutamate onto adjacent histamine receptor neurons, whereas high frequency LED stimulation induces orexin release **(Schöne et al., 2014)**. Applying frequency-dependent LED stimulation in ChR2 cell type-restricted recordings should enable mapping the neuromodulatory layer of synaptic communication between CNS neurons, and its ability to drastically improve our understanding of the conditions required and consequences resulting from neurotransmitter and neuropeptide release in the brain.

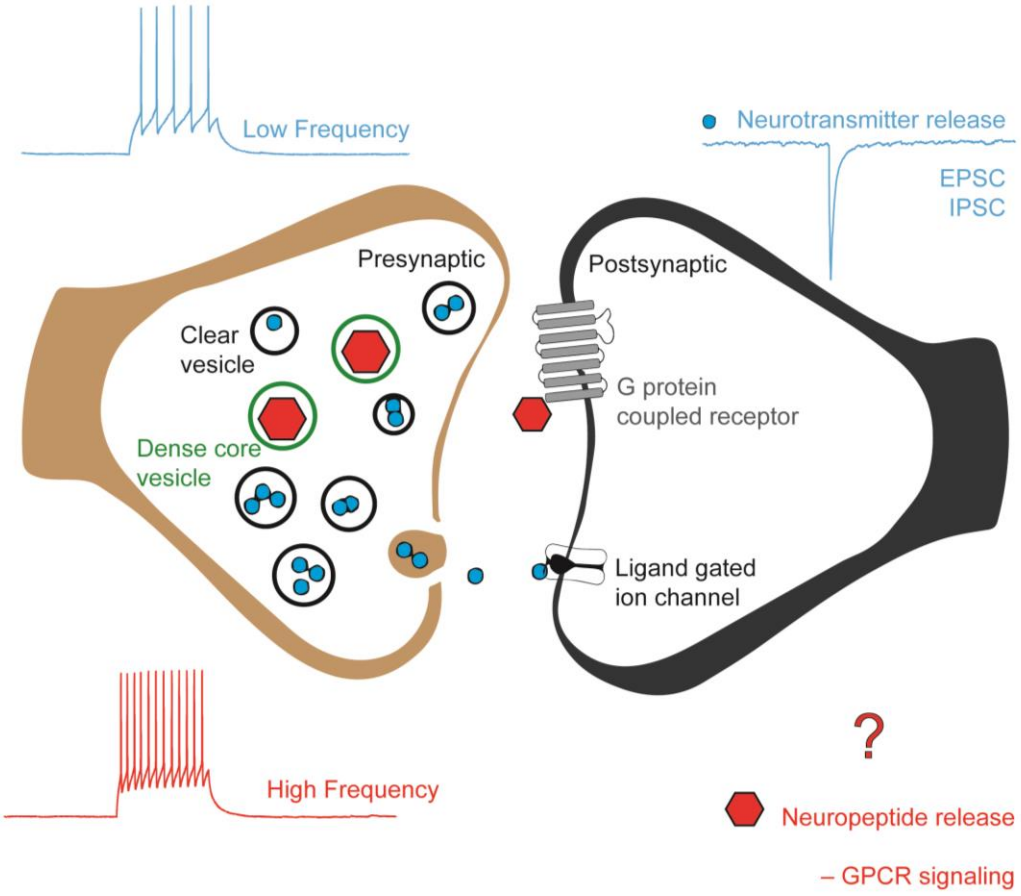

Figure 1.3. Increased presynaptic firing frequency is required for release of neuropeptides.

Example presynapse containing both neurotransmitters and neuropeptides and adjacent postsynapse containing ion channel and GPCRs. High frequency presynaptic firing trains increase presynaptic cytosolic Ca^{2+} and facilitate dense core vesicle fusion and neuropeptide release.

1.4 Neuropeptide ligands and G protein coupled receptor activation in cortex

Despite their broad structural and functional diversity, all neuropeptide ligands bind and signal exclusively through G protein coupled receptors (GPCRs). Their involvement and regulation in nearly every non-ionic synaptic communication would suggest their expression would be elevated in the CNS, and of the 367 known GPCRs in humans and 392 GPCRs in mice, strikingly, over 90% of GPCRs are expressed in the brain **(Vassilatis et al., 2003)**. Four major classes of GPCRs are found in the central nervous system - Class A, B, C, and F.

Class A, rhodopsin-like receptors include the odorant receptor gene family, which accounts for over 2% of the entire mammalian genome. Other Class A GPCRs, like oxytocin, are involved in a variety of endocrine, physiological, and cognitive functions. Class B GPCRs, secretin family receptors, coupled via G(αs) proteins to increase cAMP via adenylate cyclase and include neuropeptides and peptide hormones like calcitonin, parathyroid hormone, glucagon-like peptide, and of particular importance to these studies, CRH. Class C GPCRs, composed primarily of metabotropic glutamate receptors mGluR or metabotropic GABAQ receptor for $GABA_B$, response **(Chun et al., 2012)** are heavily involved in the modulation of $AMPA_r$ and Ca^{2+} channels **(McElligott et al., 2010)** and required for most forms of synaptic plasticity. Class F GPCRs, composed of either frizzled (FZD) or smoothened (SMO) receptor subtypes, are known mediate effects of the Wnt and hedgehog proteins signaling pathway **(Kozielewicz et al., 2020)** and are essential regulators of early embryonic development.

Following G protein-coupled receptor (GPCR) activation, the Gα and Gβγ dissociate, allowing both subunits to interact and modulate ion channel expression

downstream independently. The Gα s subunit promotes activation of Adenylyl Cyclase and Protein Kinase A, subsequently elevating cAMP levels. The Gα i/o subunit opposes Gα s and promotes the inhibition of Adenylyl Cyclase and Protein Kinase A, subsequently reducing cAMP levels. Gα q/11 subunit activates Phospholipase C Beta 1, which enhances cellular excitability **(Armbruster et al., 2007)**. Gα 12/13 induces the activation of RHO-GTPase and is heavily involved in cell proliferation, cancer metastasis and progression **(Jo et al., 2016).** The Gβγ subunit, known to inhibit G α subunits, has been found to both activate and inhibit Adenylyl Cyclase and Protein Kinase A **(Tang et al., 1991)**.

While the presynaptic mechanisms segregating neurotransmitter and neuropeptide release are well established, the countless tissue, ligand, receptor combinations and their net physiological and behavioral effect is made more complex by GPCR signaling and its downstream modulation of ion channel expression and function **(Dascal et al., 2001)**. Downstream, Gα s, Gα i/o, and Gα q/11 all modulate voltage-gated Ca^{2+}channels and K^{+} channels, whereas Gβγ directly inhibit voltage-gated Ca^{2+} channels **(Nikolova et al., 1997)** and K^{+} channels, most notably GIRK (G-Protein-Gated Inwardly Rectifying K^{+}) **(Tabak et al., 2019)**. Ultimately, presynaptic Ca^{2+} requirements and GPCR modulation of ion channels work in parallel to allow complex dynamic pre- and postsynaptic mechanisms that influence neurotransmitter and neuropeptide release and signaling.

1.5 Brain-wide expression of the neuropeptide corticotropin-releasing hormone and its cognate receptor

Corticotropin-releasing hormone (CRH), a 41-residue neuropeptide found in neurons of the paraventricular nucleus (PVN) of the hypothalamus **(Vale et al., 1982)**, is a key mediator of the stress response **(Heinrichs and Koob, 1992)**. PVN neurons secrete CRH through a network of blood vessels to the adrenal pituitary, where it promotes adrenocorticotropic hormone (ACTH) release. ACTH then acts on the adrenal cortex to promote glucocorticoid synthesis, in turn activating glucocorticoid receptors, expressed in nearly every cell type, tissue, and organ in the human body **(Oakley and Cidlowski, 2013)**.

CRH production and reception is not restricted to the regulation of the PVN or the peripheral stress response and CRH neurons have been characterized in both cortex **(Gallopin et al., 2005)** and hippocampus **(Hooper et al., 2016)**. As such and in logical fashion, *in situ* hybridization studies reveal corticotropin-releasing hormone receptor 1 (CRHR1) mRNA expressed not only in brain regions within PVN **(Jiang et al., 2018)** but also in pyramidal cells of cortex **(Li et al., 2016)** and hippocampus **(Aldenhoff et al., 1983, Hauger et al., 2006)**. In cortex, CRH acts predominantly on its receptor, CRHR1, widely expressed in excitatory pyramidal cells in the cortex. CRH-CRHR1 signaling enhances excitability, as measured via current clamp, and increases firing rate in cortical pyramidal cells **(Li et al., 2016),** mediated through Gs- coupled signaling **(Gallopin et al., 2005, Inda et al., 2016)**. However, the same CRHR1 exerts G_i-coupled inhibitory effects depending on cell type, indicating differential excitatory and inhibitory

responses based on anatomical region, cell type expression, and downstream signaling events **(Hillhouse and Grammatopoulos, 2006)**.

When assessing CRH production, immunohistochemical labeling for CRH-producing neurons reveals scattered expression across cortex, hippocampus, thalamus, to name a few. More detailed quantitative analyses of CRH cell counts systematically mapped CRH cell count and cell density across CNS **(Peng et al., 2017)** and visualized their morphology at a single cell resolution **(Wang et al., 2021)**. From highest density of CRH neurons to lowest density, CRH neurons were found in olfactory areas, hypothalamus, cerebral cortex, striatum and midbrain, thalamus, and hippocampus and exhibit both local and long-range projection morphologies, depending on anatomical region.

Chronic exposure to stressful stimuli, or an inability to dampen the stress response, results in a plethora of physiological perturbations, notably fatigue, decrease immune function, and cardiovascular and metabolic disease **(Whitnall, 1993)**. Postmortem clinical studies in early suicide patients with depression show elevated CRH receptor mRNA and protein levels in the cortex and simultaneous reduced CRHR1 mRNA and protein. These findings suggest that activation of CRHR1 cells in cortex, or increased production of CRH protein in cortex, may be associated with progression of emotional and mood disorders **(Pandey et al., 2019)**.

1.6 Methods for probing cell type function in physiological studies

1.6.1 Transgenic mouse lines for dual cell type studies and stereotaxic surgery

Animals

All animal procedures were approved by The Rockefeller University Institutional Animal Care and Use Committee in accordance with NIH guidelines. Crh-Cre, Crh-FLOX, and Vip-Flp were purchased from Jackson Laboratory (012704, 030110, 028578). Oxtr-Cre ON82 mice were generated by The Rockefeller University GENSAT Project. Crh-Flp mice were generously donated from the laboratory of Dr. Bernardo Sabatini at Harvard University. Mice were group housed according to sex, up to 5 per cage, and bred on a C57BL/6 background. Mice were weaned at 3 weeks of age, maintained on 12-hour light/dark cycle, and given ad libitum access to food and water. The following primers were used to detect valid transgene insertion or genetic deletion for molecular profiling, electrophysiological recordings, and behavior studies.

CRE Recombinase

Forward:	GCATTACCGGTCGATGCAACGAGTGATGAG
Reverse:	GAGTGAACGAACCTGGTCGAAATCAGTGCG

GFP

Forward:	GCACGACTTCTTCAAGTCCGCCATGCC
Reverse:	GCGGATCTTGAAGTTCACCTTGATGCC

CRH–FLP Recombinase

Null Forward:	CTG TCC CTG TAT GCC TCT GG
Null Reverse:	AGA TGG AGA AAG GAC TAG GCT ACA
Mutant Forward:	CTT GGA ATA AGG CCG GTG T
Mutant Reverse:	AGC TTC CAG AGG AAC TGC TTC

VIP–FLP Recombinase

27266 Common Reverse:	CAC CTC TGA TTT CAG CTC TGC
27267 Wildtype Forward:	GGC TGA TTT TCA ATA GTA TGG TCT C
27265 Mutant Forward:	AGG ATT GGG AAG ACA ATA GCA

CRH Flox

Null CRH 51706 Reverse:	TTGTCCTCTGACCTCCACCCACTTC
Mutant CRH 49959 Reverse:	CGCACACCCTAATCGCCCCC
Mutant CRH 49667 Forward:	CCAGCTGCCCATGTGCTGGA

Stereotaxic Surgeries

Mice were anesthetized with a ketamine/xylazine (100mg/kg, 10mg/kg B.W.) injected intraperitoneally (I.P.). Stereotaxic surgeries were performed on mice at 7-8 weeks of age. Mice were attached to a stereotaxic adaptor (Stoelting Co). and bilateral injections (4 x 0.25µl) were performed targeting medial prefrontal cortex (AP +1.90, +1.65, ML +/- 0.25, DV -2.00) or PVN (AP -0.15, ML +/- 0.15, DV -4.75). Mice recovered for at least 4 weeks prior to any testing. For behavioral studies, CRH-IRES-Cre mice were injected with AAV2/hSyn-DIO-mCherry (AddGene) or AAV2/hSyn-DIO-hM3Dq-mCherry (AddGene), and Crh-FLOX mice were injected with either AAV1-CMV-Cre-GFP (UNC Gene Therapy), or AAV-CMV-GFP (UNC Gene Therapy).

For anatomical and electrophysiological studies, CRH-IRES-Cre mice were injected with the following virus- AAV2.2-EF1a-DIO-hChR2(H134R)-mCherry (UNC Gene Therapy). Crh-Flp mice, crossed to Oxtr-Cre mice, were injected with AAV2.2-EF1a-fDIO-hChR2(H134R)-EYFP (UNC Gene Therapy) and AAV2.2-DIO-mCherry (UNC Gene Therapy) in a 1:1 dilution. CRH-IRES-Cre mice, crossed to Vip-Flp mice, were injected with AAV2.2-EF1a-DIO-hChR2(H134R)-mCherry (UNC Gene Therapy) and AAVDJ-fDIO-eYFP (UNC Gene Therapy) in a 1:1 dilution.

1.6.2 Molecular profiling using Translating Ribosome Affinity Purification

TRAP

Due to the low number of CRH cells present in mPFC, samples dissected from eight male mice were required for each independent TRAP replicate. Three replicate samples were collected and the resulting RNA sequenced. Normalized values from each of the replicates and their averages were obtained for both the Immunoprecipitated (IP) and input (input) fractions. The TRAP procedure was performed as described previously **(Mellén et al., 2017)**. Medial prefrontal cortices were dissected from individual mice. Tissue was immediately homogenized with a motor-driven Teflon glass homogenizer. Polyribosomes were immunoprecipitated by monoclonal anti-EGFP antibodies (custom made, a mix of 19C8 and 19F7)-coated protein L magnetic beads. RNAs from polyribosomes were extracted and further purified with an Rneasy Plus Micro Kit. RNA quantity and quality were determined with an Agilent 2100 Bioanalyzer. cDNA was synthesized from 3ng of mRNA from IP and input samples and further amplified by Ovation RNA-seq Kit. cDNA fragments of 200 bp were end-repaired and ligated with adapters for HiSeq 2000 (Ilumina Inc., San Diego, CA, USA) technology using TruSeq Nano DNA Sample kit (Illumina). Quality of libraries was assessed using HT DNA High Sensitivity Chip (Agilent) for 2100 Bioanalyzer. RNA-seq reads were aligned to the UCSC mm10 reference genome using STAR (version 2.3.0e_r291). Aligned reads were quantified by htseq-count module, part of the 'HTSeq' framework (version 0.6.0). Differentially expressed genes were identified by performing a negative binomial test using DESeq2 (R-package version 1.4.5) with default settings. Significant p values were corrected to control the false discovery rate of multiple testing at 0.05 threshold.

1.6.3 Immunolabeling approaches for anatomical studies

Fluorescence In-situ Hybridization (FISH)

Mice were sacrificed and dissected brains were submerged in OCT media at stored at -80°C. Brains were then sectioned at 14µ using a Leica CM 3050 S Cryostat and stored at -80°C for fluorescence *in situ* hybridization (FISH). FISH was conducted using RNAscope Multiplex Fluorescent Reagent Kit v2 (Advanced Cell Diagnostics 323100). The following probes were used. Mm-Crh (316091), Mm-Vip-C2 (415961), Mm-Htr3a-C3 (411141), and Mm-Crhr1-C3 (418011).

Probes were visualized using TSA Fluorescein (NEL701A001KT), TSA CY3 (NEL704A001KT), and (TSA CY5 SAT705A001EA). For dual ISH/immunofluorescence labeling, slides were rinsed in PBS-0.1% Triton X, blocked in 0.5% TSA blocking buffer, and incubated in primary antibody in 0.5% TSA blocking buffer for 2 hours. Slides were then rinsed in 0.1M Phosphate Buffer and incubated in Alexa-fluor conjugated secondary antibodies (Jackson Immuno), diluted in 0.5% TSA blocking buffer, for 1 hour. Slides were then rinsed, cover slipped, and imaged on a Zeiss LSM700 confocal microscope using ZEN acquisition software, with laser intensity set to 20% maximum power. Following imaging, slides were stored short term at 4°C.

Immunohistochemistry

Twenty-four hours prior to perfusion, mice were lightly anesthetized with ketamine/xylazine (100mg/kg, 10mg/kg B.W.) and 1µg of colchicine (2.0 µg / µl) (Sigma-Aldrich 64-86-8) was injected into the lateral ventricle (AP -0.20., ML –0.15, DV -2.50) via stereotax to induce microtubule breakdown and allow for localizing sufficient protein

concentrations to somata for cell type identification. Following 24 hours of recovery, mice were deeply anesthetized with sodium pentobarbital (Nembutal, 100mg/kg B.W.) and perfused transcardially with chilled phosphate buffered saline (PBS), followed by 4% paraformaldehyde. Brains were then dissected and postfixed in 4% paraformaldehyde at 4°C for 4 to 24 hours. Brains were then submerged in 30% sucrose for at least 24 hours prior to sectioning. Brains were frozen in dry ice and sectioned using a Leica SM2000R Sliding Microtome at 40µ. Sections were stored in cryoprotectant solution at -20°C and were rinsed thoroughly in 0.1M Phosphate Buffer and blocked in 0.5% TSA blocking buffer (Perkin Elmer).

Sections were incubated in the primary antibody, diluted in 0.5% TSA blocking buffer, for 24 to 72 hours at 4°C: Rb x GABA [1:1000] (Sigma A2052), Rat x Somatostatin [1:100] (Millipore MAB354), Ms x Parvalbumin [1:2000] (Millipore MAB1572), Rb x VIP [1:300] (Immunostar 20077), Rb x c-Fos [1:1000] (Cell Signaling 2250S), Chk x GFP [1:2000] (Abcam ab13970), Rb x mCherry [1:2000] (Rockland 600-401-379), and Ms x mCherry [1:2000] (Rockland 200-301-379).

Following primary incubation, sections were then rinsed thoroughly in 0.1M Phosphate Buffer and incubated in Alexa-fluor conjugated secondary antibodies (Jackson Immuno), diluted in 0.5% TSA blocking buffer [1:1000], for 1 hour at room temperature. Sections were then rinsed with 0.1M Phosphate Buffer, mounted onto glass slides, allowed to dry, and cover slipped with Prolong Gold Antifade and imaged on a Zeiss LSM700 confocal microscope using ZEN acquisition software. For DAB immunostaining, sections were incubated in Chk x GFP [1:2000] (Abcam ab13970) for 24 hours at 4°C. Following rinses in 0.1M Phosphate Buffer, sections were then incubated in biotinylated secondary

antibody [1:500] for 1 - 2 hours, followed by rinses in 0.1M Phosphate Buffer. Sections were then incubated in Vectastain ABC Kit Peroxidase Standard for 60 minutes, followed by rinses in 0.1M Phosphate Buffer. Visualization via SIGMAFAST™ 3,3-Diaminobenzidine tablet (D4418 Sigma Aldrich) was closely monitored for 2 – 10 minutes, after which sections were rinsed in 0.1M Phosphate Buffer, cover slipped, and imaged on a Zeiss AxioImager2 slide scanning microscope with Neurolucida acquisition software. All images were converted from ZEN and Neuolucida file formats to JPEG format using ImageJ software.

1.6.4 Electrophysiological whole cell recordings in mouse brain slices

Brain Slice Preparation

At 14-18 weeks of age, mice were deeply anesthetized with ketamine/xylazine (100mg/kg, 10mg/kg B.W.) and perfused with ice cold dissection buffer (2.5 mM KCl, 0.5 mM $CaCl_2 \cdot 2H_20$, 7.0 mM $MgCl_2 \cdot 6H_20$, 25.0 mM NaHCO3, 1.25 mM NaH_2PO_4, 11.6 mM (+)-Sodium L-ascorbate, 3.1 mM sodium pyruvate, 110.0 mM choline chloride, and 25.0 mM glucose). Brains were sectioned at 400µm on a Microslicer (DTK-1000N) and allowed to recover in artificial cerebrospinal fluid (aCSF) (2.5 mM KCl, 118 mM NaCl, 1.3 mM $MgCl_2$2.5 mM $CaCl_{2,}$, 26 mM $NaHCO_3$, 1 mM NaH_2PO_4, 10 mM glucose) at 32°C for 1 hour.

Dissection buffer and aCSF were kept constantly gassed for at least 45 minutes prior to the start of dissection and for the remainder of the recording. Sections were transferred to room temperature and underwent whole cell electrophysiological recordings following 30 minutes of recovery in aCSF. Slices were transferred to a

recording chamber and visualized under an Olympus microscope using a Q-Imaging QIClick PCI extended camera. Sections were constantly perfused in aCSF gassed with carbogen and temperature controlled to 32°C (TC-324B). 4-9MΩ glass capillary pipettes were pulled, depending on cell type somata size, and filled with internal solution for current clamp (130 K-Gluconate, 5 KCl, 10 HEPES, 2.5 MgCl2. 4 Na2ATP, 0.4 Na3GTP, 10 Na-phosphocretine, 0.6 EGTA) or voltage clamp (115 CsMeSO3, 20 CsCl, 10 HEPES, 2.5 MgCl2, 4 Na2-ATP, 0.4 Na-GTP, 10 Na-phosphocreatine, and 0.6 EGTA).

Electrophysiological Recordings

After establishing a stable GΩ seal, the membrane was disrupted with short bursts of negative pressure to achieve a whole cell configuration. Series resistance was measured and ranged between 3 to 30MΩ and cells were excluded where the holding current to achieve a -70mV voltage hold exceeded -20pA. In current clamp recordings, 0pA current injection was used to measure the resting membrane potential, and a 200ms -50pA hyperpolarizing pulse was used to measure membrane resistance. Tau, the membrane time constant, was determined via the time required to reach 63% maximum voltage response to a -50pA hyperpolarizing pulse. Spike width was determined at 50% maximum amplitude from spike threshold 50pA current injection. In voltage clamp recordings, cells were clamped to -70mV and 0mV to isolate AMPA and GABA currents, respectively.

All voltage and current sweeps were separated by 15 second intertrial intervals to allow cells to recover from their previous sweep. Recordings were collected on a Scientifica SliceScope Pro 1000 with data filtered at 2.4 kHz and digitized at 10 kHz using

a Digidata 1440A interface (Molecular Device) driven by pClamp 9.2 (Molecular Device). Liquid junction potential, measured at -11.2mV, was left uncorrected. Following collection, all data traces were analyzed using AxoGraph software.

1.6.5 Optogenetics and pharmacology in synaptic studies

Optogenetics

AAV2.2-EF1a-DIO-hChR2(H134R)-mCherry-WPRE was injected in mPFC to isolate ChR2 expression to select neurons for optogenetics studies **(Boyden et al., 2005)**. 5ms LED pulses were delivered to evoke action potential firing and to measure LED-induced postsynaptic currents. The minimal LED % illumination required to generate consistent action potential firing and postsynaptic currents varied between 5% - 10% and was kept at 5%, unless an immature LED response was observed. Five sweeps were collected at each potential, with a 15-second delay between sweeps.

Postsynaptic currents were excluded when recordings could not be collected at both -70mV and 0Mv, when series resistance was greater than 30MΩ, and when postsynaptic currents were not repeatable and time-locked across sweeps.

In vitro pharmacology

Bath application of pharmacological agents was used to characterize postsynaptic currents and were applied directly to circulating aCSF and kept constantly gassed with carbogen. For select optogenetic studies, sections were incubated in selective CRHR1 antagonist NBI 27914 (5μM) for 60 minutes prior to the start of the recordings and were recorded in NBI 27914-containing aCSF. CNQX (20mM) and D-

AP5 (20μM) wash in was used to block AMPA and NMDA currents, respectively, while picrotoxin (100μM) wash in was used to block $GABA_A$. Targeted single cell GPCR transduction blockade was accomplished using GDP-β-S (5μM) applied in the pipette solution.

1.6.6 Behavioral paradigms for the characterization of anxiety-like behavior and preference for novelty and sociosexual interaction

Behavioral Tests

Mice underwent an array of behavioral paradigms to characterize anxiety-like behavior, novelty preference, and sociosexual preference **(Figure 1.3)**. Animals were tested from Postnatal Day 90-104, with the behavioral testing separated by a minimum of 5 days. Behavioral instrumentations were cleaned with 70% ethanol and water between test runs and with Clydox when switching between sexes. In all experiments, mice were habituated to the testing room for at least 1 hour prior to testing and were run during their light cycle. All experimental groups were run during the same session to exclude batch effects.

The experimenter was blind to the treatment for each group except for hM3Dq clozapine-N oxide (CNO) and vehicle injected cohorts. Crh-hM3Dq were injected via intraperitoneal with either 2mg/kg CNO or vehicle 30 minutes prior to behavioral testing. Behavioral data was analyzed with no binning. Following behavioral testing, mice were subject to immunohistochemistry to validate viral expression.

Elevated Plus Maze. The elevated plus maze consisted of two open and two closed arms with an intersecting center point, elevated 120 cm from the ground. Mice

were lowered into the center point and allowed to freely roam for 10 minutes. The maze was illuminated to 60 lumens and curtained off during testing. Mouse location, vertical rears, and velocity was automatically measured using Ethovision v7.0 (Noldus). Zones were established in the software to partition the arena into open arms, closed arms, and center point. Duration in seconds and number of entries were automatically calculated for each zone within the arena.

Open Field Test. In the open field test, mice were lowered into and allowed to explore a clear plexiglass 50 x 50 x 30 cm open-top cube, elevated 120 cm from the ground, for 1 hour. The arena was illuminated to 230 lumens. Crh-hM3Dq were injected with either 2mg/kg clozapine-N oxide or vehicle at the start of testing, with the 30-minute peak efficacy time of clozapine-N oxide occurring half-way during the trial. Up to 8 mice per trial were run in separate arenas. Mouse location, vertical rears, and velocity was measured automatically using Fusion Software. A zone map delineating the center zone (4x4) and the periphery zone (7-4 x 7-4) was used to determine duration in the center and periphery.

Light Dark Box. The light dark test consisted of a black acrylic apparatus, partitioned into an exposed (light, 230 lumens) and closed (dark, 0 lumens) compartment, placed in a clear plexiglass 50 x 50 x 30 cm open-top cube, elevated 120 cm from the ground. Mice were lowered into the dark partition and their location and velocity was tracked automatically using Fusion Software. A zone map partitioning the exposed and close compartment was used to track duration in both compartments and latency to enter the exposed compartment.

Novel Object Recognition Test. The novel object recognition test consisted of a 50 x 50 x 30 cm open-top cube, elevated 120 cm above the ground. Illumination was set to 60 lumens and the arenas was curtained off. On day one, following testing room habituation, mice were habituated to the testing arena for 10 minutes. On day two, mice were again habituated to the test room for one hour. Mice were then lowered into the testing arena and allowed to freely investigate two identical objects for 5 minutes. Mice were then removed from the testing arena, and one of the identical objects was replaced with a novel object. After a delay of 60 minutes, mice were reintroduced to the arenas and allowed to freely investigate the novel and familiar object for 10 minutes. Mouse location and velocity was tracked automatically using Ethovision v7.0 (Noldus). An experimenter manually scored the duration of object interaction, defined as physical contact with novel and familiar objects. The objects consisted of two plastic 3-D triangles and two iron hose valves. Objects were placed in the upper left and upper right corner of the arena. To exclude potential bias, the side and identity of the novel and familiar objects were varied across groups. Objects were cleaned with 70% ethanol between trials and with Clydox when switching between sexes.

Three-chamber sociability test. In the three-chamber sociability test, mice were allowed to freely explore 3 connected 50 x 50 x 30 cm open-top plexiglass containers elevated 120 cm from the ground, with illumination set to 60 lumens. A cohort of wild type males and females, age matched to the experimental group, were habituated to a wire cup for 15 min daily three days prior to testing. On testing day, mice from the experimental groups were lowered into the central chamber and gates were removed allowing free access to both adjacent chambers. After 10 minutes of exploration, mice were removed

from the arena and temporarily housed in a cage. In phase one of the task, a novel, conspecific wildtype mouse of the opposite sex was placed under a wire cup in one of the outer chambers, while a plastic Lego was placed under a wire cup in the other outer chamber. The experimental mouse was reintroduced to the center chamber, and gates were removed allowing free access to both adjacent chambers for 10 minutes. Mouse location and velocity were tracked automatically using Ethovision v7.0 (Noldus). In phase two, an experimenter manually scored the duration of physical interaction between the experimental mouse and the Lego and conspecific mouse. In phase three, duration of physical interaction between the novel and familiar mouse were scored manually.

Figure 1.4. Experimental timeline for behavioral testing with CNO.

a) Elevated plus maze experimental timeline. Mice undergo testing 30 minutes after intraperitoneal injection
b) Open field test experimental timeline. Mice undergo testing immediately after I.P. injection
c) Light dark box experimental timeline. Mice undergo testing 30 minutes after I.P. injection
d) Novel object testing experimental timeline, lasting two days. Mice undergo testing 30 minutes after I.P. injection
e) 3-Chamber social interaction test. Novel conspecific mouse of the opposite sex used. Mice undergo testing 30 minutes after I.P. injection

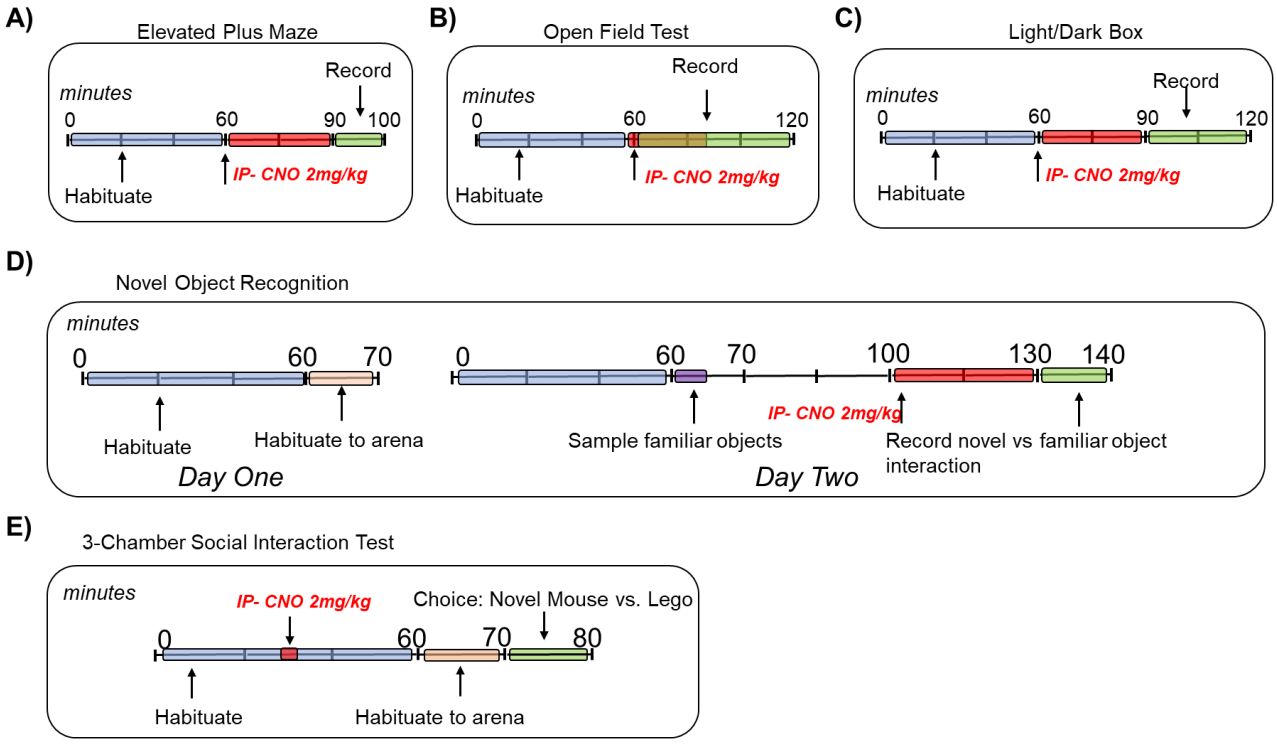
A)
Elevated Plus Maze
minutes
0
60
90
100
Record
Habituate
IP- CNO 2mg/kg
B)
Open Field Test
minutes
0
60
120
Record
Habituate
IP- CNO 2mg/kg
C)
Light/Dark Box
minutes
0
60
90
120
Record
Habituate
IP- CNO 2mg/kg
D)
Novel Object Recognition
minutes
0
60
70
Habituate
Habituate to arena
Day One
0
60
70
100
130
140
IP- CNO 2mg/kg
Sample familiar objects
Record novel vs familiar object interaction
Day Two
E)
3-Chamber Social Interaction Test
minutes
IP- CNO 2mg/kg
Choice: Novel Mouse vs. Lego
0
60
70
80
Habituate
Habituate to arena

CHAPTER 2. Modulation of OxtR interneurons, L2/3 pyramidal cells, and social behaviors by Corticotropin Releasing Hormone interneurons

2.1 Introduction

To understand the impact of cortical CRH production and signaling on local circuit functions and to determine whether CRH release from cortical neurons has roles independent from hypothalamic release of the hormone, we have studied in detail the small subset of cells expressing CRH in the mPFC. We show by TRAP translational profiling, immunolabeling, and viral injections in double transgenic mice that ~75% of CRH expressing cells in the mPFC are VIP expressing interneurons, which we refer to as CRH interneurons (CrhINs).

We demonstrate that, despite their rarity, CrhINs have profuse projections covering superficial cortical layers, and that their intrinsic electrophysiological properties are consistent with their molecular identity, matching previous studies of VIP/5-HT_{3A}R interneurons **(Lee et al., 2010)**. VIP interneurons, one of the three molecularly distinct cortical interneurons subtypes **(Rudy et al., 2010)**, have been shown to be important in disinhibition, the non-selective and transient silencing of pyramidal cell inhibition by selective and direct suppression of SST and, to some extent, PVALB interneuron firing **(Pfeffer et al., 2013, Kepecs & Fishell 2014)**.

We provide further functional evidence supporting the classification of CrhINs as VIP interneurons by demonstrating that LED activation of CrhINs during simultaneous

recordings from genetically labelled OxtR-INs *in vitro* results in time-locked postsynaptic currents (PSC) that result in strong inhibition of OxtR-INs.

In postsynaptic mPFC layer L2/3 pyramidal cells (L2/3 PCs), high frequency LED stimulation of CrhINs elicits increases in postsynaptic current (PSC) frequency, not amplitude, in a subpopulation of L2/3 cells which can be blocked both by bath application of the CRHR1 specific antagonist NBI27914 HCl or by *in vitro* intracellular dialysis of GDP-β-S, a competitive inhibitor of G-protein activation. Optogenetic activation of CrhINs evoked PSCs targeting L2/3 pyramidal cells that were larger in males than in females, suggesting that CrhINs may play a significant role in the sexually dimorphic social behaviors.

Cre-mediated excision of CRH in mPFC strongly increases male sociability with novel female mice but has no impact on female sociability with novel male mice or on anxiety related behaviors regulated by hypothalamic release of CRH **(Zhang et al., 2017)**. In parallel, chemogenetic activation of mPFC CrhINs reduces male sociability with novel female mice and again has no impact on female sociability and anxiety related behaviors.

Taken together, these data demonstrate that CrhINs regulate L2/3 pyramidal cells by both classical disinhibition via the inhibition of OxtR-INs and by direct CRH release, provide additional support for the reciprocal roles CrhINs and OxtR-INs in regulating gender specific social behaviors **(Li et al., 2016)**, and demonstrate that local release of CRH in the mPFC has functional roles distinct from those mediated by the hypothalamus.

2.2 Local vs. remote expression of CRH in medial prefrontal cortex

To begin to address the role of CRH in cortical microcircuits and identify which cell types express CRH in the mPFC, we crossed CRH-IRES-Cre mice **(Taniguchi et al., 2011)** to a Cre-dependent L10a-EGFP (TRAP) reporter mouse line and visualized EGFP immunoreactive CRH expressing cells. As expected, we observed dense labeling of the paraventricular nucleus of the hypothalamus (PVN) **(Figure 2.1B)** but also noted a sparse population of EYFP immunoreactive cells scattered across the mPFC **(Figure 2.1A)**.

We next examined the potential interaction between hypothalamic efferents to mPFC inputs compared to local projections of prefrontal CRH-Cre- expressing cells. For this purpose, we injected CRH-ires-Cre mice with AAV2/hSYN-DIO-mCherry and AAV2/hSYN-DIO-EYFP into PVN and mPFC respectively **(Figure 2.2)**. Local mPFC injections revealed robust EYFP+ immunoreactivity and dense innervation from cortical CRH-CRE cells **(Figure 2.2A)** and we observed scarce mCherry+ hypothalamic projections afferents targeting mPFC **(Figure 2.2B)**.

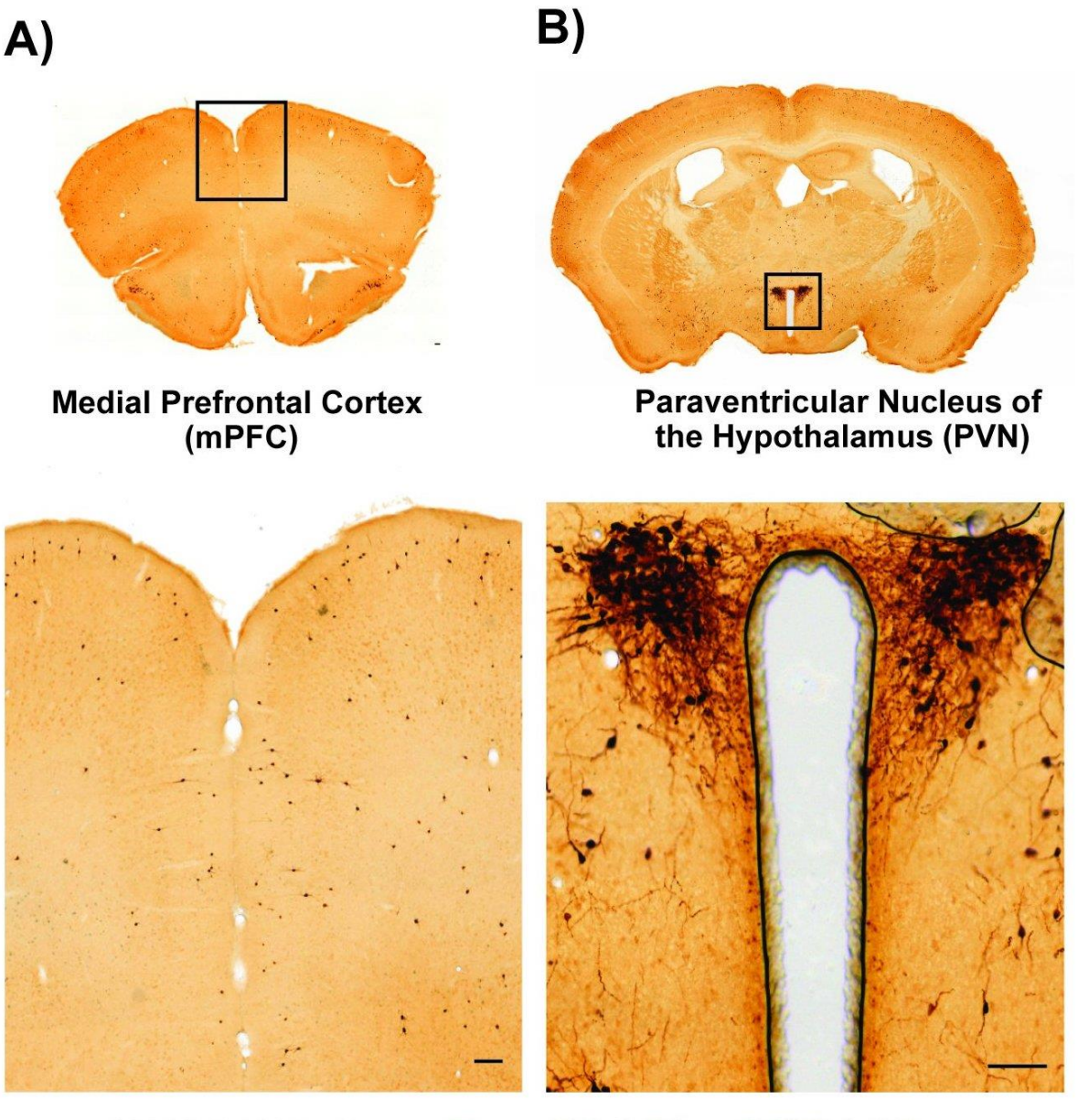

Figure 2.1. Hypothalamic and cortical expression of CRH and their respective innervation of mPFC.

a) Visualization of CrhINs in the mPFC of CRH-IRES-Cre x Rosa26-LSL-eGFP-L10a mice by DAB immunostaining against eGFP
b) DAB immunostaining reveals canonical CRH cell type localization in the PVN of the hypothalamus in CRH-IRES-Cre x Rosa26-LSL-eGFP-L10a mice

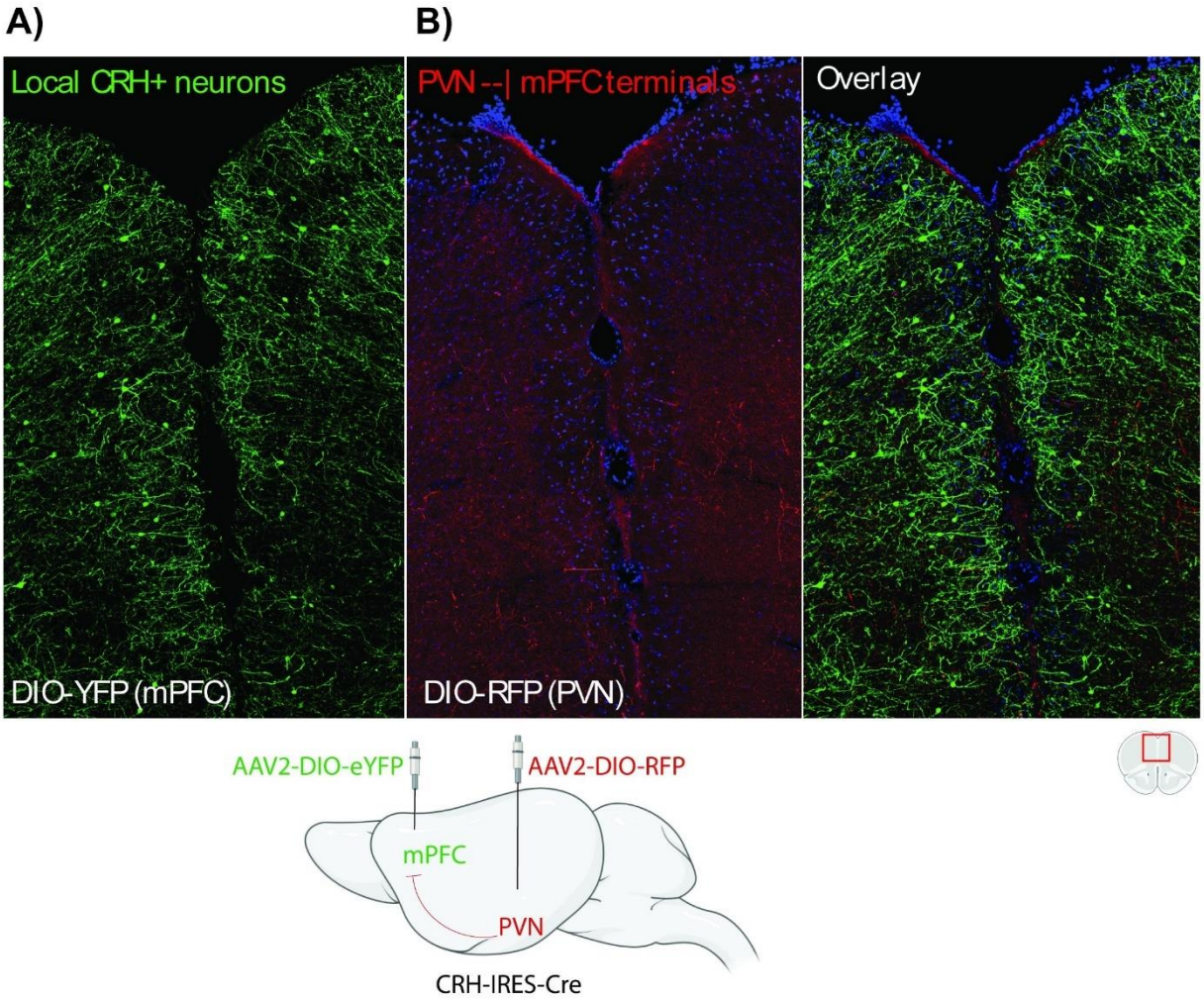

Figure 2.2. Qualitative assessment of CRH+ hypothalamic and cortical innervation of mPFC.

a) CRH-ires-Cre mice were injected with AAV2/hSYN-DIO-mCherry and AAV2/hSYN-DIO-EYFP into PVN and mPFC respectively
b) Hypothalamic injection label sparse mCherry+ projections into mPFC and local mPFC injections revealed eYFP+ immunoreactivity in dense local projections from few scattered CRH-CRE cells

2.2.1 Molecular profiling of CRH neurons in medial prefrontal cortex

Dense innervation, together with the localized expression of CRH to select cell types in cortex, suggests that CRH may be enriched in a molecularly distinct subset of cortical neurons and that cortical CRH production could modulate adjacent CRH receptor bearing cells. To evaluate this possibility, we next proceeded to determine the molecular profile of mPFC CRH-IRES-CRE cells using TRAP (Translational Ribosome Affinity Purification) profiling **(Heiman et al., 2008)**, after which enriched molecules were validated via histological methods.

To identify mRNAs expressed and translated in this small population of cortical cells, we used TRAP profiling from the mPFC of CRH-IRES-Cre x Rosa26-LSL-eGFP-L10a mice **(Figure 2.3A)** (n = 8, 3 replicates).When compared to the molecular profiles of other cortical interneurons (**Figure 2.3B)**, we noted cell type specific markers in CRH-IRES-CRE cells and demonstrated enrichment in *Gad1*, *Dlx1*, *Crh*, *Vip* and *Htr3a* mRNAs, and their depletion of *Pvalb*, *Crhbp*, *Oxtr* and a variety of excitatory neuronal markers in the EGFP-L10a expressing cell population **(Figure 2.4) (Table 2.3).**

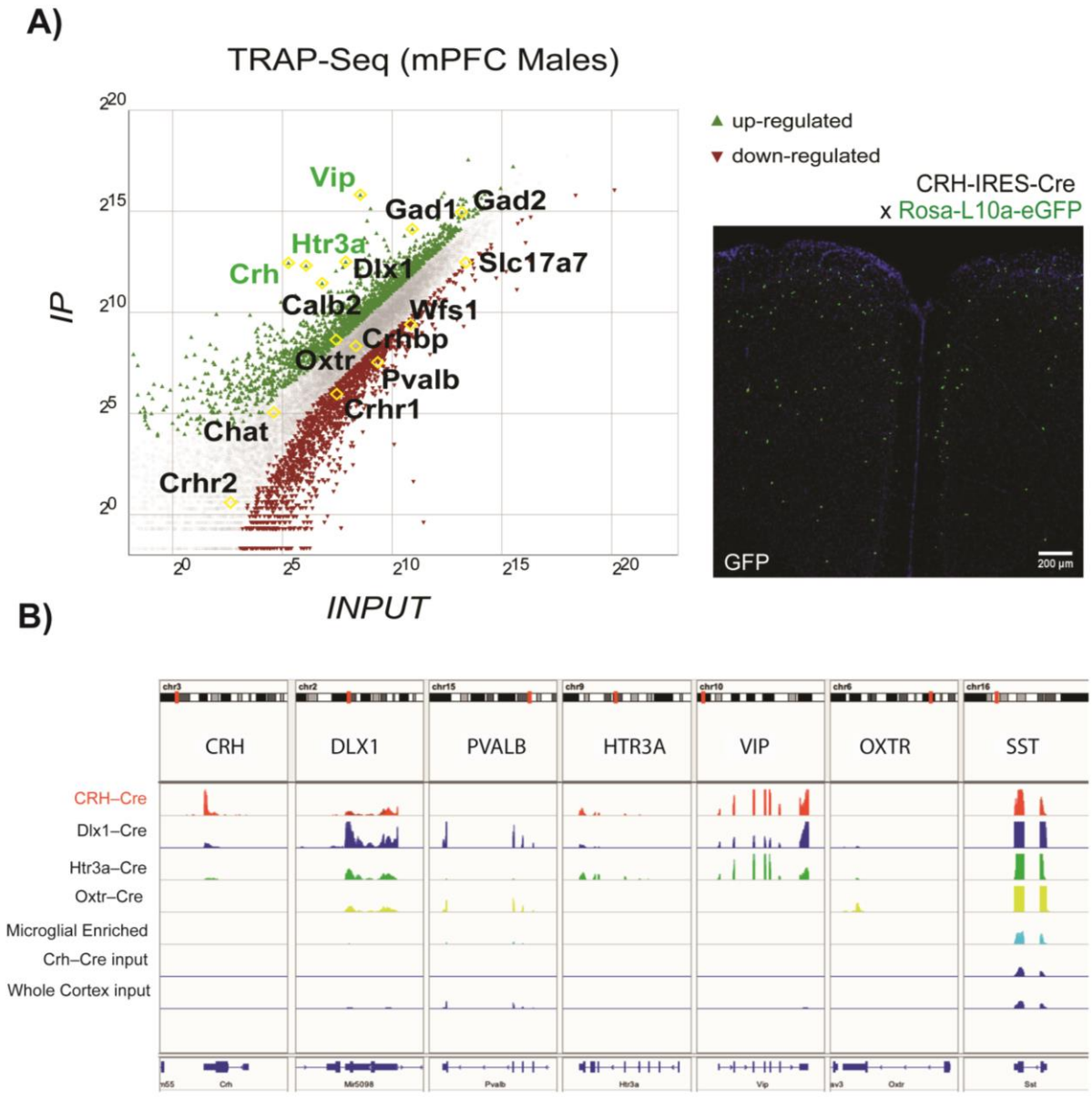

Figure 2.3. Molecular profiling and histological validation of CRH neuron subtype in mPFC.

a) TRAP-seq molecular profiling of mPFC CRH-Cre-eGFP-L10a neurons reveals an abundance of transcripts associated with VIP/5-HT_{3A}R interneurons. Enriched genes of interest (green) and depleted genes of interested (red)
b) IGV gene enrichment plot for mPFC CRH-IRES-Cre x Rosa26-LSL-eGFP-L10a neurons and other interneuron lines across cortex

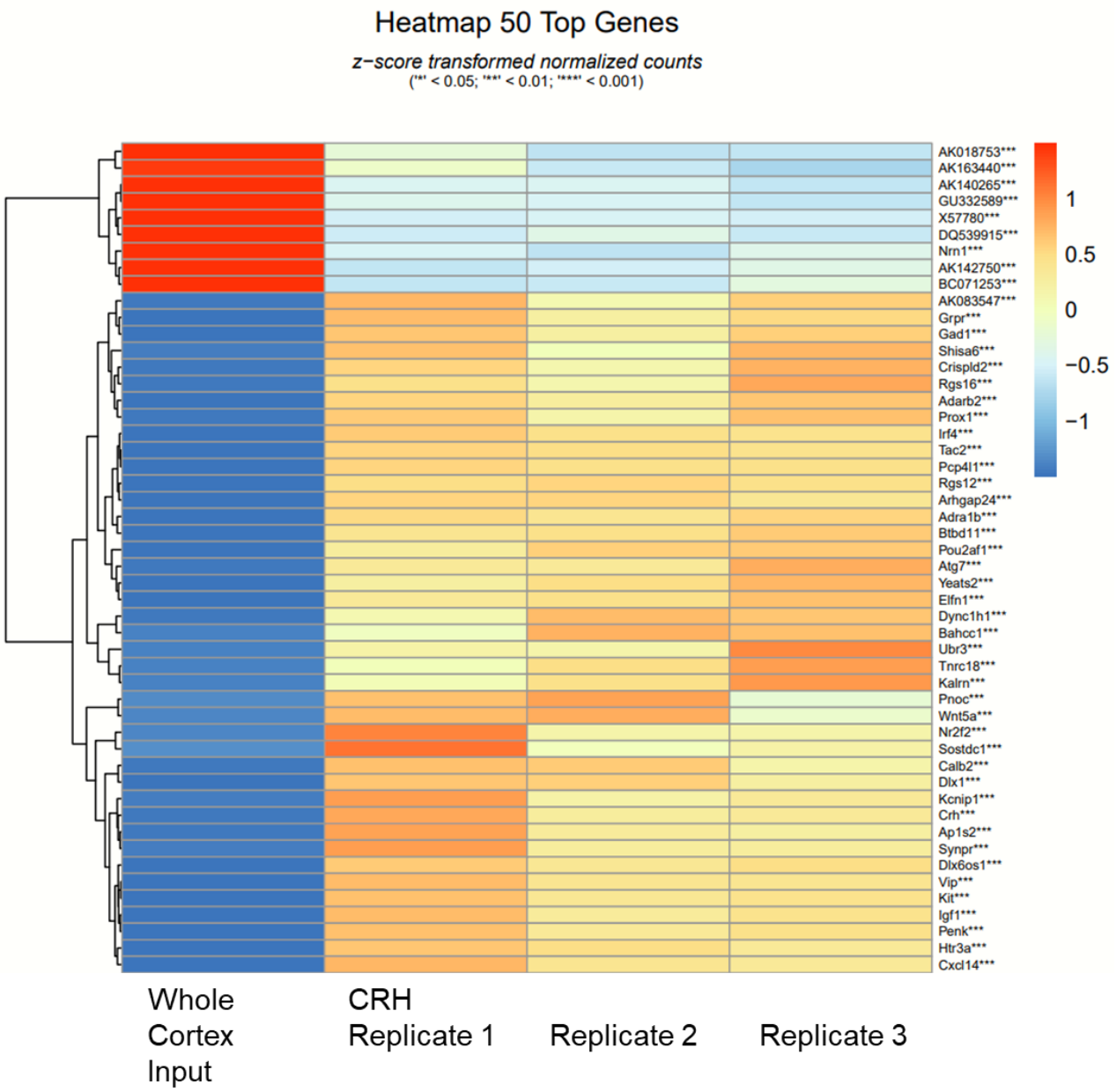

Figure 2.4. Heat maps results from molecular profiling of mPFC CRH neurons in males.

Heatmap for top 30 genes enriched in TRAP seq molecular profiling of mPFC CRH-Cre-eGFP-L10a neurons reveals an abundance of transcripts associated with VIP/5-$HT_{3A}R$ interneurons

Table 2.3. *TRAP RNAseq results for CRH-IRES-CRE mPFC cells from male mice.*

Gene	Description	Average Input	Average IP	log2Fold Change	p Value	p adj. Value
Crh	corticotropin releasing hormone	17.201388	3711.9758	7.7539808	1.471E-28	3.609E-25
Vip	vasoactive intestinal polypeptide	459.52279	38329.582	6.3822171	1.839E-37	9.023E-34
Htr3a	Serotonin receptor 3A	61.433528	3374.9519	5.779924	6.389E-26	1.045E-22
Calb2	calbindin 2	54.061505	1851.5438	5.0981816	8.881E-16	4.842E-13
Dlx1	distal-less homeobox 1	202.32109	3855.6698	4.2523649	9.378E-16	4.844E-13
Gad1	glutamate decarboxylase 1	1268.8071	11805.657	3.2180117	1.475E-11	4.669E-09
Gad2	glutamic acid decarboxylase 2	3921.9164	21107.111	2.4281336	1.163E-07	0.00002238
Oxtr	oxytocin receptor	89.283394	265.8136	1.5725599	0.1997469	0.9999533
Chat	choline acetyltransferase	8.191137	22.054564	1.4320593	0.5734294	NA
Crhbp	corticotropin releasing hormone binding protein	150.71692	214.84355	0.5087413	0.6279239	0.9999533
Pvalb	parvalbumin	274.40309	123.06308	-1.1624187	0.3621889	0.9999533
Slc17a7	solute carrier family 1, member 7	8551.5471	3753.5304	-1.1882971	0.0319517	0.5238714
Crhr2	corticotropin releasing hormone receptor 2	2.4573411	1.0093043	-1.3375229	0.8046076	NA
Wfs1	Wolfram syndrome 1 homolog	1163.1415	449.4836	-1.3733058	0.0386005	0.5748482
Crhr1	corticotropin releasing hormone receptor 1	114.67592	41.418433	-1.4730339	0.3622248	NA

2.2.2 Histological validation of molecular profiling results

Immunohistochemistry (IHC) co-staining for known interneuron markers against EGFP confirmed **(Figure 2.5A)** that CRH-Cre-eGFP cells are predominantly VIP interneurons (70.83% ± 7.352 S.E.M) **(Figure 2.5B)**, although we noted a small percentage of CRH-Cre-eGFP neurons were positive for SST (6.71% ± 1.80 S.E.M) and observed no co-localization with PVALB. To confirm the identity of CRH expressing mPFC neurons as a subpopulation of VIP/5-HT_{3A}R interneurons, we used RNAscope multiplex *in situ* hybridization (ISH) to localize *Crh*, *Vip* and *Htr3a* mRNAs. The co-localization of these markers in mPFC sections from wild type mice **(Figure 2.6A, B)** and their close agreement with previous IHC results demonstrates clearly that mPFC CRH expressing cells are interneurons of the VIP/5-HT_{3A}R subtype.

Given the presence of numerous VIP labeled cells that did not express *Crh* in the ISH experiments and the relative rarity of mPFC CrhINs in CRH-IRES-Cre mice, we next determined the fraction of VIP interneurons in mPFC that co-express CRH. To measure this and visualize directly CrhIN cell morphology in adult mPFC, we crossed CRH-IRES-Cre to VIP-Flp mice and performed stereotaxic injections of AAV virus encoding Cre-dependent mCherry (AAV2-DIO-mCherry) to detect CRH expressing neurons as red and a Flp-dependent eYFP (AAV2-fDIO-eYFP) to detect VIP cells as green **(Figure 2.7A)**. Quantification of these results revealed that 73% of mPFC CRH neurons are VIP interneurons **(Figure 2.7B)**, which we refer to as CRH interneurons (CrhINs), and that they account for 18% of all mPFC VIP interneurons.

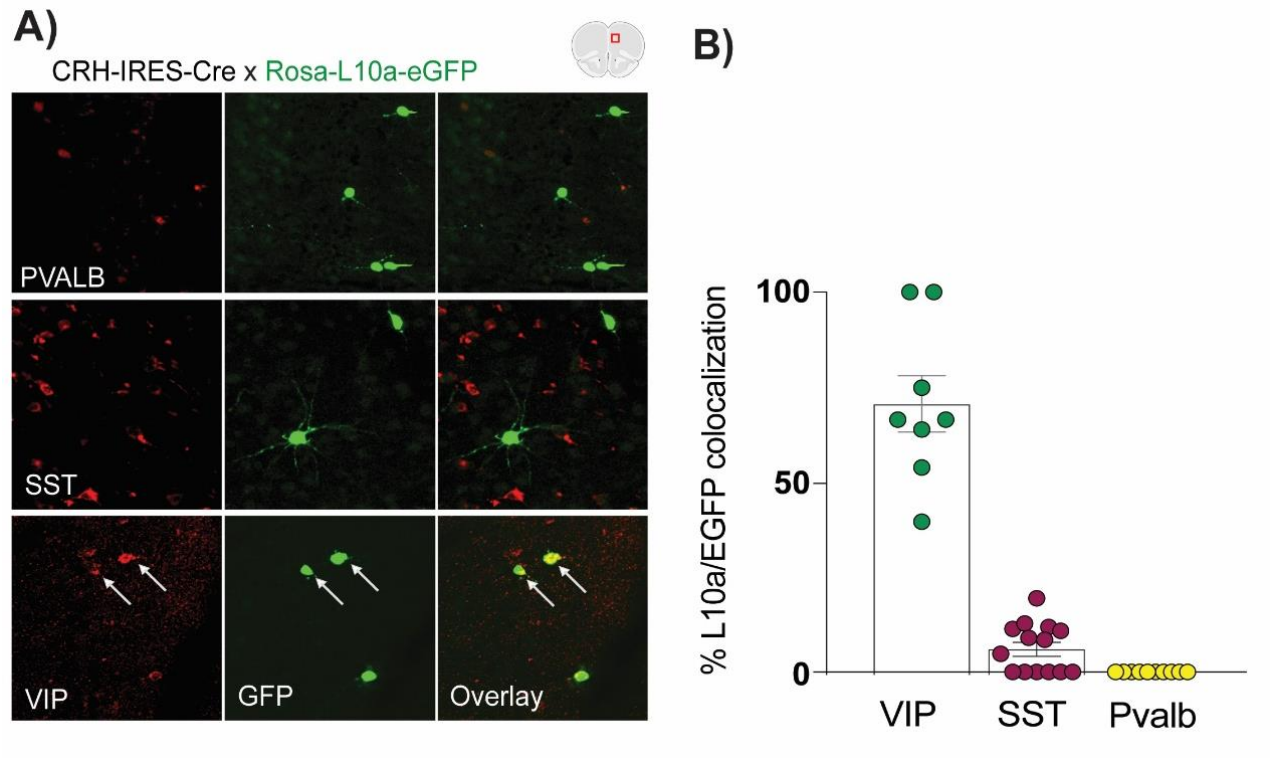

Figure 2.5. IHC validation of molecular profiling results.

a) Immunohistochemistry for interneuron markers and colocalization against eGFP in CRH-IRES-Cre x Rosa26-LSL-eGFP-L10a mice
b) Quantification of IHC results reveals 70.83% (± 7.352 S.E.M) of GFP cells colocalize with VIP, 6.71% (± 1.80 S.E.M) of GFP cells colocalize with SST, and we observe no evidence of PVALB colocalization with GFP

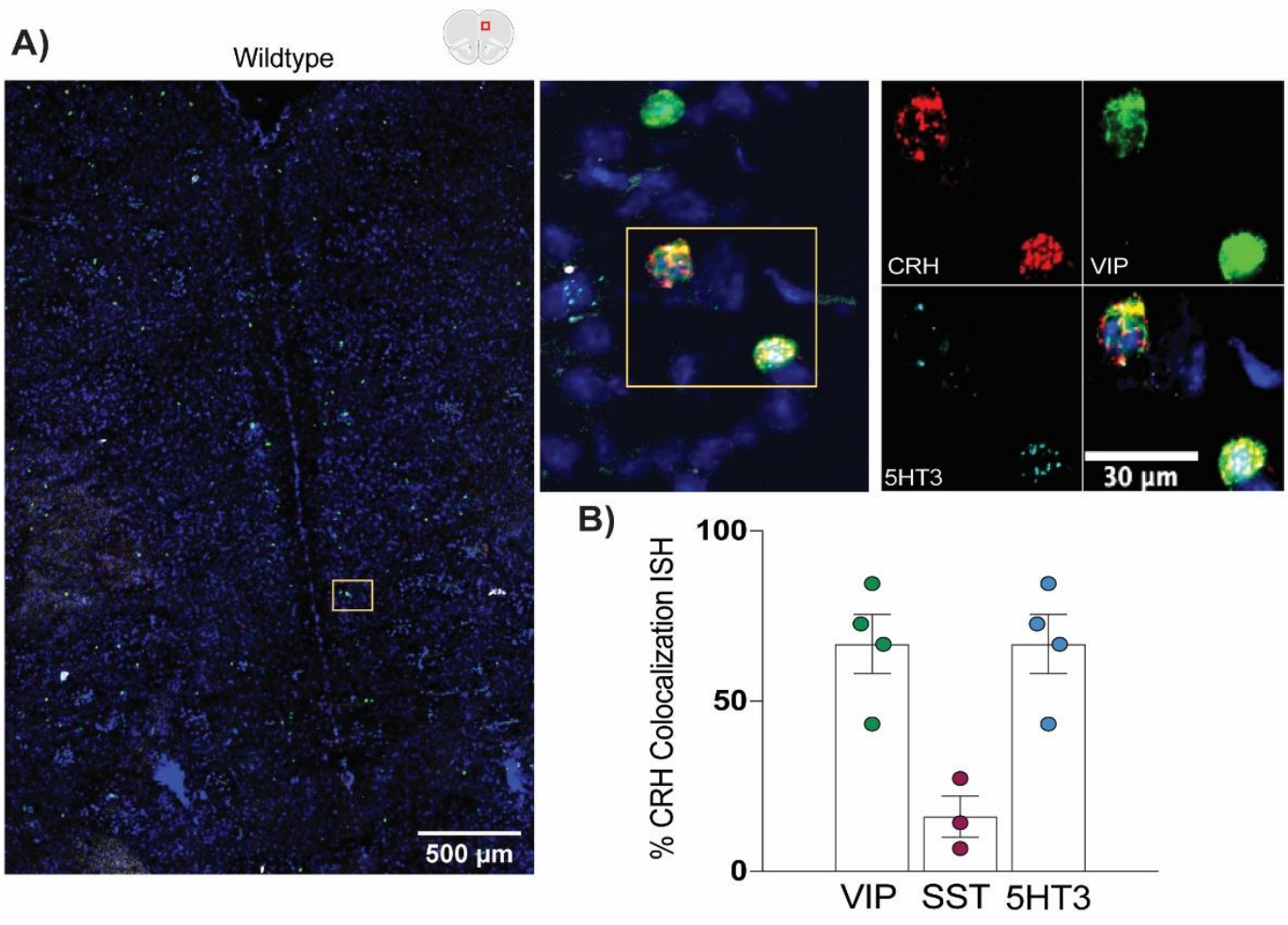

Figure 2.6. ISH validation of molecular profiling results.

a) RNAscope *in situ* hybridization (ISH) studies in wildtype mice again observed co-expression of CRH, VIP, and 5-HT_{3A}R transcripts in mPFC
b) Quantification of ISH results again reveals mPFC CrhIN are predominantly VIP+

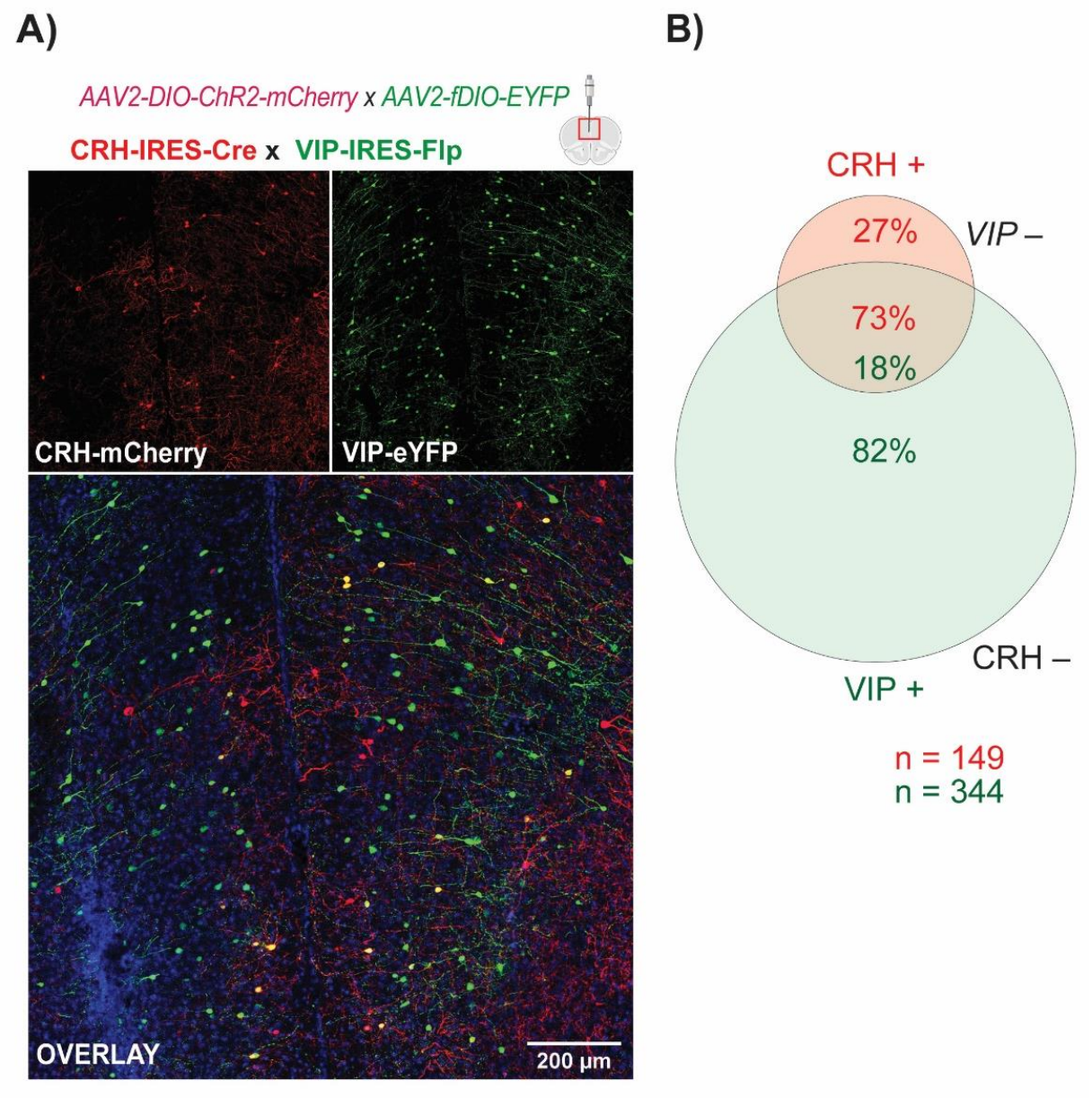

Figure 2.7. Validation of molecular profiling results by dual transgenic viral labeling.

a) CRH-Cre mice crossed with VIP-Flp mice underwent stereotaxic injection of Cre-dependent AAV virus encoding RFP (AAV2-DIO-RFP) and Flp-dependent AAV virus encoding eYFP (AAV2-fDIO-eYFP)
b) Quantification of CRH-Cre crossed to VIP-Flp colocalization study. Over 50% of mPFC CRH neurons express VIP, and those CRH neurons represent approximately 20% of all mPFC VIP neurons

2.2.3 Intrinsic electrophysiology properties of CRH interneurons

To better visualize the morphology of CrhINs and measure their intrinsic electrophysiological properties, we used whole cell current clamp recordings in CRH-IRES-Cre mice after stereotaxic injections of AAV2-DIO-ChR2-mCherry in mPFC. Despite their small numbers, CrhINs arborize extensively in mPFC, particularly in the superficial cortical layers **(Figure 2.8A)**. We proceeded to use fluorescence-guided whole cell current clamp recordings from CrhINs in mPFC **(Figure 2.8B)** to characterize their baseline electrophysiological intrinsic properties.

Upon achieving a whole cell configuration, we observed large voltage decreases in response to a -25pA hyperpolarizing current injection and repetitive burst firing in response to a +25pA depolarizing current injection in both males **(Figure 2.9A)** and females **(Figure 2.9B)**. Current injections as low as 50pA produce high frequency AP firing in both males **(Figure 2.9C)** and females **(Figure 2.9D)**. AP frequency-current curves generated by 25pA stepwise current injections **(Figure 2.9E)** revealed CrhINs quickly increase AP firing in response to current injections and plateau at sustained AP frequencies upon high current injection. Both male **(Figure 2.10A-D)** and female CrhINs **(Figure 2.10E, F)** display repetitive AP firing following a single 5 msec 470nm LED pulse at low illumination intensity.

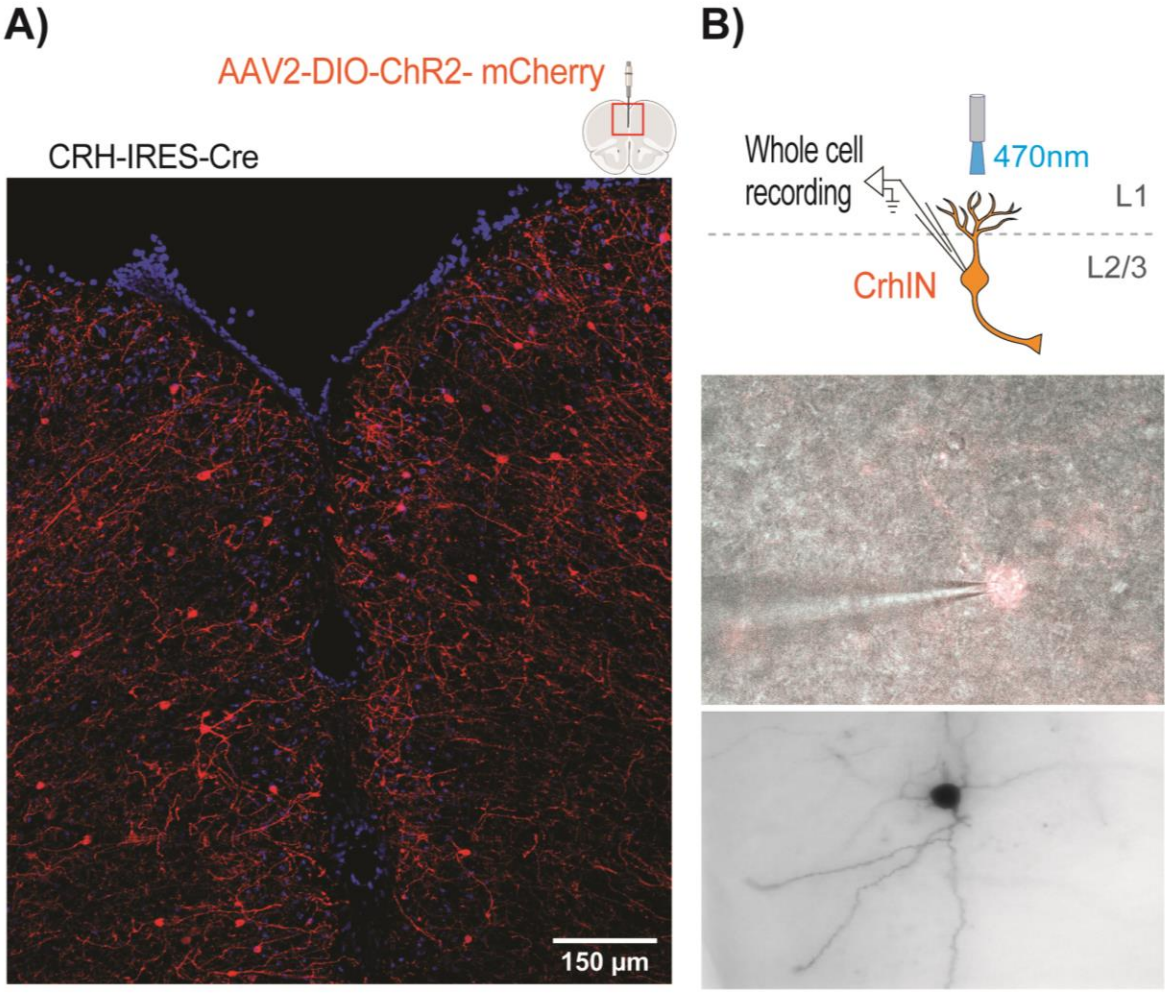

Figure 2.8.Viral expression of ChR2 restricted to CRH-IRES-CRE cells in mPFC. Whole cell recording from mPFC CrhINs.

a) Optogenetic validation of CRH-IRES-Cre mice in a 400µm section after stereotaxic injections targeting mPFC with Cre-dependent AAV virus encoding ChR2 (AAV2-DIO-ChR2-mCherry) and whole cell recording. CrhINs arborize extensively in mPFC, particularly in the superficial cortical layers
b) Schematic showing whole cell recording configuration for CRH-Cre cell upon LED optogenetic stimulation. Following dialysis of neurobiotin, DAB immunostaining visualizes the stellate morphology of mPFC CrhINs

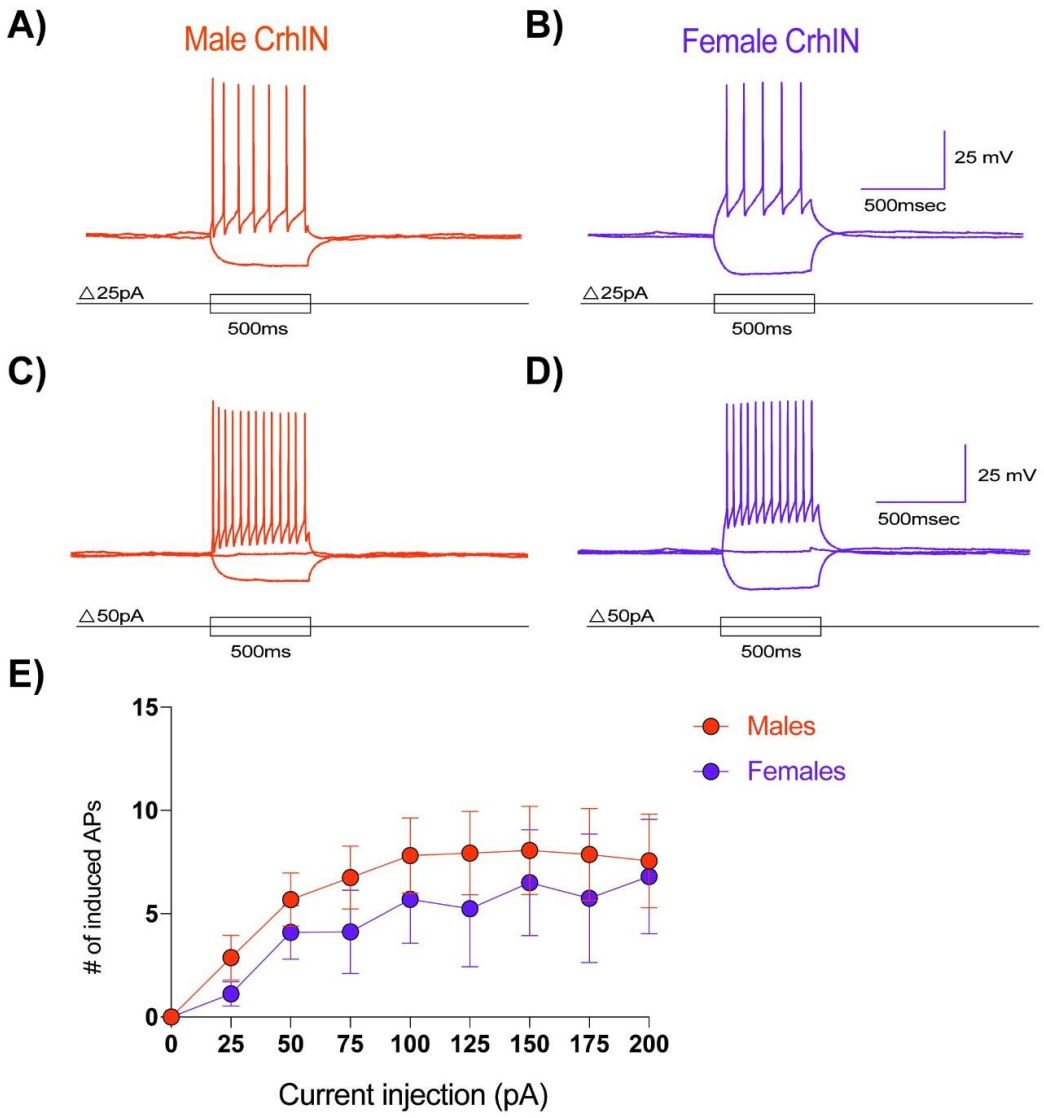

Figure 2.9. Current clamp injections in mCherry+ CRH-IRES-CRE cells in male and female mPFC.

a) Male CrhINs respond with large voltage decrease following a -25pA hyperpolarizing current injection and repetitive burst firing in response to a +25pA current injection
b) Similar current-AP responses seen in female CrhINs
c) High frequency AP firing in male CrhINs in currents as low as +50pA
d) Similar current-AP responses seen in female CrhINs following +50pA current injection
e) Action potential frequency– current (FI) curves resistance for male (n=17) and female (n=10) CRH-Cre cells demonstrate mPFC CRH-Cre cells have low rheobase current and firing multiple action potentials at low current injections

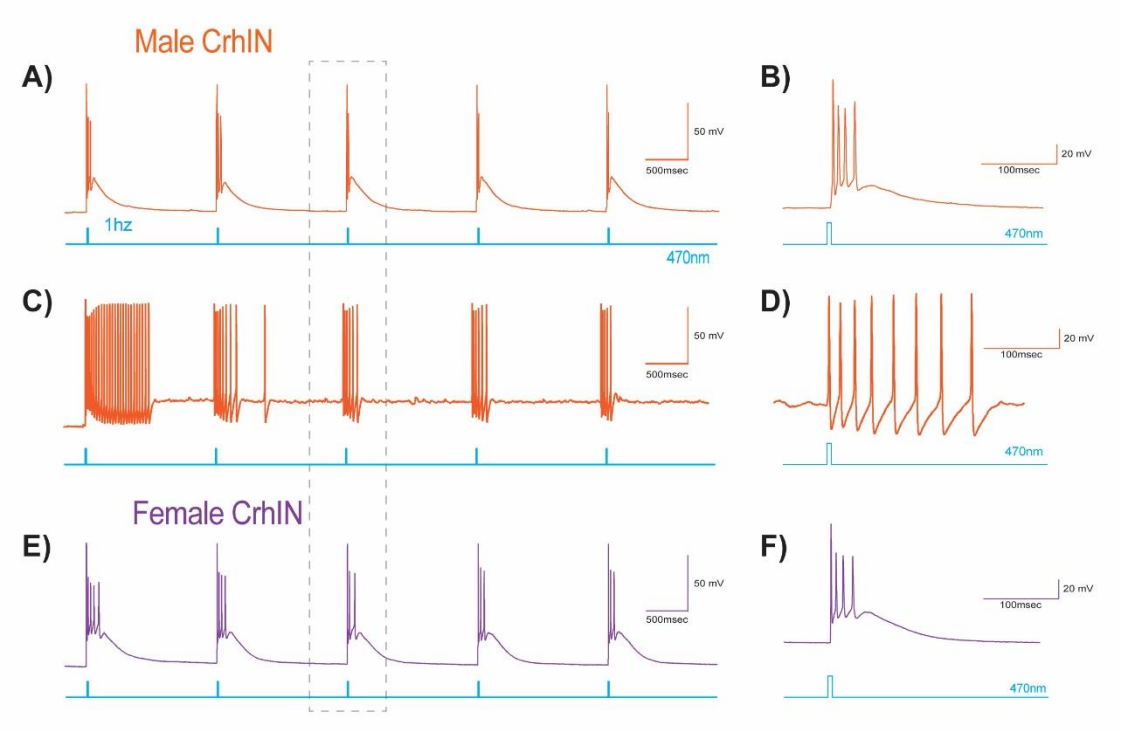

Figure 2.10.ChannelrhodospIn validation in male and female mPFC CrhINs.

a) LED evoked action potentials in mCherry+ mPFC CRH-Cre cells. Optogenetic validation of ChR2 expression via 1hz LED stimulation results in multiple time-locked APs in male CrhINs
b) Zoomed in plot of 3rd LED pulse and AP response in males
c) Repetitive burst action potential firing responses following 1hz LED illumination in another example male CrhIN, likely a result of high membrane resistance
d) Zoomed in plot of 3rd LED pulse and AP response in males
e) LED evoked action potentials in female mCherry+ mPFC CRH-Cre cells
f) Zoomed in plot of 3rd LED pulse and AP response in females

Measurement of whole cell intrinsic properties **(Table 2.4)** revealed that CrhINs have a high input membrane resistance **(Figure 2.11A),** which likely accounts for the large voltage responses **(Figure 2.9)** and burst AP firing **(Figure 2.10)** following single pulse LED stimulation**.** High membrane resistance is a result of their small somata and has been reported previously for cortical 5-HT_{3A}R expressing interneurons **(Lee et al., 2010)**. CrhINs rest at hyperpolarized resting membrane potentials **(Figure 2.11B)** and AP firing threshold did not vary significantly between males and females **(Figure 2.11C).**

When taken together, the molecular, anatomical, and electrophysiological properties of CrhINs are clearly consistent with that of the VIP/5-HT_{3A}R interneuron subtype. VIP interneurons are known to preferentially synapse with and inhibit SST interneurons **(Pfeffer et al., 2013),** and since OxtR-INs are a subclass of SST interneurons that secrete CRHBP **(Li et al., 2016)**, the endogenous inhibitor of CRH, the molecular and electrophysiological features of CrhINs suggested to us that their activation may lead to both the inhibition of SST interneurons and also the release of CRH onto mPFC CRHR1 expressing neurons.

Table 2.4. *Male and female CRH interneuron intrinsic properties, as measured via current clamp.*

CrhIN Intrinsic Properties	Males	Females
Resting membrane potential [mV]	-59.32 ± 1.72	-53.85 ± 2.748
Membrane Resistance [mΩ]	487.23 ± 45.08	598.43 ± 50.78
AP Threshold [mV]	-40.59 ±-1.54	-39.84 ±-1.72
AP Amplitude[mV]	62.68 ± 4.90	57.47 ± 6.05
Membrane time constant τm [ms]	21.99 ± 2.65	30.67 ± 4.08
AP spike width [ms]	3.65 ± 0.68	3.78 ± 0.67
n	17	10

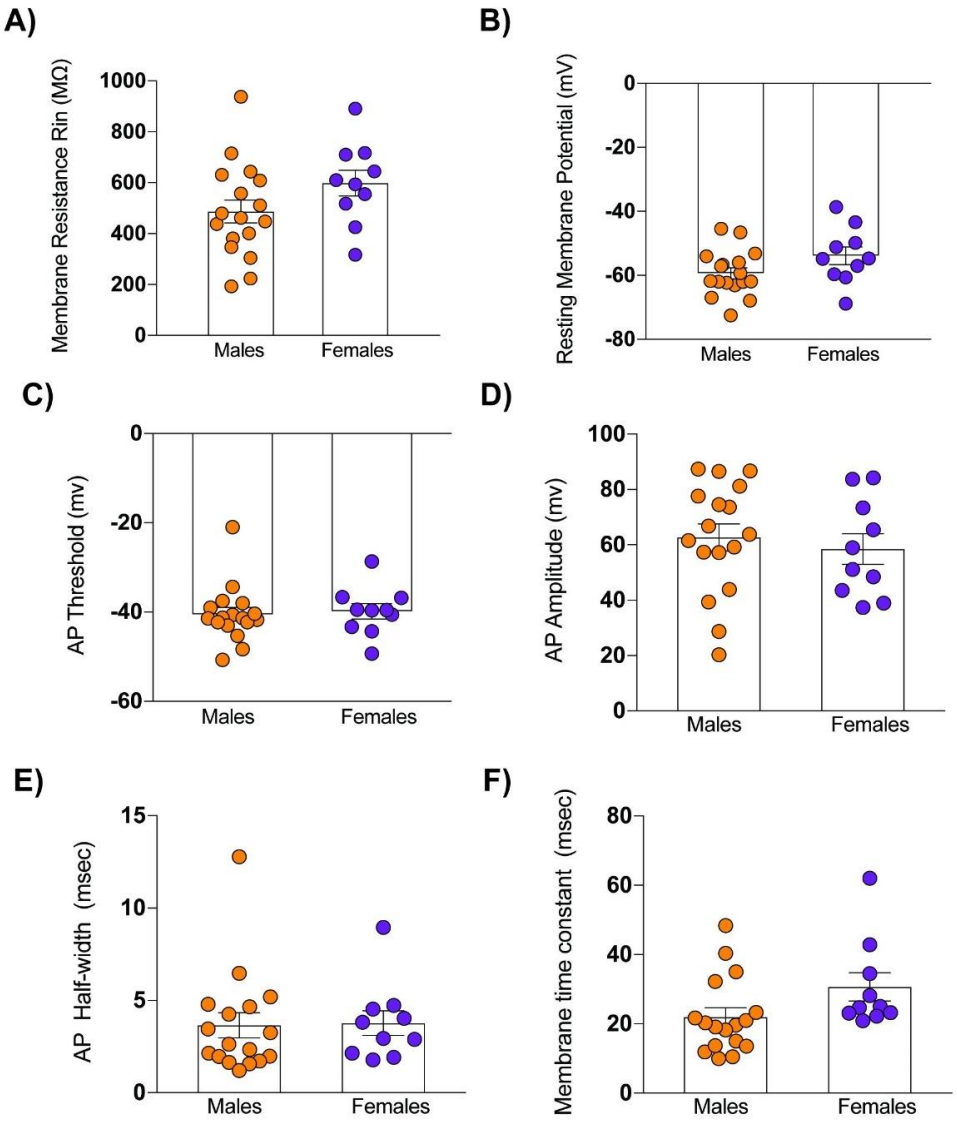

Figure 2.11.Male and female CrhIN electrophysiological intrinsic properties.

a) High membrane resistance for both male and female CrhINs, characteristic of VIP interneurons
b) Resting membrane potentials for both male and female CrhINs
c) Membrane AP firing threshold for AP waveform transition threshold for both male and female CrhINs
d) Male and female CrhIN AP amplitude, as measured via the difference between AP threshold and AP peak
e) AP half width, as measured via the width at half amplitude between AP threshold and AP peak, for both male and female CrhINs
f) Male and female CrhINs membrane time constant, as measured via time required to reach 63% of maximum voltage response to -50pA hyperpolarizing current injection

2.3 Modulation of cortical cell types by local CRH interneurons

Molecular profiling of CRH interneurons in mPFC and histological validation, demonstrates that CRH interneurons represent approximately 18% of all VIP/5-HT3AR interneurons **(Figure 2.5, 2.6, 2.7)** present in mPFC. This suggests that inhibition of SST interneurons, a well-established characteristic of VIP interneurons, may be coupled to release of CRH by mPFC CrhINs, collaboratively enhancing excitability of cortical pyramidal cells. To map this cortical microcircuit and determine whether CrhINs modulate the cortical activity through either GABAergic inhibition or through CRH release, we used whole cell voltage clamp recordings from select postsynaptic cell types in mPFC while simultaneously evoking CrhIN AP firing via LED pulse stimulation in ChR2 expressing CRH interneurons.

2.3.1 CRH interneurons inhibit Oxytocin Receptor Interneurons

As a first step in characterization of CrhIN modulation of local mPFC circuits, Crh-Flp mice, crossed to Oxtr-Cre expressing mice, were injected in mPFC with AAV2-fDIO-ChR2-mCherry and AAV2-DIO-eYFP **(Figure 2.12A),** at 1:1 dilution, to allow for simultaneous optogenetic stimulation of CrhINs and fluorescence-guided recordings from OxtR-INs. 400μm thick mPFC sections were prepared for whole cell voltage clamp recordings of isolated CrhIN – OxtR-IN postsynaptic currents (PSCs) **(Figure 2.12B)**. In both male and female mice, OxtR-INs were held at -70mV to isolate excitatory postsynaptic currents (EPSC) and at 0mV to isolate inhibitory postsynaptic currents (IPSCs).

Optogenetic activation of male CrhINs elicits a multi-phasic postsynaptic current (PSC) targeting OxtR-INs that are largely inhibitory **(Figure 2.13A, C)** and we observed blunted responses in females **(Figure 2.13B, D).** Similar PSC waveforms have been reported when activating CRH neurons outside of the mPFC **(Partridge et al., 2016)**, likely a result of repetitive burst firing of CrhINs in response to single LED pulses **(Figure 2.10)**. In both males and females, OxtR-IN PSCs evoked by optogenetic stimulation of CrhINs are predominantly inhibitory, as IPSC amplitude were consistently larger than that of corresponding EPSC amplitudes **(Figure 2.13E)**. We observed a CrhIN LED-induced PSC response in 6/7 (85.7%) male OxtR-IN cells and 6/7 (85.7%) female OxtR-INs cells and noted a statistically significant difference between male and female OxtR-IN PSC response following CrhIN LED activation, as determined via a one-way ANOVA ($F(3, 17) = 9.909$, $p = 0.0005$) ($n = 1$-2 mice per group). However, a Bonferroni post hoc multiple comparison test noted no significant difference between male and female OxtR-IN PSC amplitude size at both -70mV ($p = 0.9835$) and 0mV ($p = 0.1030$).

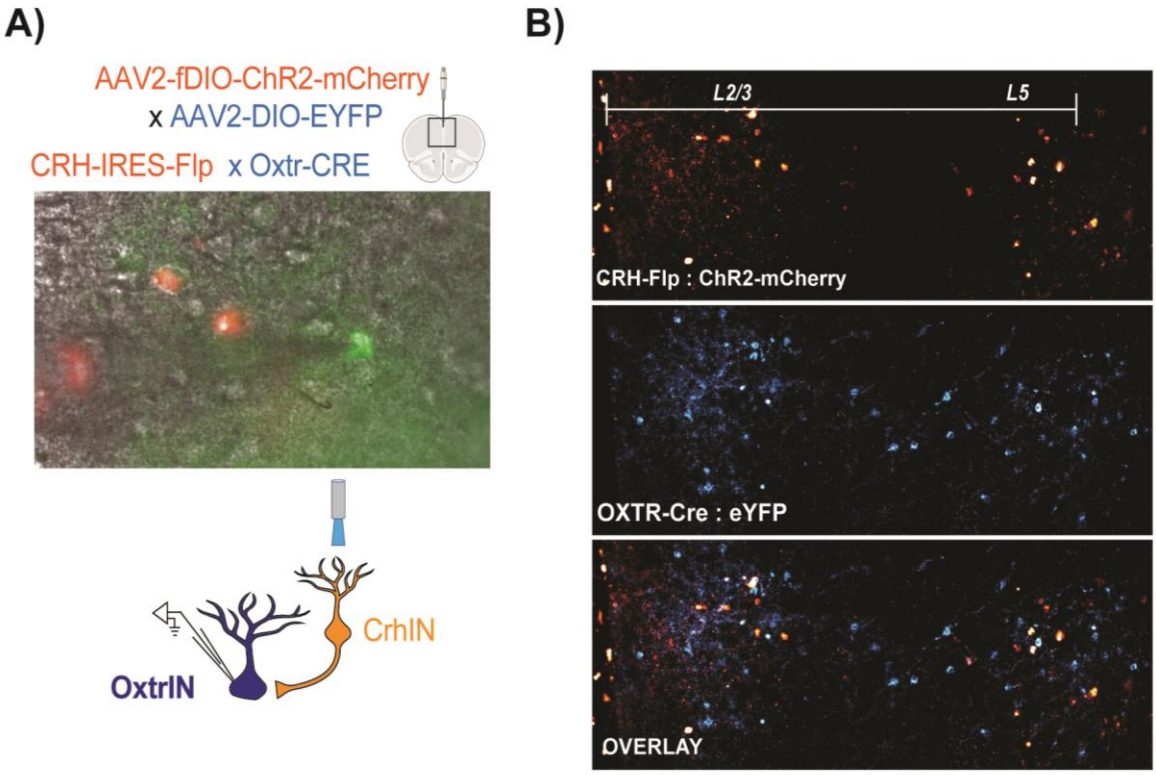

Figure 2.12. CrhIN OxtR-IN dual labeling approach for whole cell voltage clamp synaptic studies.

a) Crh-Flp mice crossed with Oxtr-Cre mice underwent stereotaxic injection of Flp-dependent AAV virus encoding ChR2 (AAV2-fDIO-ChR2-mCherry) and Cre-dependent AAV virus encoding eYFP (AAV2-DIO-eYFP). Cartoon schematic showing whole cell recording configuration for OxtR-Cre cell plus simultaneous LED optogenetic stimulation of CRH-Flp ChR2+ cells
b) IHC immunolabeling for 300μM thick mPFC slices post recording. CRH-Flp cells visualized via anti-RFP antibody (red), Oxtr-Cre cells visualized via anti-GFP antibody (blue). CrhINs somata are concentrated near L2/3 and L5, whereas OxtR-IN somata are more distributed across cortical layers

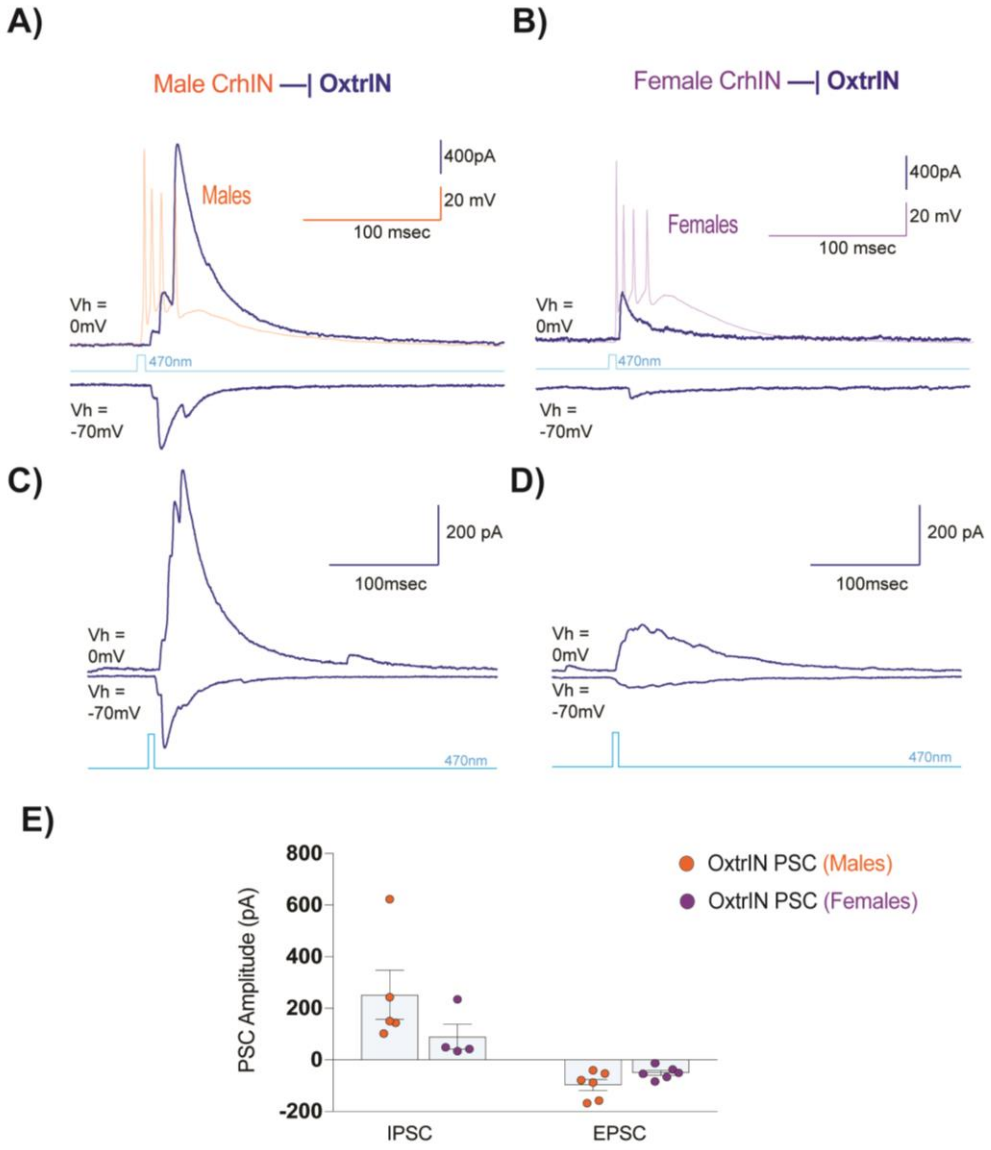

Figure 2.13. CrhINs target OxtR-IN with inhibitory postsynaptic currents.

a) Voltage clamp recording from male OxtR-INs during LED stimulation of CRH-Flp mice crossed with Oxtr-CRE mice, following injection of AAV2-fDIO-ChR2-mCherry and AAV2-DIO-eYFP. CrhIN APs, recorded in separate slices via current clamp, are overlaid onto OxtR-IN PSCs. OxtR-IN PSCs are multiphasic due to repetitive CrhIN burst firing and demonstrate that CrhINs inhibit OxtR-INs in males
b) Voltage clamp recording from female OxtR-INs during CrhIN LED stimulation show reduced amplitudes, as compared to male OxtR-INs
c) Separate example of voltage clamp responses in male OxtR-INs
d) Separate example of voltage clamp responses in female OxtR-INs
e) Quantification of maximum CrhIN – OxtR-IN PSC amplitudes between males and females (n=3)

2.3.2 CRHR1 expression in L2/3 pyramidal cells in mPFC

Given the established role of OxtR-INs in the modulation of L2/3 excitability **(Li et al., 2016)**, we next proceeded with determining if mPFC CrhINs modulate CRHR1 L2/3 pyramidal cells. We first confirmed scattered Crhr1 expression in a subset of mPFC L2/3 PCs via ISH in wildtype mPFC sections **(Figure 2.14)**.

Before measuring CrhIN modulation of mPFC L2/3 via both GABA and CRH production, we performed whole cell voltage clamp recordings from putative CRHR1 expression L2/3 pyramidal cells in wildtype mPFC **(Figure 2.15A)** and found that bath application of 1μM CRH enhances spontaneous EPSC frequency across all L2/3 cells recorded **(Figure 2.15B, C)**, although with a large degree of variability in terms of magnitude, onset, and duration. Previous studies have noted that CRH bath application can vary drastically by concentration **(Zemkova et al., 2016)**, obscuring the effect of endogenously released neuropeptides presumably released at the picomolar concentration.

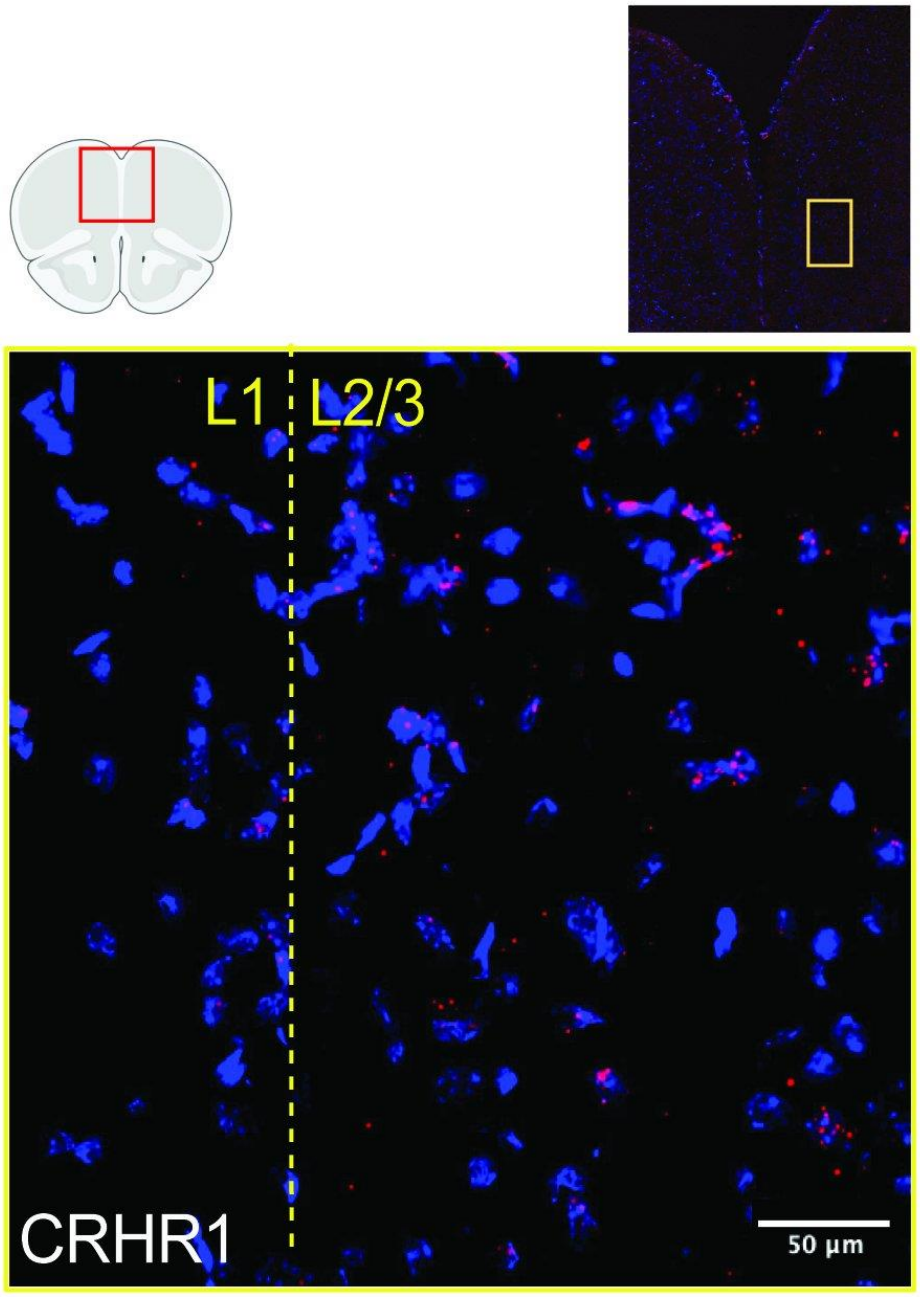

Figure 2.14. CRH receptor 1 mRNA in L2/3 pyramidal cells in wildtype mPFC sections

L2/3 cells in mPFC have the highest abundance of the CRH receptor CRHR1, visualized via an RNAscope probe targeting the CRHR1 gene in a wildtype mouse.

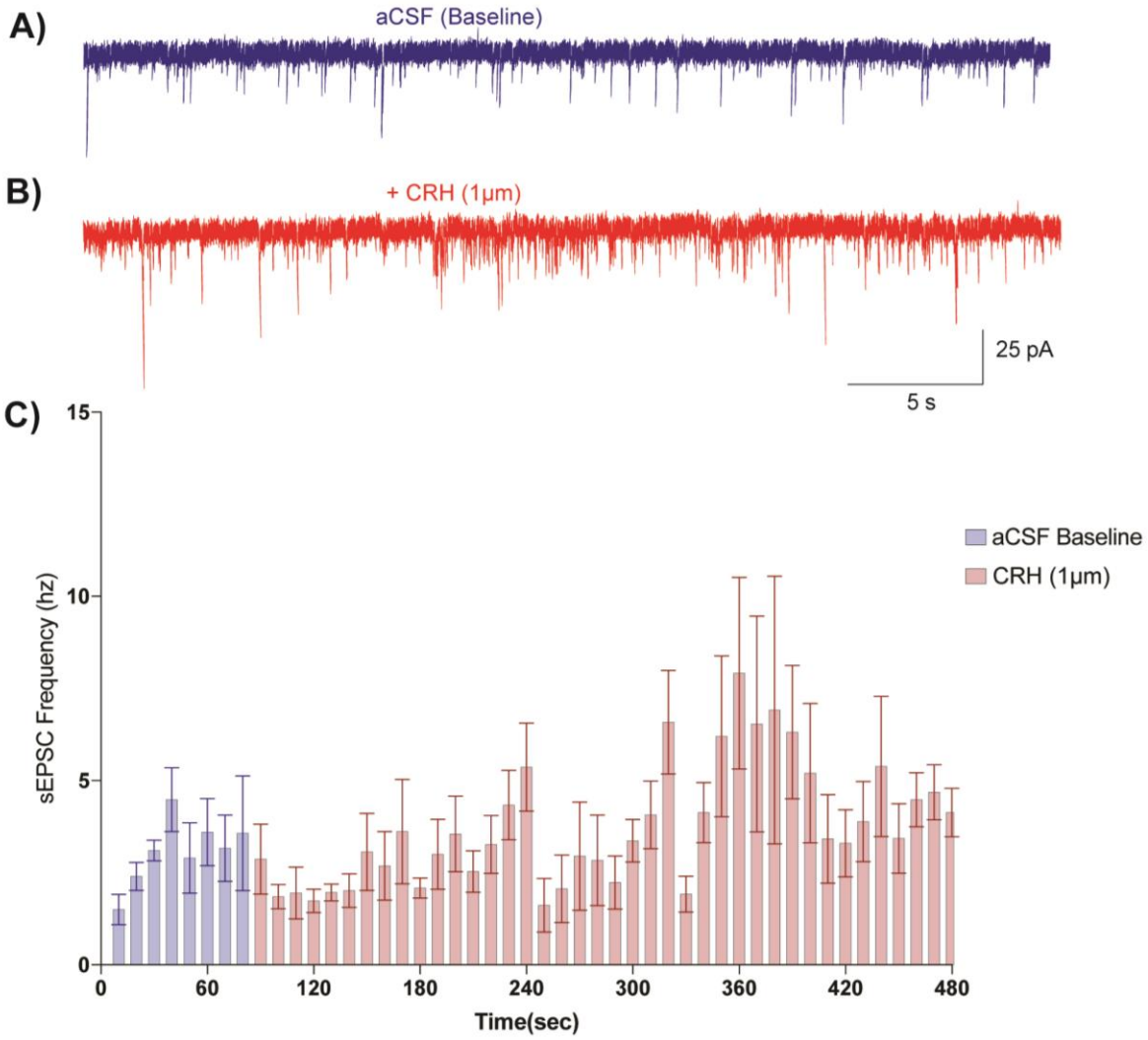

Figure 2.15. Whole cell voltage clamp recordings measuring spontaneous EPSCs in L2/3 before and after 1µM CRH bath application.

a) Whole cell voltage recordings of spontaneous EPSCs, recorded at -70mV, in L2/3 mPFC in aCSF in males
b) Pharmacological application of CRH produces a moderate increase in EPSC frequency in a subset of L2/3 pyramidal cells
c) Quantification of sEPSC in male L2/3 mPFC (n = 7) at 10 second bins for 8 minutes

2.3.3 CRH interneurons elicit GABAergic postsynaptic currents in L2/3 pyramidal cells

To analyze the extent to which CrhIN activation produces EPSC and IPSCs targeting mPFC L2/3 pyramidal cells, we performed whole cell voltage clamp recordings of L2/3 cells in CRH-IRES-CRE mice following stereotaxic injections of AAV2-DIO-ChR2-mCherry in mPFC **(Figure 2.16B)**. Given the stereotyped somatic morphology and clear laminar organization, we used DIC-based optics to identify L2/3 pyramidal cells in mPFC **(Figure 2.16A)**. We performed voltage clamp recordings in L2/3 by holding the membrane potential (Vh) at -70mV or 0mV, respectively. Measurements of PSC amplitudes in male **(Figure 2.17A, C)** and female mice **(Figure 2.17B, D)** demonstrate that L2/3 PSCs evoked by optogenetic activation of CrhINs were more pronounced in males than in females **(Figure 2.17E)**. We observed a L2/3 PSC response in 71% (13/21) of L2/3 cells recorded in male mice and in 66.6% (10/14) of L2/3 cells recorded in female mice.

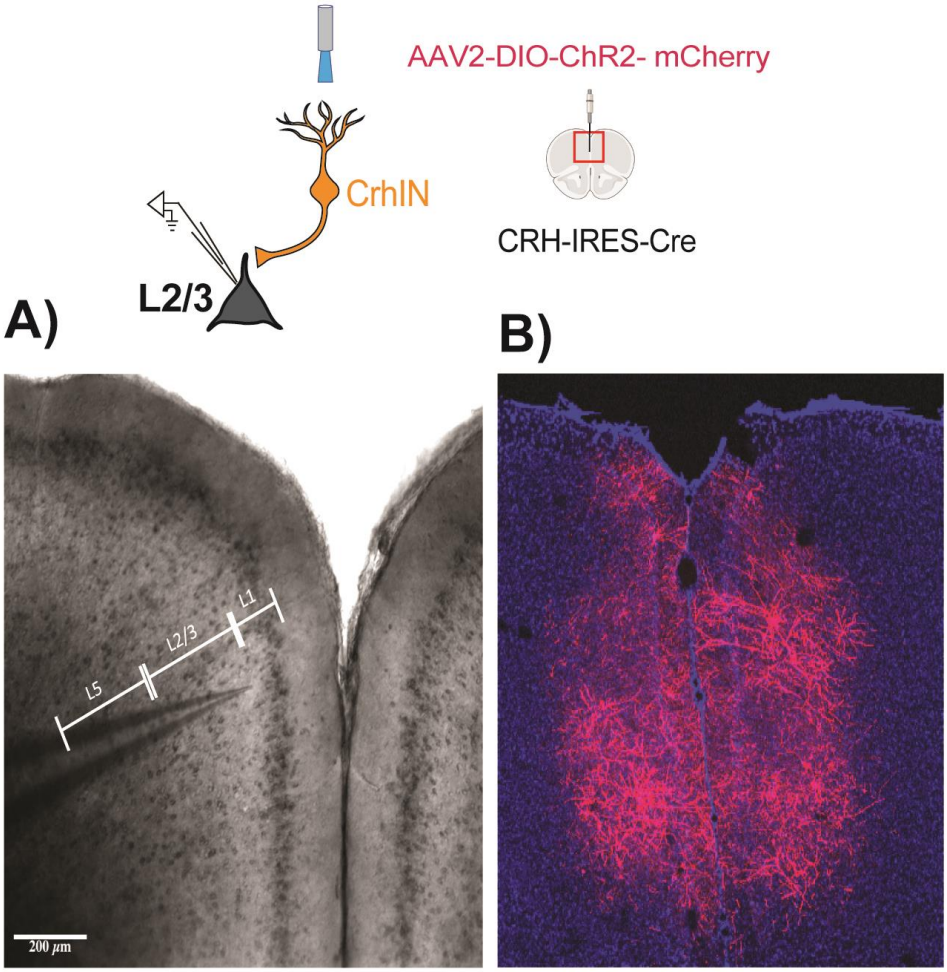

Figure 2.16. L2/3 pyramidal cells in electrophysiological mouse brain slices. Amplification of viral reporter for post hoc validation.

a) DIC-guided whole cell recordings targeting L2/3 mPFC pyramidal cells in CRH-IRES-Cre mice after stereotaxic injections targeting mPFC with Cre-dependent AAV virus encoding ChR2 (AAV2-DIO-ChR2-mCherry)
b) IHC validation of mPFC ChR2 expression in 400μm thick section post recording

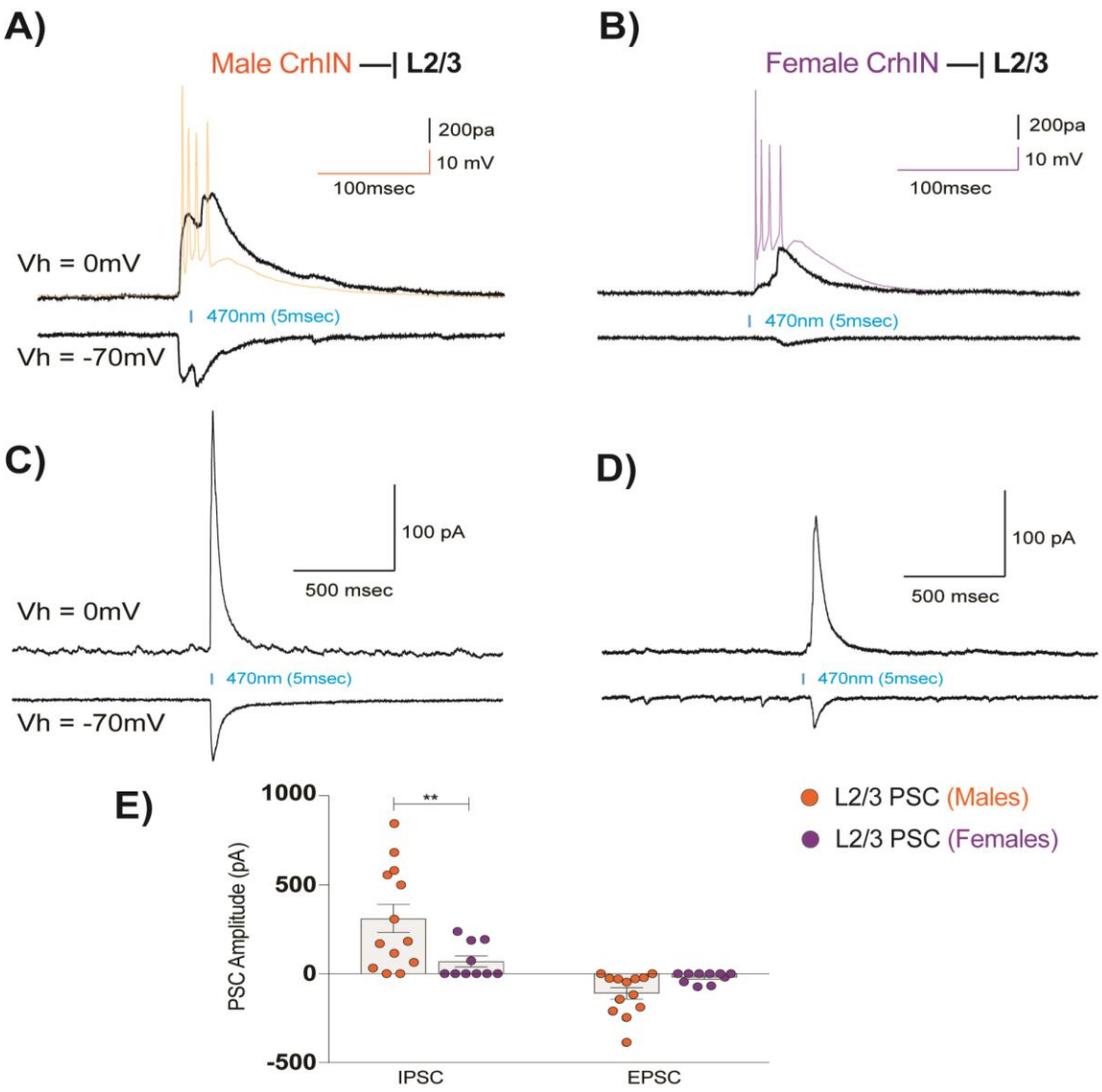

Figure 2.17. CrhIN postsynaptic currents targeting L2/3 pyramidal cells are larger in males than in females.

a) Whole cell voltage clamp recordings in male mPFC L2/3 pyramidal cells at -70mV and 0mV were used to isolate and measure CrhIN – L2/3 excitatory and inhibitory postsynaptic currents (PSCs). CrhIN APs, recorded in separate slices via current clamp, are overlaid onto L2/3 PSC traces (n = 21)
b) Whole cell voltage clamp recordings in female mPFC L2/3 pyramidal cells (n = 14)
c) Male L2/3 PSC recordings at larger time scales
d) Female L2/3 PSC recordings at larger time scales
e) Quantification of maximum L2/3 PSC amplitude reveals IPSCs are larger in males than in females

Given their complex waveform, we next clamped male L2/3 pyramidal cell membrane potentials from -70mV to +40mV in 10mV increments and delivered a single LED pulse to measure the evoked PSC reversal potential **(Figure 2.18A)**. This revealed that the evoked PSC reversal potential is near -50mV (trace in orange) **(Figure 2.18B, C)**, close to the reversal potential for GABAergic PSCs measured previously in cortical L2/3 PCs **(Szabadics et al., 2006)**.

To determine the relative contribution of $AMPA_R$ versus $GABA_A$ currents in L2/3 PSCs evoked by optogenetic activation of CrhINs, we delivered single LED pulses before and after bath application of the AMPA receptor antagonist cyanquixaline 6-cyano-7-nitroquinoxaline-2,3-dione (CNQX) **(Figure 2.19A)** or the $GABA_A$ receptor antagonist picrotoxin (PTX) **(Figure 2.19B)**. This revealed that CrhIN LED-induced L2/3 PSCs are largely CNQX-resistant and PTX-sensitive **(Figure 2.19C)**, indicating that they are mediated predominantly by $GABA_A$ receptors and consistent with their disinhibitory nature. Taken together, these results demonstrate that single LED pulse stimulation is sufficient to induce PTX-sensitive L2/3 PSCs from mPFC CrhINs. Strikingly, in a small subset of L2/3 pyramidal cells recorded in males, we observed that single LED pulse stimulation of mPFC CrhINs resulted in classic disinhibition of local excitatory neurons **(Figure 2.20)**, potentially a result of the direct inhibitory relationship between CrhINs and OxtR-INs. While exceedingly rare and occurring in just 4% of all male mPFC cells recorded (3/68), these results further validate the characterization of CrhINs as a disinhibitory population of VIP interneurons. Of interest, we observed no classical disinhibitory responses in 300μM thick slice preparations from mPFC, suggesting that an intact dendritic arborization may be essential for recording disinhibitory responses *in vitro*.

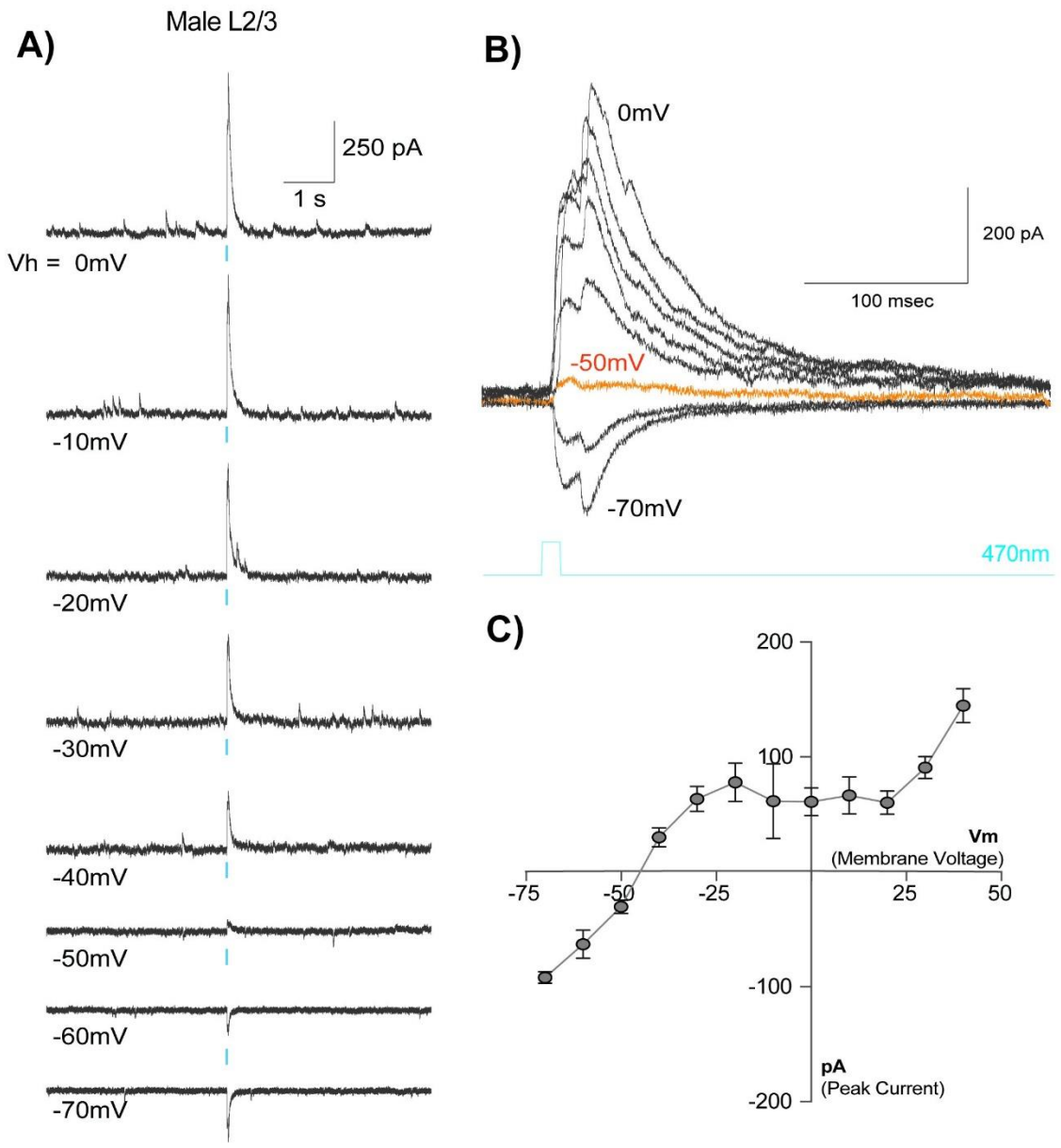

Figure 2.18. L2/3 PSC reversal potential suggests an inhibitory conductance.

a) Voltage clamp of L2/3 pyramidal cells across increasing membrane potentials (-70mV → 40mV, delta 10mV) reveal CrhIN – L2/3 PSCs reverse direction near -50mV
b) Ascending L2/3 voltage sweeps, overlayed
c) Quantification of CrhIN – L2/3 PSC reversal potential nearing -50mV (n = 12)

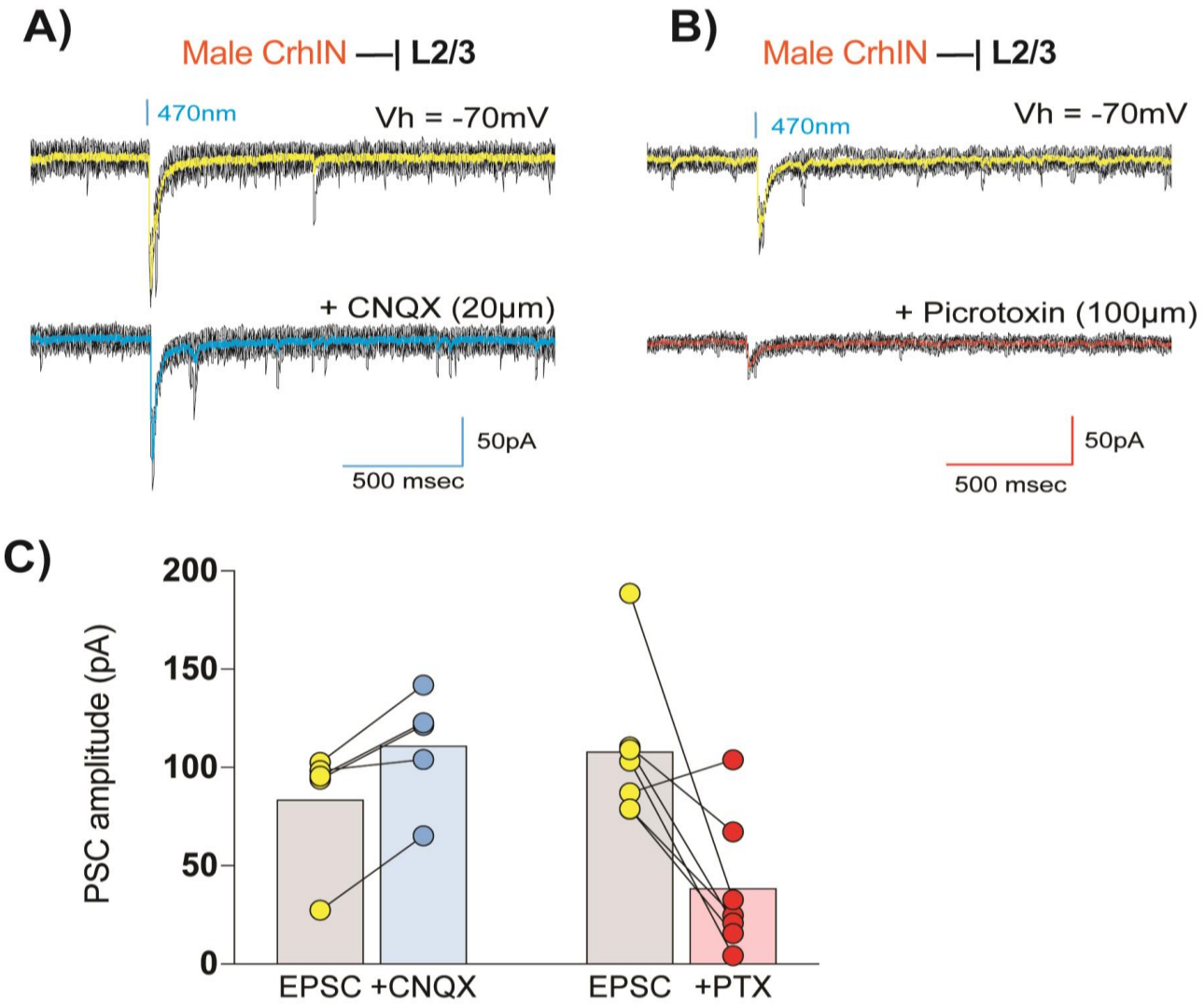

Figure 2.19. Pharmacological validation of L2/3 PSC GABAergic tone.

a) Bath application of AMPAr antagonist CNQX (20µM) did not block CrhIN – L2/3 PSCs
b) L2/3 PSCs can be blocked by 100µm picrotoxin bath application
c) Quantification of CrhIN – L2/3 PSCs before and after 20µm CNQX bath application (n = 4) or 100µm picrotoxin bath application (n=7)

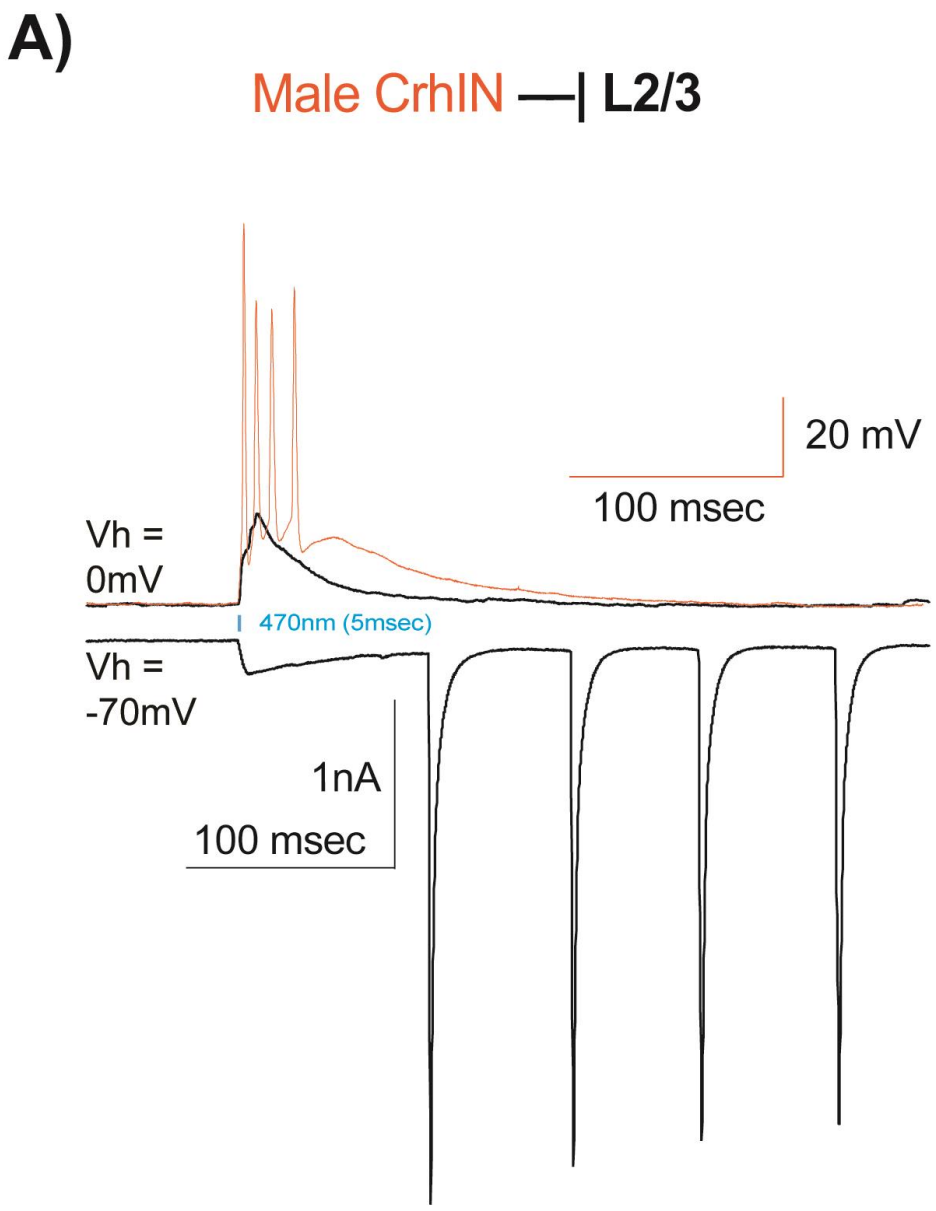

Figure 2.20. *In vitro* disinhibition of L2/3 pyramidal cells following CrhINs activation.

a) Disinhibitory responses observed in 4% of all male mPFC cells recorded (3/68) and occur approximately 100 msec following LED pulse stimulation of CrhINs

2.3.4 High frequency optogenetic stimulation evokes CRH neuropeptide release

Recent technical advancements have allowed for temporally precise control of neuropeptide signaling *in vitro* and therefore circumvent the limitations of pharmacology **(Figure 2,.15)**. High frequency (~20hz) optogenetic stimulation has been used to selectively evoke neuropeptide transmission in orexin neurons of the hypothalamus **(Schöne et al., 2014)**, whereas low frequency stimulation only evoked neurotransmitter release. We therefore set out to characterize the postsynaptic electrophysiological properties of mPFC CrhINs and selectively evoke the endogenous release of CRH and GABA using high and low frequency optogenetic stimulation combined with pharmacology.

Studies of dense core fusion and neuropeptide release have suggested that, in contrast to release of fast acting neurotransmitters **(Bargmann, 2012, Arrigoni et al., 2014)**, efficient release of neuropeptides requires high-frequency stimulation **(Muschol and Salzberg, 2000)**. We set out to confirm if high frequency optogenetic stimulation, sufficient for inducing neuropeptide transmission in orexin neurons of the hypothalamus **(Schöne et al., 2014)**, can elicit CRH release from CrhINs *in vitro*. To ensure that CrhINs expressing ChR2 in mPFC could fire at sustained high rates in response to high frequency LED stimulation, we first performed whole cell current clamp recordings from AAV2-DIO-ChR2-mCherry expressing neurons **(Figure 2.21A)**. These studies revealed robust firing in response to both 1hz **(Figure 2.21B**, orange trace**)** and 20hz **(Figure 2.21C,** orange trace**)** stimulation. Electrophysiological studies of the 5-HT_{3A}R expressing interneurons in mPFC have established that these neurons can fire at high frequency (>50hz) when stimulated with a 5-HT_{3A}R agonist **(Lee et al., 2010)**,

however, far less is understood regarding the postsynaptic L2/3 effects of high frequency 5-HT_{3A}R interneuron firing.

To address this, we used voltage clamp recordings from L2/3 PCs to measure PSCs elicited by optogenetic stimulation of CrhINs. Stimulation at 1 hz revealed time-locked PSCs that were variable in amplitude **(Figure 2.21D**, black trace**).** Following 60 seconds of recovery, we delivered 20hz stimulation for 20 seconds, which elicited a two-component PSC response in L2/3 PCs consisting of a sharp initial inward current followed by an intense train of PSCs **(Figure 2.21E**, black trace**)**. Approximately 38% of L2/3 PCs did not respond to 20hz stimulation.

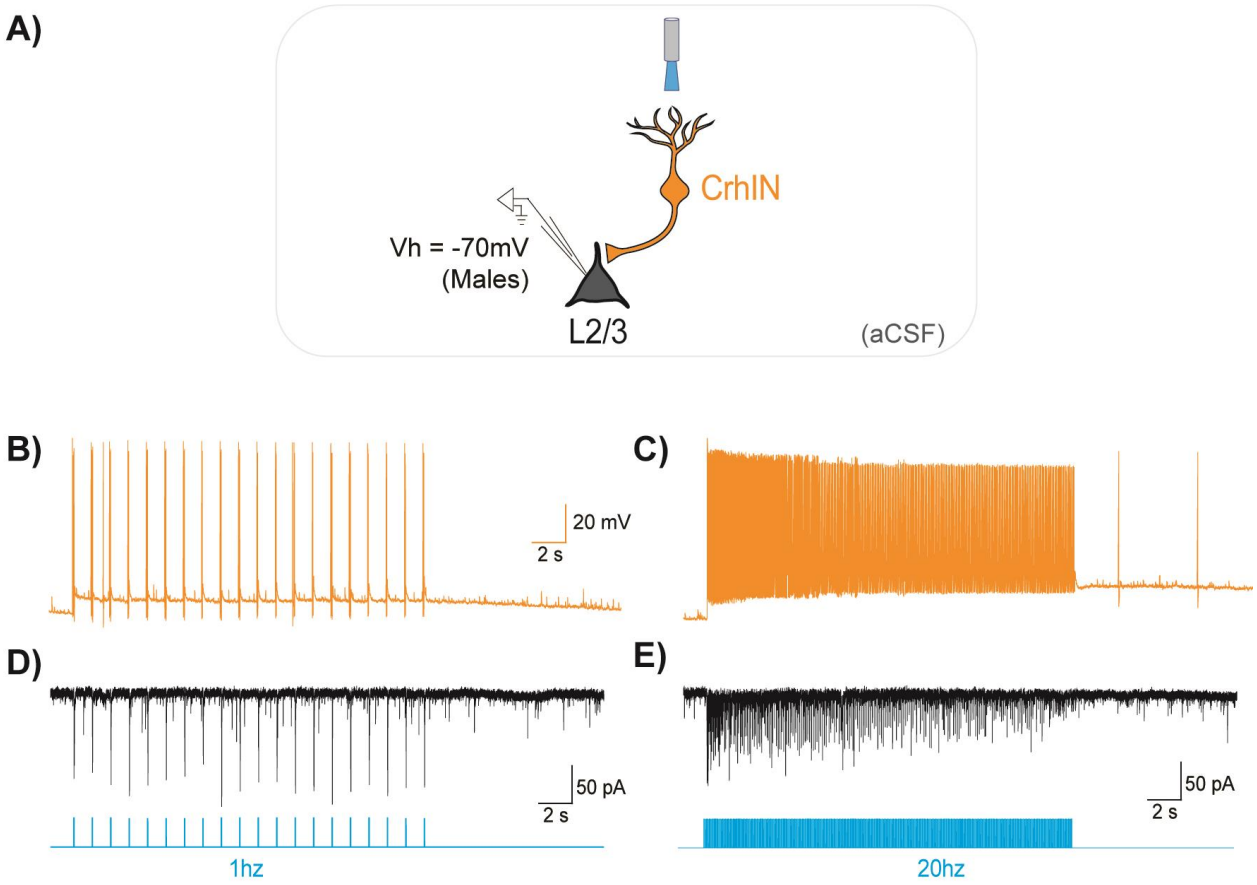

Figure 2.21. High frequency optogenetic stimulation of CrhINs. Whole cell voltage clamp recordings measuring evoked EPSCs in L2/3.

a) Whole cell current clamp recordings from mPFC CrhINs in CRH-IRES-Cre mice after stereotaxic injections targeting mPFC with Cre-dependent AAV virus encoding ChR2
b) CrhINs maintain stereotyped AP firing during 1hz LED stimulation, delivered for 20seconds, followed by 10seconds of recovery
c) mPFC CrhINs can maintain persistent fast firing during 20hz LED stimulation
d) Whole cell CrhIN – L2/3 PSC voltage clamp recordings at Vh-70mV during 20 seconds of 1 hz LED stimulation, followed by 10 seconds of recovery (n = 20)
e) A subset of mPFC L2/3 pyramidal cells display a strong initial inward current followed by a high frequency PSC train following 20hz LED stimulation

2.3.5 Pharmacological validation of frequency-dependent mPFC CRH release

To confirm that the observed two-component postsynaptic response upon high frequency stimulation is mediated through CRH release and CRHR1 signaling, we performed two types of control experiments using a selective CRHR1 antagonist or an inhibitor of GPCR signaling added to the intracellular voltage clamp solution. Pretreatment of cortical slices with the selective CRHR1 antagonist NBI 27914 HCl (5μm) **(Figure 2.22A)** did not affect CrhIN induced L2/3 PSCs at 1hz stimulation **(Figure 2.22B)**. In stark contrast, 20hz stimulation in the presence of the CRHR1 antagonist resulted in a sharp initial inward current but no longer elicited the dramatic increase in PSC frequency evident in its absence **(Figure 2.22C)**.

Since CRHR1 receptors are Class B G-protein coupled receptors (GPCRs) **(Inda et al., 2016)**, we next determined whether GDPβ-S, an inhibitor of GPCR transduction, would mimic effects of the CHRH1 antagonist bath application. GDPβ-S (5μm) was applied to the pipette solution in whole cell configuration to block GPCR signaling only in the recorded L2/3 PCs **(Figure 2.22D)**, thus preventing global disruption of GPCR signaling in the slice and potential network effects. Following dialysis of the pipette solution and intracellular milieu, we repeated 1hz and 20hz stimulation protocols. Although we observed a small effect of GDP-β-S on the initial inward peak, no major effect of GDP-β-S on EPSC responses to 1hz stimulation was evident **(Figure 2.22E)**. Again, and in stark contrast to 1hz PSC results, 20hz optogenetic stimulation no longer induced train of high frequency EPSCs **(Figure 2.22F)** following GDPβ-S dialysis.

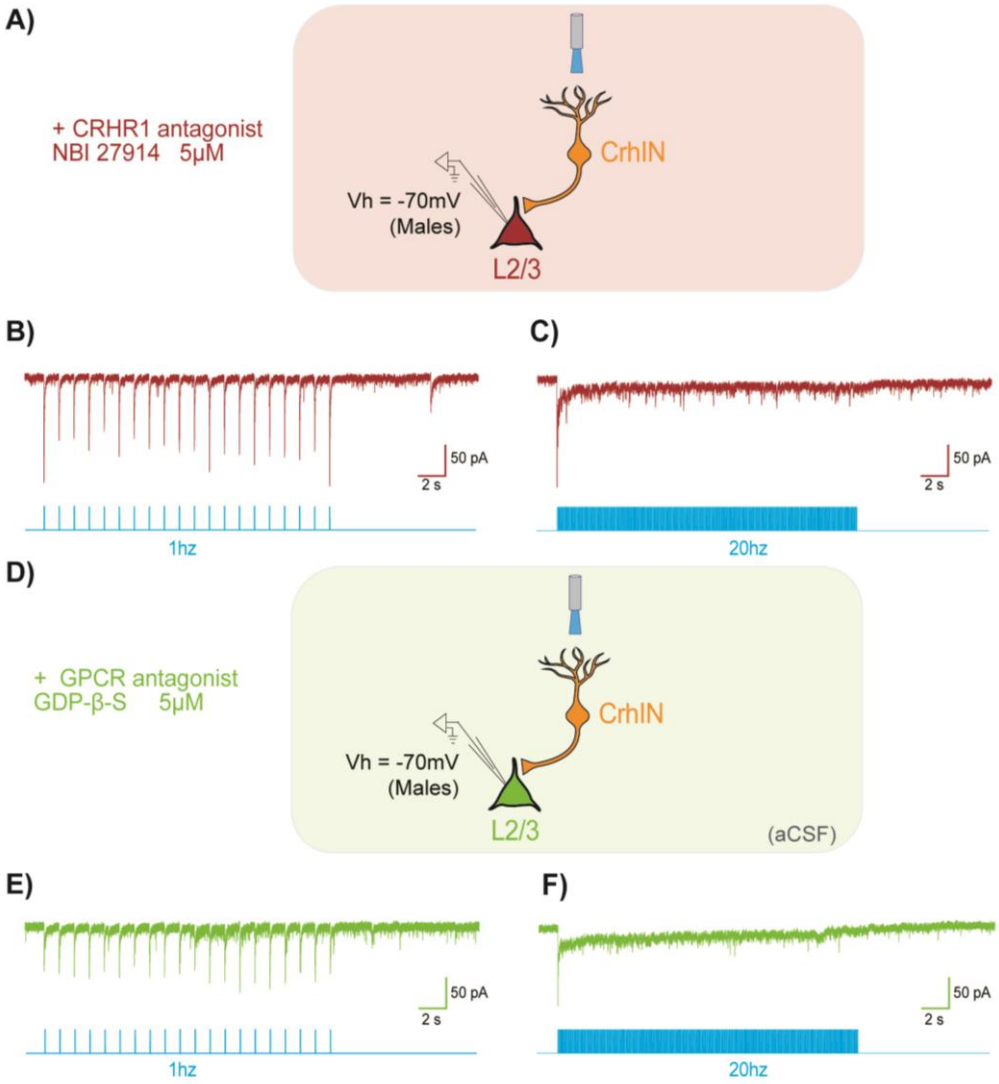

Figure 2.22. High frequency optogenetic stimulation can be blocked by GPCR subunit antagonist GDP-β-S and the CRHR1 antagonist.

a) Voltage clamp recordings from mPFC L2/3 pyramidal cells after 1 hour recovery in aCSF + CRHR1 antagonist NBI 27914 (5μM) (n = 18)
b) 1hz CrhIN – L2/3 PSCs are largely unaffected by CRHR1 blockade
c) 20hz CrhIN – L2/3 PSC response is noticeably altered by CRHR1 pre-treatment. The initial inward current remains while the following high frequency PSC train is blocked
d) Targeted single cell GPCR transduction blockade using 5μM GDP-β-S applied in the pipette solution following whole cell recording of mPFC L2/3 pyramidal cells in aCSF (n = 11)
e) 1hz CrhIN – L2/3 PSC is not affected following GPCR transduction blockade
f) Acute GPCR blockade via GDP-β-S mimics the effects of CRHR1 pre-treatment. 20hz CrhIN – L2/3 PSCs are blocked while the initial inward current is still pronounced

Quantification of these results revealed L2/3 PSC amplitudes evoked by CrhIN optogenetic activation **(Figure 2.23A)** did not vary significantly across 1hz and 20hz optogenetic stimulation, however CrhIN-L2/3 PSC frequency increased strongly between 1hz and 20hz in a 57% (16/23) of L2/3 pyramidal cells **(Figure 2.23B)**. We noted a statistically significant difference between L2/3 PSC frequency, not amplitude, across baseline, CRHR1, and GDPβ-S conditions, as determined via a one-way ANOVA ($F(5, 84) = 9.45$, $p < 0.0001$) (n= 2-6 mice per group). A Bonferroni post hoc multiple comparison test found a significant difference at baseline between 1hz and 20hz ($p = 0.0109$), 20hz baseline vs. 20hz CRHR1 antagonist ($p < 0.0001$), and 20hz baseline and 20hz GDPβ-S ($p = 0.0121$). We observed no difference ($p = 0.7078$) between 20hz CRHR1 antagonist treatment and 20hz GDPβ-S treatment.

These data clearly establish that, in contrast to the direct inhibition of OxtR-INs following a single optogenetic pulse, CRH release from CrhINs and its effects on postsynaptic L2/3 PCs require high frequency stimulation and intact GPCR subunit dissociation and downstream signaling. The striking similarity between 20hz stimulation after CRHR1 bath application or with GDPβ-S intracellular solution further demonstrate the validity behind using low and high frequency optogenetic stimulation and pharmacology to selectively evoke and measure CrhIN neurotransmitter (GABA) and neuropeptide (CRH) release. In this manner, 20hz stimulation induces a CRHR1, GPCR dependent effect in a subpopulation of L2/3 and likely reflects endogenous release of CRH from local ChR2 expressing CrhINs.

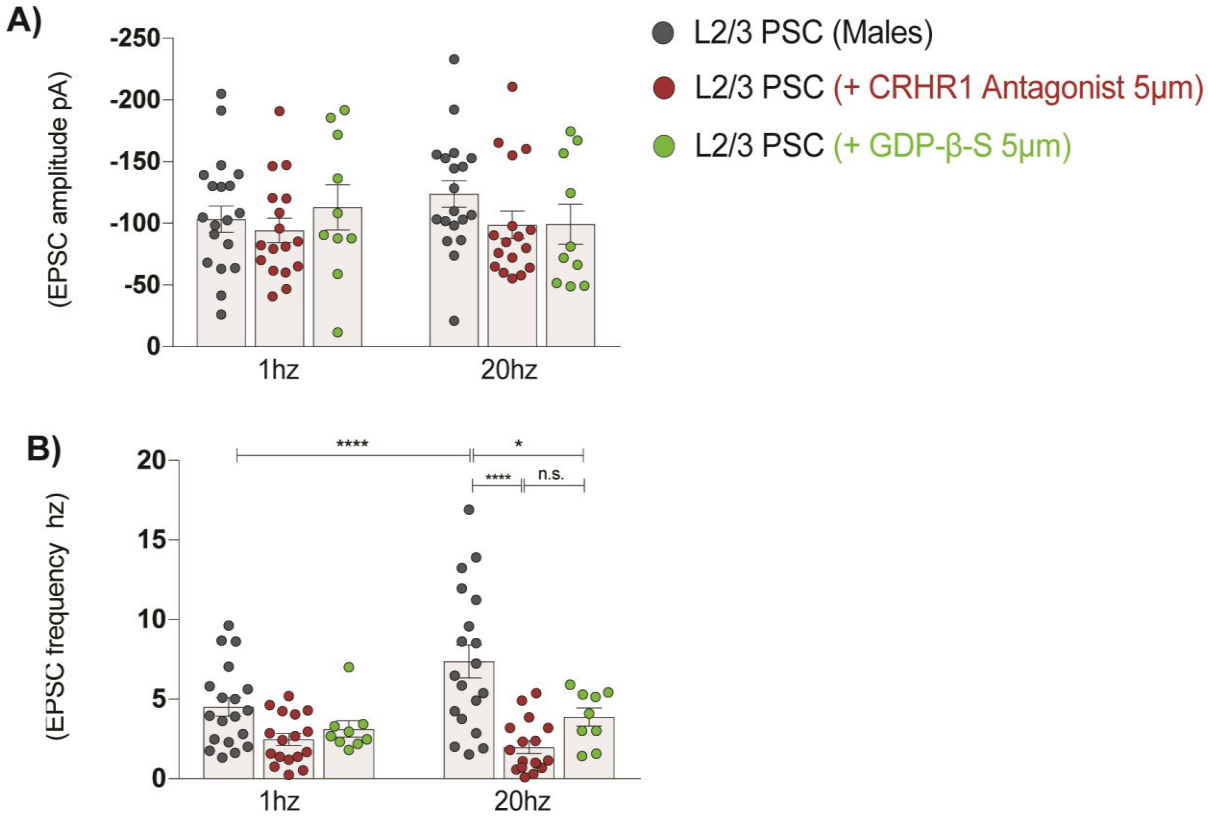

Figure 2.23. Quantification of high frequency optogenetic stimulation studies in male mPFC.

a) Quantification of CrhIN – L2/3 PSC amplitude does not reveal any significant differences across recording conditions
b) CrhIN – L2/3 PSC frequency is significantly increased between 1hz and 20hz LED stimulation. 1hz LED stimulation is not affected by CRHR1 pretreatment or acute GPCR blockade. At 20hz LED stimulation, the CRHR1 pre-treatment and acute GPCR blockade significantly reduce CrhIN – L2/3 PSC frequency

2.4 Behavioral influence of CRH interneurons in medial prefrontal cortex

A likely consequence of CrhIN inhibition of OxtR-INs and release of CRH may be the modulation of mPFC dependent behaviors. To determine the relative extent to which CrhINs affect classical anxiety-like behavior or object preference and sociability, we used two opposing approaches to manipulate mPFC CRH production and determine its behavioral impact.

Previous studies have demonstrated that specific deletion of CRH in the hypothalamus alters several approach/avoidance behaviors that indicate reduced anxiety **(Zhang et al., 2017)**. A more extensive deletion of *Crh* from all GABAergic neurons in cortex, hippocampus, central nucleus of the amygdala and bed nucleus of the striatum alters stress resilience and baseline social interactions **(Dedic et al., 2019)**. Since both studies employed intersectional targeting with transgenic mice that might express Cre-recombinase in early development, and since neither study reported gender specific behavioral alterations suggested by the modulatory function of CrhIN – OxtR-IN signaling in mPFC circuitry, we next examined the effects of *Crh* deletion and CrhIN activation in the adult mPFC. Before proceeding, we first quantified total CRH-IRES-CRE cell counts in mPFC between males **(Figure 2.24A)** and females **(Figure 2.24B)** and found no differences in the number of immunoreactive cells between males and females **(Figure 2.23C).**

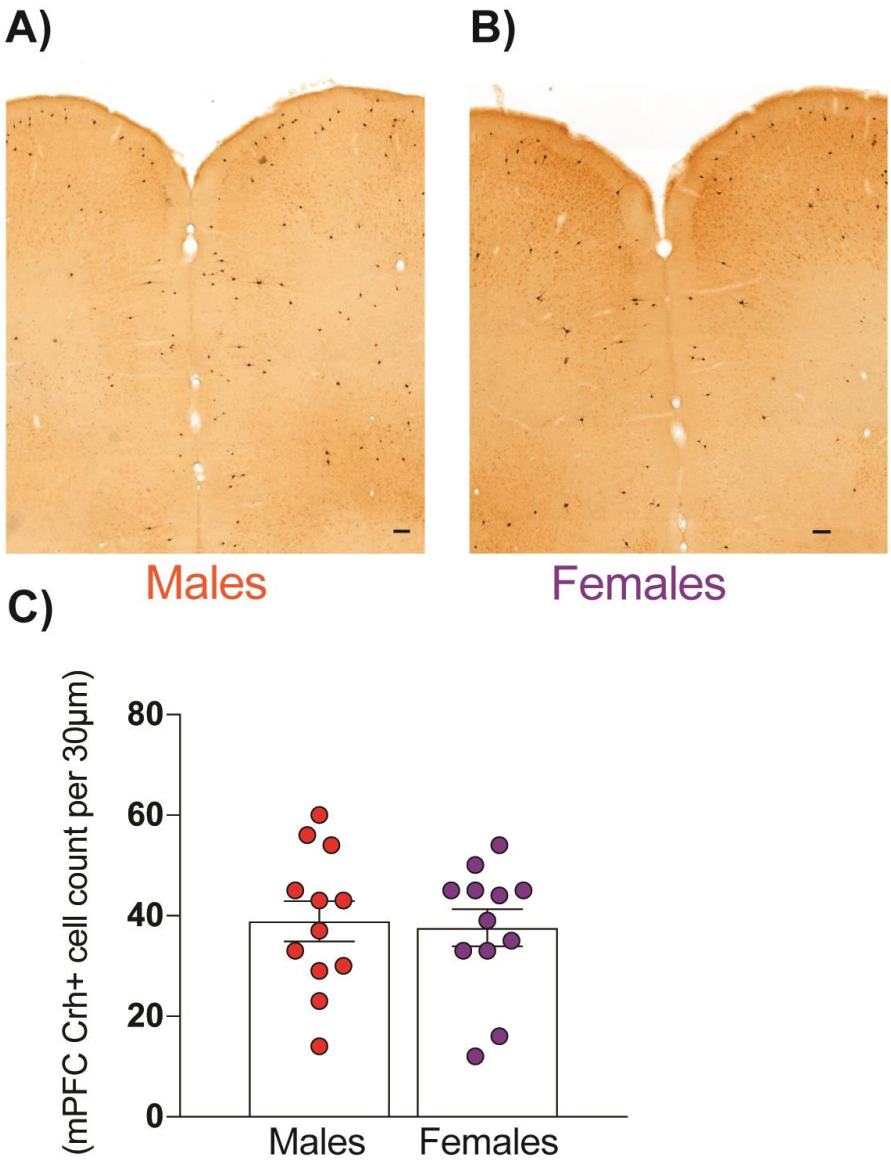

Figure 2.24. CRH interneuron cell counts, as measured via DAB immunolabeling for EYFP in mPFC sections from male and female Crh-EGFP-L10a mice.

a) Total mPFC cell CRH cell counts in male CRH-IRES-Cre x Rosa26-LSL-eGFP-L10a mice
b) As compared to males, total mPFC cell CRH cell counts in females did not differ significantly, as evidenced by DAB immunostaining against eGFP
c) Quantification of mPFC CRH-Cre cells between males and females

2.4.1 Validation of transgenic approaches for behavioral testing

Stereotactic injections of either AAV-CMV-eGFP **(Figure 2.25A)** control virus or AAV-CMV-Cre-GFP **(Figure 2.25B)** into mPFC of Crh-FLOX mice **(Zhang et al., 2017)** were first analyzed by ISH to assess the efficiency of *Crh* deletion in mPFC. Relative to motor cortex **(Figure 2.25B,** *middle***)** and piriform cortex **(Figure 2.25B,** *right***)**, the majority of *Crh* expression restricted to mPFC was lost in mice injected with AAV-CMV-Cre/eGFP **(Figure 2.25B,** *left***)**, relative to mice injected with the AAV-CMV-eGFP control virus **(Figure 2.25A)**.

We next performed intraperitoneal injections of the selective hM3Dq ligand Clozapine N-oxide (CNO) (2mg/kg) in CRH-IRES-CRE mice following stereotaxic injections of AAV2-DIO-hM3Dq-mCherry in mPFC **(Figure 2.26A)**. We observed that upon CNO injection, hM3dq-mCherry labeled neurons showed increased colocalization with c-fos **(Figure 2.26B)** as well as a robust increase in the number of c-fos positive neurons, indicating that chemogenetic activation of CrhINs increases neuronal activity of CrhINs in both male and female CrhINs.

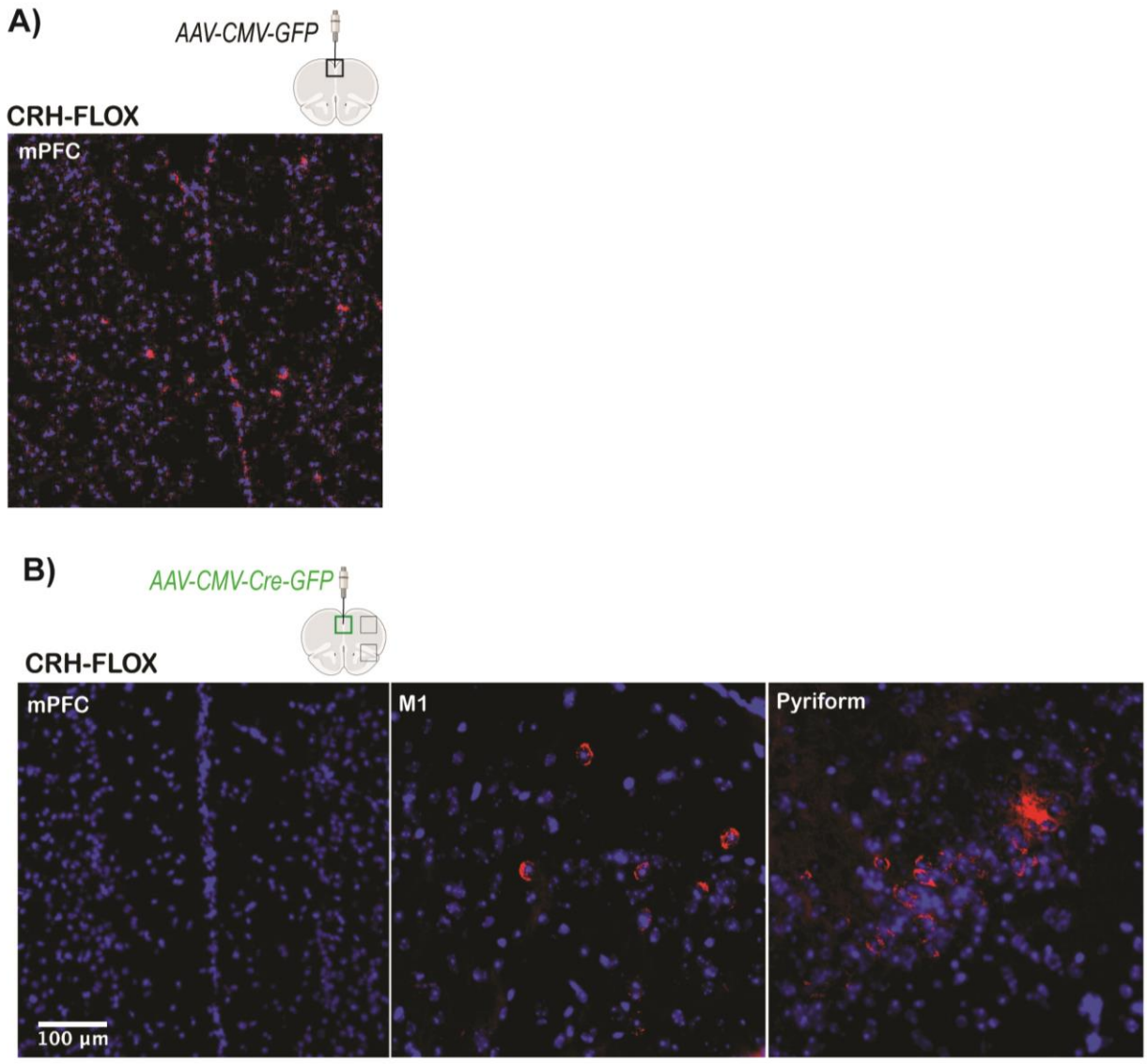

Figure 2.25. Scattered mRNA labeling for *CRH* in mPFC is absent after CRE-mediated excision of CRH.

a) ISH for CRH mRNA confirms that stereotaxic injection of CMV-GFP in mPFC of *Crh-FLOX* mice does not affect mPFC CRH mRNA expression
b) CMV-CRE/GFP stereotaxic injection in *Crh-FLOX* mice selectively excised mPFC CRH while maintaining robust CRH expression in noninjected areas, notably M1 and piriform cortex

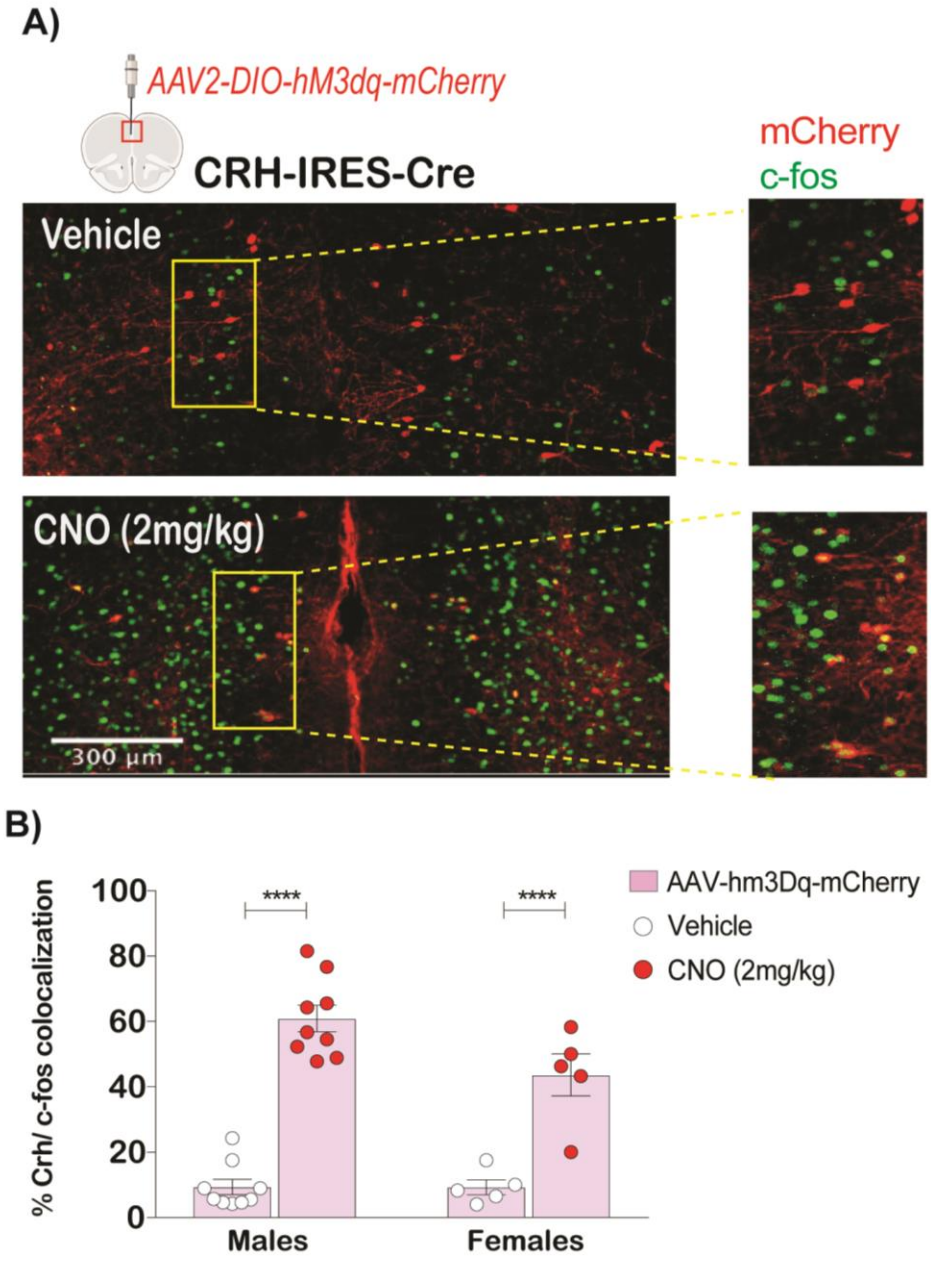

Figure 2.26. Chemogenetic activation of mPFC CrhINs in male and female Crh-hM3Dq mice, as measured via IHC labeling for c-fos induction.

a) A chemogenetic approach using stereotactic delivery of AAV-DIO-hM3Dq in CRH-IRES-Cre mice, was coupled with intraperitoneal injections of the selective hM3 ligand Clozapine N-oxide (CNO), and was used to increase mPFC CrhIN activity
b) Quantification of c-fos/hM3dq-mCherry colocalization in *Crh-hM3Dq* mice injected with CNO (2mg/kg), as compared to vehicle, in both and females, indicating DREADDs are equally efficacious

2.4.2 mPFC CRH interneurons do not influence approach avoidance behaviors

To evaluate whether loss of CRH production in the mPFC of *Crh-FLOX mice* or CrhIN activation with chemogenetics, in adult mice could impact behavior, we performed a series of behavioral tests to assess alterations in social and stress-related behaviors. Surprisingly, we observed that mPFC knockdown of CRH in either male or female *Crh-FLOX* mice did not alter behavioral responses across a battery of approach/avoidance tests, including the elevated plus maze **(Figure 2.27A, B)**, open field test **(Figure 2.27C, D)**, and light/dark box **(Figure 2.27E, F)**. Consistent with the fact that mPFC CRH signaling had no effect in these paradigms, we observed that chemogenetic activation of CrhINs had no effect in the elevated plus maze **(Figure 2.28A, B)**, open field test **(Figure 2.28C, D)**, and light/dark box **(Figure 2.28E, F).** We did note potential anxiolytic effects of CNO in female mice injected with control virus **(Figure 2.28B, D)**, however these effects were absent from hM3Dq experimental mice and may be due to the relatively high CNO dosage used or potentially due to a sexually dimorphic interaction resulting from non-selective CNO receptor binding in the absence of hM3Dq.

We next assayed for novelty preference in both *Crh-FLOX* and *Crh-hM3Dq* mice using the novel object interaction behavioral paradigm. Regardless of object identity or object location, mPFC deletion of CRH in males did induce a significant increase in novel and not familiar object preference **(Figure 2.29A)**. Consistent with the sexual dimorphism detected in the electrophysiological characterization of CrhINs across postsynaptic recordings with OxtR-INs **(Figure 2.12)** and L2/3 pyramidal cells **(Figure 2.17)**, we observed no robust changes in preference for novelty in female *Crh-FLOX* **(Figure 2.29B)**.

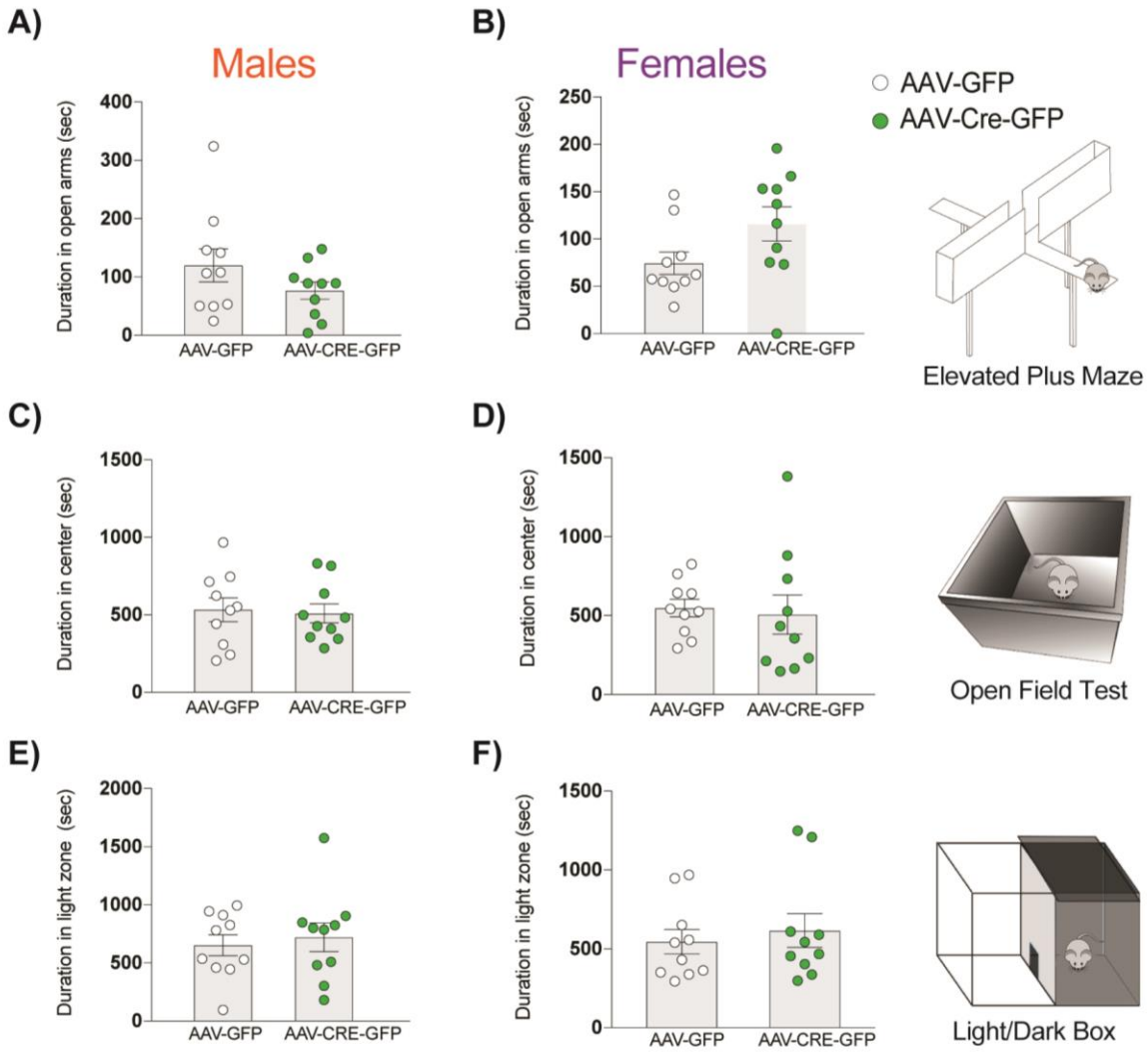

Figure 2.27. mPFC CRH knockdown in both adult male and female mice does not affect approach avoidance paradigms.

a) mPFC CRH knockdown in male *Crh-FLOX* mice has no effect on open arm exploration
b) Knockdown of mPFC CRH has no effect on open arm exploration in the elevated plus maze in females
c) mPFC CRH knockdown in male *Crh-FLOX* mice has no effect on open field test center exploration
d) Knockdown of mPFC CRH mice has no effect on open field test center exploration in in females
e) mPFC CRH knockdown in male *Crh-FLOX* mice has no effect on light/dark box latency
f) Knockdown of mPFC CRH mice has no effect on light/dark box latency in females

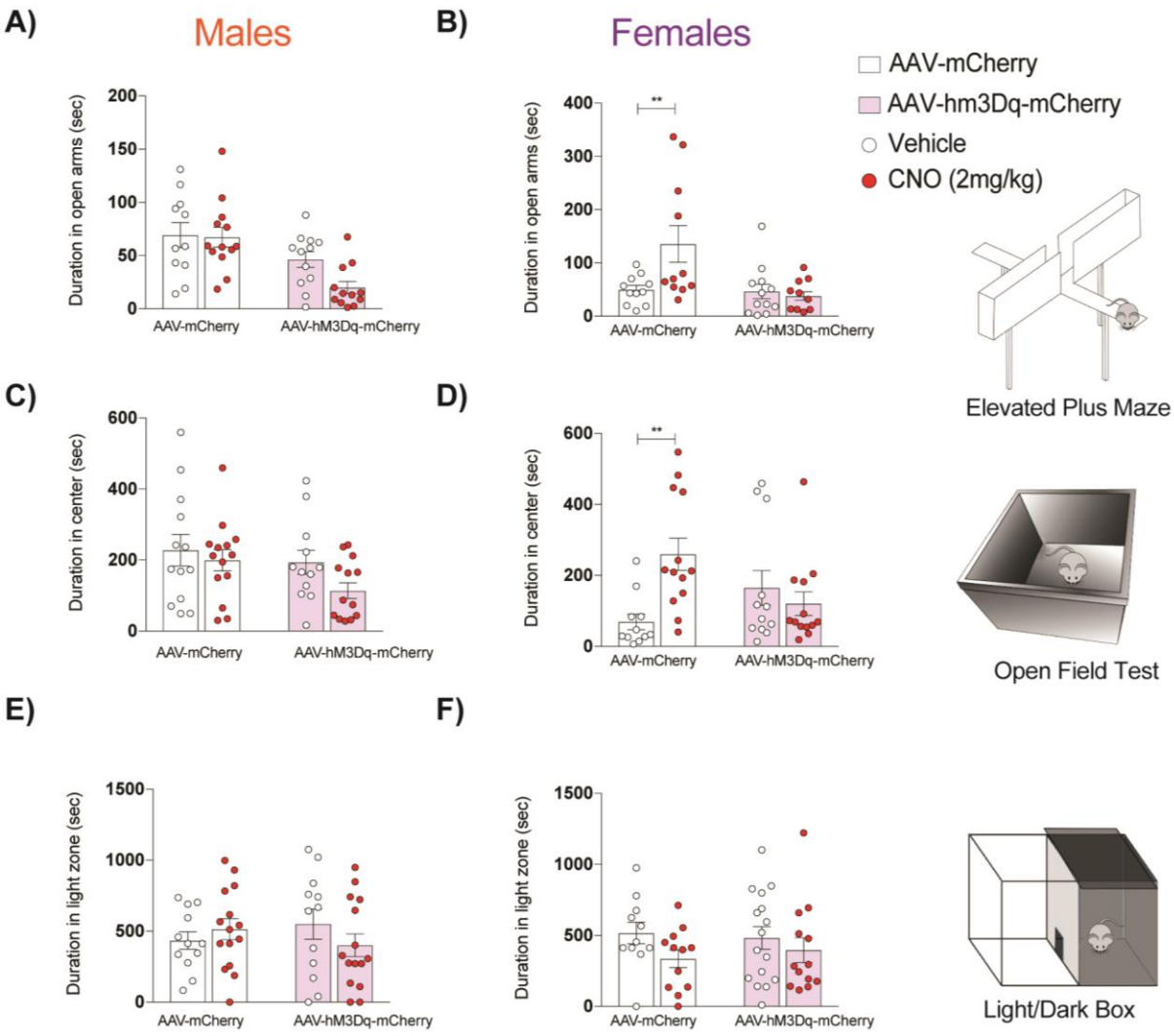

Figure 2.28. Activation of CrhINs via DREADDs in both males and females does not affect approach avoidance anxiety.

a) Activation of mPFC CrhINs in male *Crh-hM3Dq* mice via C.N.O. I.P. injection (2mg/kg) has no effect on open arm exploration
b) No observed effect on open arm exploration in elevated plus maze in female *Crh-hM3Dq* mice. CNO I.P. injection increases exploration in control females
c) Activation of mPFC CrhINs in male *Crh-hM3Dq* mice has no effect on open field test center exploration
d) No significant changes in center exploration in open field test in female *Crh-hM3Dq* mice. CNO I.P. injection increases exploration in control females
e) Activation of mPFC CrhINs in male *Crh-hM3Dq* mice has no effect on light/dark box latency
f) No significant changes in latency behavior in light/dark box in female *Crh-hM3Dq* mice

2.4.3 CRH interneurons influence preference for novelty and sociability in males

Quantification of results revealed a statistically significant difference between novel object interaction duration in male Crh-FLOX mice injected with AAV-CMV-Cre/eGFP, as determined via a one-way ANOVA ($F(3, 36) = 4.849$, $p = 0.0062$). A Bonferroni post hoc multiple comparison test found a significant difference between novel, not familiar, object interaction ($p =- 0.0070$) (n= 10 mice per group).

In parallel with these results, male Crh-hM3Dq mice treated with CNO displayed a reduction in novel **(Figure 2.30B)**, but not familiar **(Figure 2.30A)**, object interaction time. Quantification revealed a statistically significant difference for novel object interaction duration between Crh-hM3Dq mice injected with CNO when compared to vehicle, as determined via a one-way ANOVA ($F(3, 50) = 4.605$, $p = 0.0064$). A Bonferroni post hoc multiple comparison test found a significant difference between novel, not familiar, object interaction ($p =- 0. 0.0303$) (n= 12 - 15 mice per group). Again, consistent with the sexual dimorphisms revealed thus far, we again observed no significant changes in female *Crh-hM3Dq* mice treated with CNO in both familiar **(Figure 2.30C)** and novel **(Figure 2.30D)** object interaction time. These results delineate a role for cortical CRH production from that of classical approach avoidance behaviors, known to be influenced by hypothalamic CRH **(Zhang et al., 2017)**.

As novelty seeking behavior is closely associated with sociability **(Moy et al., 2004)**, we next assayed both *Crh-FLOX* and *Crh-hM3Dq* mice in the 3-chamber sociability test, which allows for unrestricted interaction with a Lego or conspecific mouse of the opposite sex, housed in a wire cup.

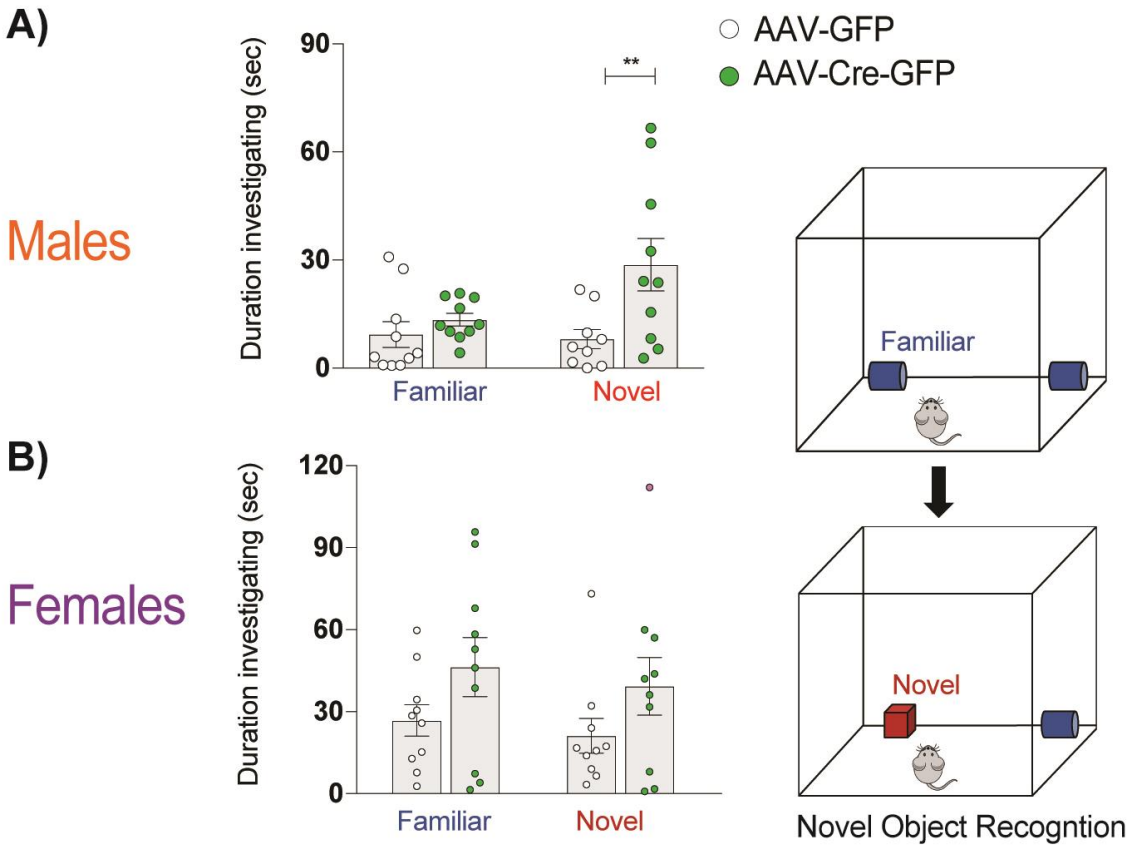

Figure 2.29. mPFC CRH excision increased preference for novel and not familiar objects.

a) Crh-FLOX increased novel object interaction in males, not females. Male mice displayed a significant increase in novel object interaction time, again regardless of object identity or location
b) No effect of Crh-FLOX in female object novelty preference

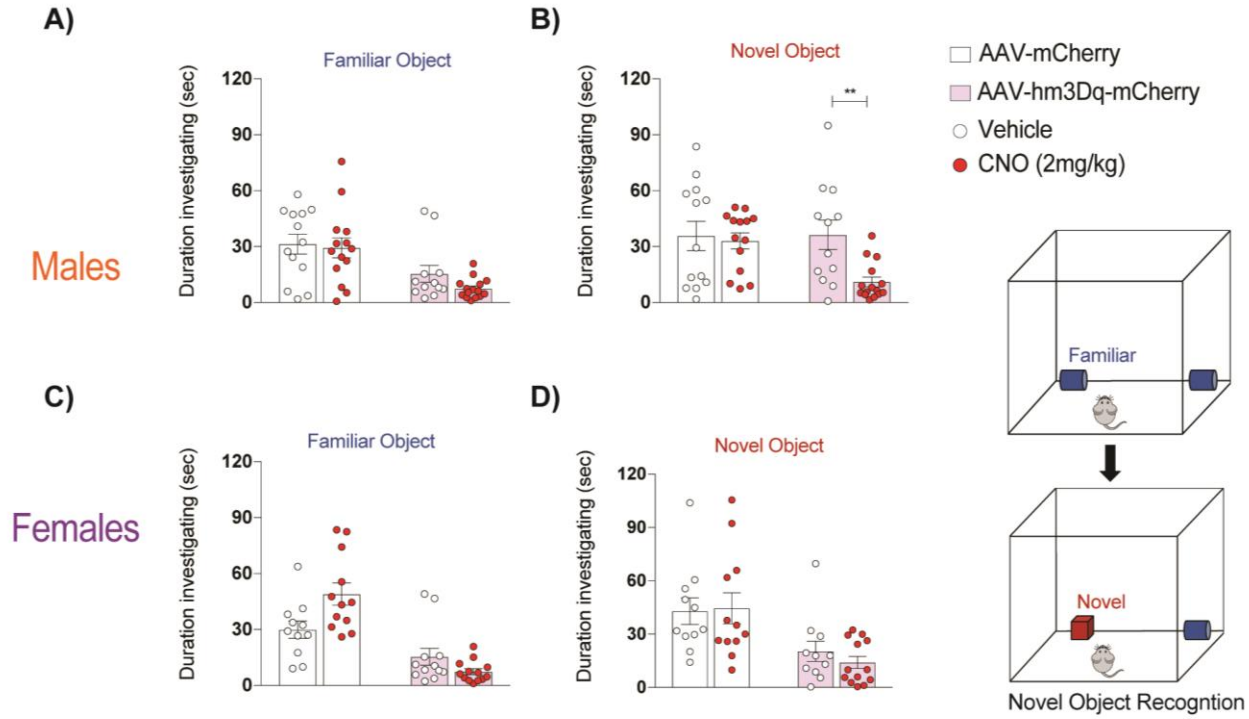

Figure 2.30. mPFC CrhIN activation reduces preference for novel objects in males.

a) In male *Crh-hM3Dq* mice treated with CNO, novel object interaction time was reduced with no effect on familiar object interaction. Again, male mice displayed a significant reduction in novel object interaction regardless of object identity or location
b) No effect of *Crh-hM3Dq* in female object novelty preference

When assayed for its impact on sociability, mPFC deletion of *Crh* via AAV-CMV-Cre/eGFP induced a significant increase in male *Crh-FLOX* sociability with novel females **(Figure 2.31A)** and we again observed no significant changes in sociability behaviors in female *Crh-FLOX* mice **(Figure 2.31B)**. Quantification revealed a statistically significant difference for male to female interaction time between Crh-FLOX male mice injected with AAV-CMV-Cre/eGFP as compared to AAV-CMV-eGFP injected mice, determined via a one-way ANOVA ($F(3, 36) = 14.26$, $p < 0.0001$). A Bonferroni post hoc multiple comparison test found a significant difference between female interaction time (p =- 0. 0.0359) (n= 10 mice per group).

We next tested *Crh-hM3Dq* mice using the 3-chamber sociability test. Male *Crh-hM3Dq* mice treated with CNO spent less time interacting with the female mouse **(Figure 2.31C)**, and in agreement with all findings thus far, we observed no significant changes in sociability behaviors in female *Crh-hM3Dq* mice **(Figure 2.31D)**. Quantification revealed a statistically significant difference for male to female interaction duration between male Crh-hM3Dq mice injected with CNO when compared to vehicle, determined via a one-way ANOVA ($F(3, 42) = 3.57$, $p = 0.0218$). A Bonferroni post hoc multiple comparison test found a significant difference in male to female interaction time between CNO and vehicle injected male Crh-hM3Dq mice ($p = 0.0104$) (n= 10-14 mice per group). Example heatmap traces for both novel object interaction test **(Figure 2.32A)** and 3-chamber sociability test **(Figure 2.32B)** visualize the extent to which preference is altered across *Crh-FLOX* and *Crh-hM3Dq* conditions.

The results indicate that, in contrast to its proven role in hypothalamic control of stress- and anxiety-related behaviors **(Zhang et al., 2017)**, CRH production in mPFC

interneurons modulates male but not female sociosexual and novelty seeking behavior. Taken together, these data establish that the behavioral states regulated by local production of CRH in mPFC are distinct from those governed by its release from afferent fibers originating in the hypothalamus. Ultimately, these findings contribute to our growing understanding of molecularly distinct cell types and their respective impacts on the sexually dimorphic and opposing nature that is well established between OXT and CRH signaling. In addition, in cases where neuromodulators are expressed both in distal sites that project to the cerebral cortex and in local interneurons, it was not known whether the source of production contributes differentially to function. The results address this and demonstrate a functionally divergent role for mPFC CRH production, as compared to that of the well understood PVN.

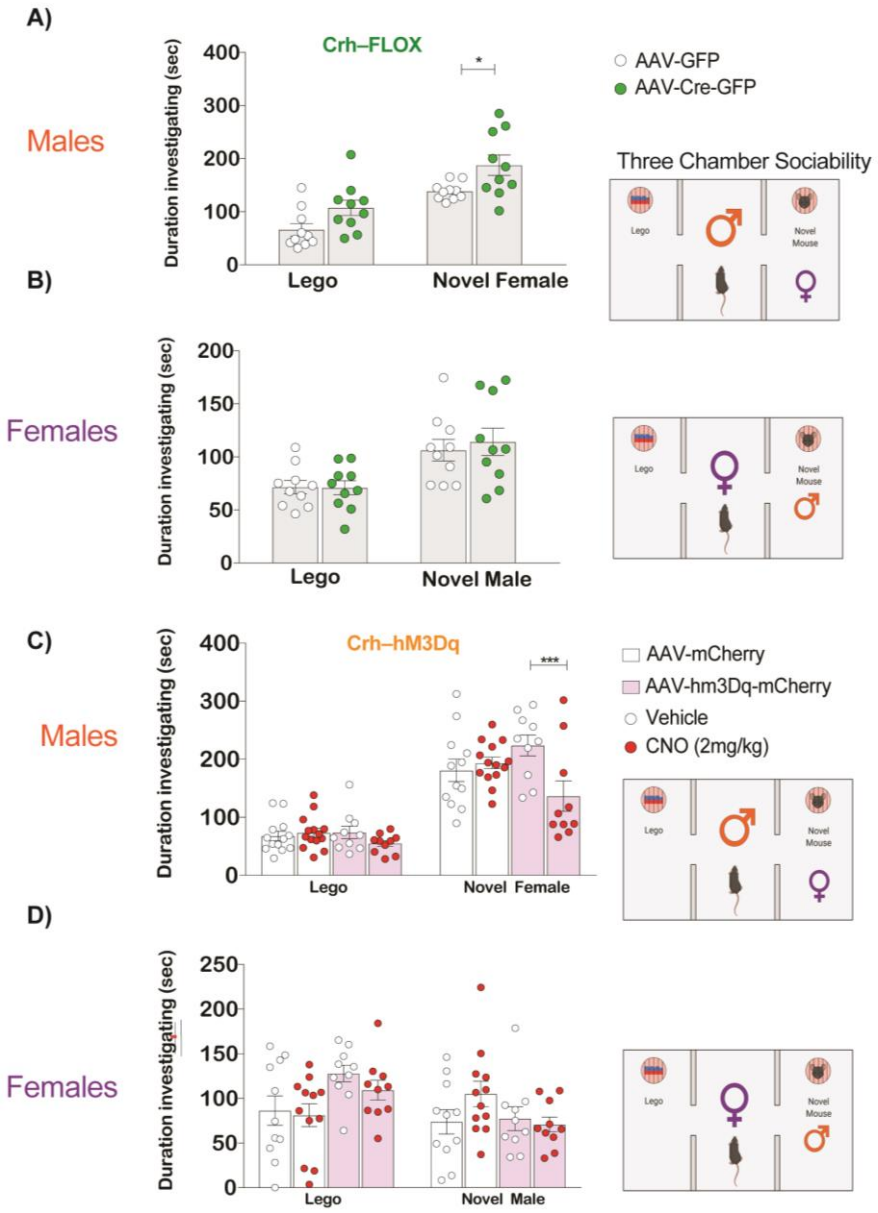

Figure 2.31. mPFC CRH excision and mPFC CrhIN activation affects sociability in males and not females.

a) Knockdown of PFC CRH in male Crh-FLOX increased interaction duration with novel female mice
b) No effect of Crh-FLOX in female sociability with novel male mice
c) Activation of mPFC CrhINs in male *Crh-hM3Dq* mice via CNO increased interaction duration with novel female mice
d) CNO treatment did not noticeably affect female *Crh-hM3Dq* interaction with novel male mice

Figure 2.32. Body tracking for novel object recognition and 3-chamber sociability behavioral paradigms.

a) Exploration heatmap visualized 10 minutes of cumulative interaction time in the novel object interaction test across *Crh-FLOX* and *Crh-hM3Dq* conditions
b) Exploration heatmap visualized 10 minutes of cumulative interaction time in the 3-chamber sociability test across *Crh-FLOX* and *Crh-hM3Dq* conditions

A)

Novel Object Recognition (Males)

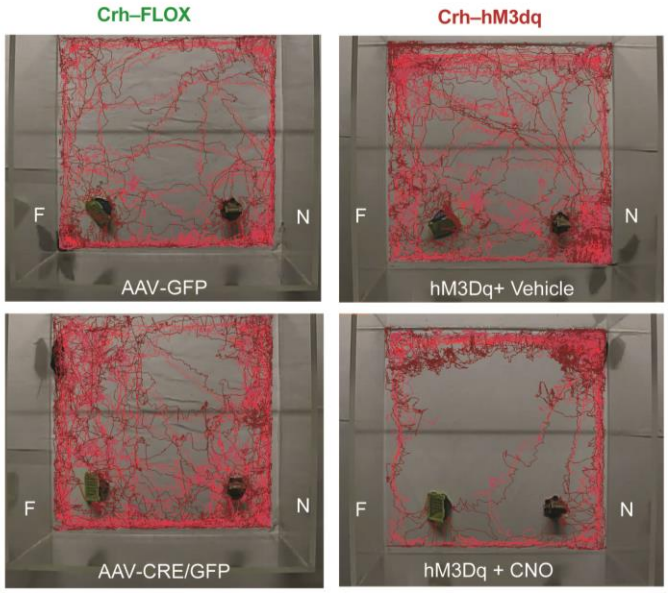

B)

Three Chamber Sociability (Males)

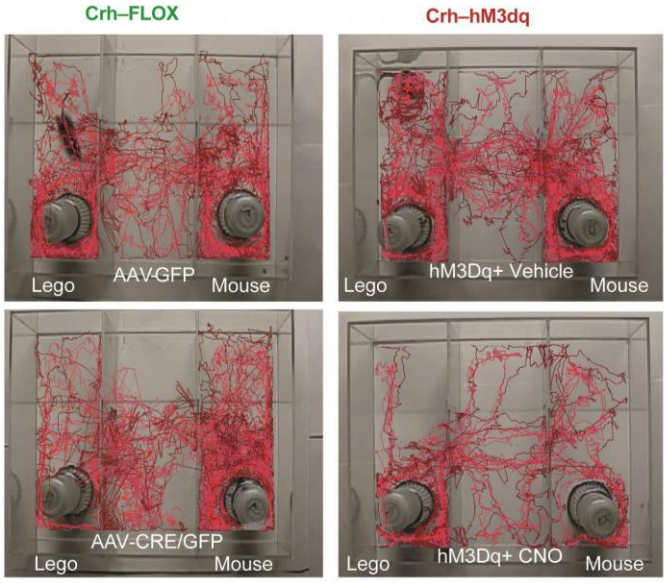

CHAPTER 3. Discussion and Future Directions

3.1 Discussion

The pursuit of cell type functional studies is intended to improve our understanding of the brain activity patterns underlying advanced cognitive functions. Information processing in the cerebral cortex is dependent on a wide variety of interneuron cell types that gate signal flow and modulate local circuitry **(Barbas, 2015, Tremblay et al., 2016)**. Cortical interneurons often express specific neuropeptides, hormones, and other neuromodulatory substances in addition to fast acting neurotransmitters **(Granger et al., 2016)**. Regulation of neuronal activity in response to neurotransmitters, neuropeptides, and other neuromodulators is centrally important for normal function of the nervous system in all species **(Marder and Bucher, 2007, Bargman, 2012)**. Genes required for both the synthesis of these factors and for their reception are amongst the most diverse and cell type-restricted in the central nervous system **(Zeisel et al., 2018)**.

Transcriptional and epigenetic profiling of cell types in both mouse **(Tasic et al., 2018)** and human brains **(Luo et al., 2017)** has refined our understanding of the histological complexity of the cerebral cortex first documented more than a century ago **(Cajal et al., 1888)**. Although a consensus definition of cell type has not clearly emerged from these data, it has been demonstrated that the cortex is composed of scores of molecularly distinct cell classes with different electrophysiological properties. Expression of optogenetic **(Tsai et al., 2009)** and chemogenetic tools **(Armbruster et al., 2007)** in

select cell types has begun to reveal the consequences of their activation or silencing on behavior. In some cases, a connection between the molecular properties specific to cell classes, their electrophysiological properties, and their contributions to behavior has been deciphered **(Carter et al., 2013)**.

Genes required for neuropeptide synthesis and reception are expressed in the cerebral cortex, or in afferent neurons that communicate directly with the cortex from distal sites. For example, oxytocin (OXT) neurons of the hypothalamus project extensively throughout the brain with neuromodulatory-releasing afferents to activate its receptor, oxytocin receptor (OxtR). We have previously shown that OXT acts on OxtR expressing interneurons (OxtR-INs) in the mPFC to regulate sexually dimorphic behaviors and modulate local circuit function. In female mice, specifically during estrus, OXT activation of OxtR-INs enhances female interactions with male mice **(Nakajima et al., 2014)**. Surprisingly, OxtR-INs are highly enriched with corticotropin-releasing hormone binding protein (CRHBP**) (Li et al., 2016)**, the endogenous antagonist to corticotropin-releasing hormone (CRH). In CRH receptor (CRHR1) expressing mPFC L2/3 cells, pharmacological application of CRH enhances excitability and can be blocked by optogenetic activation of OxtR-INs **(Li et al., 2016)**, presumably through CRHBP release.

The production and release of CRHBP by OxtR-INs furthers our understanding of the already well-established opposing behavioral roles of OXT and CRH **(Gobrogge & Wang., 2015)**. And although the main site of CRH production is also the hypothalamus, in contrast to OXT, CRH is also expressed by small populations of neurons in other brain structures including the cerebral cortex **(Uribe-Mariño et al., 2016, Peng et al., 2017)**. In this case, and in many others in which a neuropeptide or neuromodulator can be

produced both locally within the cortex and in afferent projections to cortex, the circuit mechanisms impacted by its release and their consequences for cortical function may depend critically on its source. Release of the corticotropin-releasing hormone (CRH) from a specific class of medial prefrontal cortex (mPFC) interneurons (CrhINs) requires high frequency stimulation, and local CRH production acts to enhance cell excitability of CRH receptor (CRHR1) expressing cortical L2/3 pyramidal neurons. GABA release by low frequency stimulation of CrhINs suppresses the inhibitory effects of OxtR-Ins, which should result in disinhibition of L2/3 pyramidal cells.

Conditional deletion of CRH in the mPFC or chemogenetic activation of CrhINs alters sexually dimorphic social behaviors but does not affect anxiety-related behaviors, and our data establish the importance of local CRH release for modulation of mPFC circuits from that of the well-established PVN. We demonstrate that CrhIN regulation of local circuit function involves both classical disinhibition of L2/3 pyramidal cells mediated (at least in part) through direct GABA dependent inhibition of OxtR-INs, and that high frequency stimulation of CrhINs results in increased excitability of CRHR1 expressing L2/3 pyramidal cells.

These findings indicate that an understanding of local circuit modulation by a specific interneuron class in the cerebral cortex must incorporate knowledge of the concerted actions of multiple, functionally distinct, cell autonomous molecular mechanisms, that it must include delineation of reciprocal interactions with other defined interneuron types as well as pyramidal cell targets, and that it must consider the possibility that local release of a specific neuropeptide or neuromodulator may have roles distinct from those of the same substance released into the cortex from distal sites.

Using optogenetics, pharmacology and molecular profiling results, we have demonstrated that mPFC CrhINs modulate CRHR1-expressing L2/3 pyramidal cells and OxtR-IN activity through frequency-dependent release of GABA and CRH. In totality, the molecular, electrophysiological, and behavioral results collected here suggest that future studies delineating the distinct roles of local production of neuropeptides across brain regions will enhance our understanding of cell type interactions and their role in driving neural activity and complex sensory and cognitive behaviors.

Ultimately, these data reveal a sophisticated and multi-molecular circuit **(Figure 3.1)** whereby a net excitatory effect of CrhIN activation on L2/3 pyramidal cells can be achieved through CrhINs inhibition of OxtR-INs **(Figure 2.12, 2.13)** and their release of CRHBP and GABAergic inhibition of L2/3 pyramidal cells, through classical disinhibitory responses **(Figure 2.20**), and finally, through CRH release following high frequency CrhIN AP firing **(Figure 2.21, 2.22, 2.23)**.

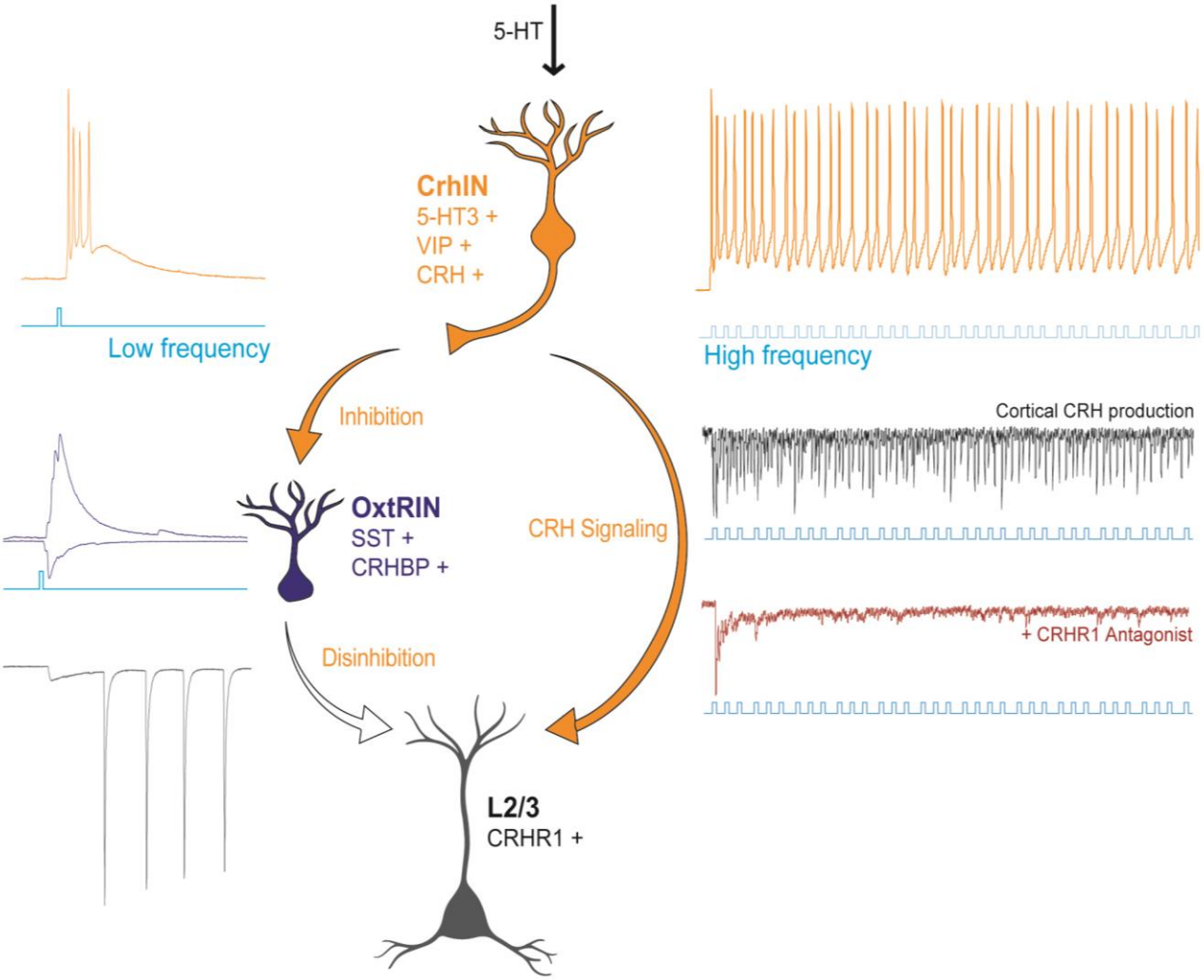

Figure 3.1. Cortical microcircuit schematic for mPFC CrhINs.

Model of cortical microcircuits for CrhIN modulation of mPFC OxtR-INs and L2/3 CRHR1 pyramidal cells. Low frequency optogenetic activation evokes release of GABA and produces robust IPSCs targeting OxtR-INs, releasing their inhibition of L2/3 pyramidal cells, resulting in disinhibition. High frequency stimulation presumably increases presynaptic cytosolic Ca^{2+} to a sufficient level to facilitate dense core vesicle fusion and CRH release, resulting in a GPCR and CRHR1-dependent high frequency train of postsynaptic currents in L2/3 pyramidal cells.

CrhINs are cortical interneurons that exert disinhibitory control

It has been previously demonstrated that release of the CRH antagonist CRHBP from OxtR-INs in the mPFC modulates anxiety-related behaviors in male mice **(Li et al., 2016)**. This is consistent with studies demonstrating that CRH release from the hypothalamus modulates these same approach avoidance behaviors **(Zhang et al., 2017)**. However, CRH is also produced locally in small numbers of cells in the cerebral cortex and other brain structures **(Peng et al., 2017)**, raising the interesting possibility that local release of CRH may have functions distinct from those controlled by the hypothalamus.

Here, we employed molecular profiling **(Figure 2.3, 2.4)**, immunohistochemistry, **(Figure 2.5)** and *in situ* hybridization **(Figure 2.6)** to identify CRH producing cells in the mPFC **(Figure 2.1)** as a small population of VIP/5-HT_{3A}R expressing interneurons (CrhINs) that arborize extensively within the mPFC **(Figure 2.8)**. CrhINs are equally abundant in the mPFC of male and female mice **(Figure 2.24)**, and they display the expected intrinsic properties of the VIP/5-HT_{3A}R class of interneurons, including high input resistance and robust and repetitive burst firing in response to depolarizing current injection **(Figure 2.9, 2.10, Table 2.5).**

It has been demonstrated that VIP interneurons target SST and PVALB interneurons **(Letzkus et al., 2011, Pfeffer et al., 2013)**, blocking inhibition of pyramidal cells, and thereby resulting in strong pyramidal cell excitation **(Lee et al., 2013)**. While we did observe an electrophysiological signature consistent with disinhibition *in vitro* **(Figure 2.20)**, further validation should employ a dual synaptic blocker strategy to confirm if these responses are CNQX-sensitive, i.e., mediated by glutamate, or PTX-sensitive, i.e.,

mediated by GABA. Should the latter prove inaccurate, these recordings may not reflect disinhibition *in vitro* and may instead result from other molecular signaling cascades influenced by CrhIN activation and OxtrIN inhibition.

A distinctive function for local production of CRH in the mPFC

CRH neurons in the hypothalamus project to several brain structures, including cerebral cortex **(Figure 2.2.)**, brainstem and raphe nuclei **(Geerling et al., 2010)**, nucleus of the solitary tract **(Wang et al., 2019**), and the lateral hypothalamus **(Füzesi et al., 2016)**, to name a few. Deletion or loss of CRH production from hypothalamic neurons leads to a strong anxiolytic phenotype, as demonstrated by alterations of a number of approach avoidance behaviors in male mice **(Zhang et al., 2017)**. Production of CRHBP by OxtR-INs in the mPFC blocks the CRH-induced potentiation of postsynaptic L2/3 pyramidal cell activity of male, but not female, mice, also producing an anxiolytic effect **(Li et al., 2016)**.

We demonstrate, however, that deletion of CRH from the mPFC has no impact on anxiety-like behaviors assessed by these same tests: elevated plus maze, open field test, and light/dark box. Rather, male mice in which *Crh* has been deleted from the mPFC of *Crh-FLOX* mice using AAV-CMV-Cre/eGFP display increased interest in novel, not familiar, objects and novel, conspecific female mice.

Consistent with this finding, chemogenetic stimulation of CrhIN cells in the mPFC results in a strong reduction in male exploration of novel female mice **(Figure 2.31)** and novel object interaction duration. No change in behavior was evident in female mice in response to either of these manipulations. The finding that local production of CRH in the

mPFC modulates different behaviors than that of release of CRHBP within the mPFC by OxtR-INs **(Li et al., 2016)**, or by hypothalamic CRH release into the cortex **(Zhang et al., 2017)** is surprising and interesting. When taken together, however, these results can be understood as complementary mechanisms for optimizing the impact of CRH production locally within the mPFC. Thus, CrhINs employ several different pathways to activate L2/3 pyramidal cells.

First, consistent with their identification as VIP/5-HT_{3A}R expressing interneurons **(Figure 2.3, 2.4, 2.5, 2.6)** CrhINs participate in classical disinhibition by releasing GABA onto other interneurons to suppress their inhibitory effects on local excitatory neurons.

Second, they directly inhibit OxtR-IN activation **(Figure 2.12, 2.13)** suppressing release of the CRH antagonist CRHBP. Since we have shown previously that activation of OxtR-INs results in release of sufficient CRHBP to block L2/3 pyramidal cell responses to exogenously added CRH and that blocking CRHBP production in OxtR-INs results in increases in anxiety-like behaviors in males **(Li et al., 2016)**, we believe this mechanism is most likely to be important for inhibiting the effects of hypothalamic release of CRH into the mPFC.

Third, CrhINs synthesize and release CRH within the mPFC which acts directly on CRHR1 expressing L2/3 pyramidal cells to enhance their excitability in male mice **(Figure 2.21, 2.22, 2.23)**. The net result of these three different mechanisms upon activation of CrhINs is to decrease specifically male novelty seeking behavior and social interactions with female mice.

Conditions for CRH release from CrhINs differ from those required for GABA

As we have shown, both GABA mediated disinhibition of L2/3 pyramidal cells by CrhINs and inhibition of OxtR-INs by CrhINs **(Figure 2.12, 2.13)** can occur in response to single LED pulses. However, to observe the dramatic increases in CRHR1 dependent PSCs in L2/3 pyramidal cells in response to CrhIN activation requires high frequency stimulation **(Figure 2.21, 2.22, 2.23)**. The requirement for high frequency stimulation to elicit L2/3 pyramidal cell responses to local production of CRH in the mPFC cortex is interesting given the identification of CrhINs as a subpopulation of the broad class of 5-HT_{3A}R expressing cortical interneurons.

5-HT_{3A}R is the only ionotropic serotonin receptor **(Table 1.2)** and when activated by its neurotransmitter 5-hydroxytryptamine (5-HT; serotonin) causes fast, depolarizing responses **(Derkach et al., 1989)**. It has been demonstrated directly that all 5-HT_{3A}R expressing interneurons can fire at high frequency in response to the 5-HT_{3A}R agonist mCPBG **(Lee et al., 2010)** and that CRH neurons receive direct monosynaptic inputs from raphe serotoninergic neurons **(Zhang et al., 2019)**.

5–HT release in mPFC, which presumably activates the broad majority of 5–HT receptors, although to varying extent, enhances anxiety-like behavior **(Meloni et al., 2008)** and freezing responses **(Marcinkiewcz et al., 2016)**. Thus, it seems likely that stimulation of a subset of these afferents may be important for activation of CrhINs. However, given the dispersion of serotonergic fibers in the cortex and the many 5-HT receptors expressed in cortical neurons, further studies will be required to delineate the conditions for CrhIN modulation of male social behavior in response to 5-HT.

Sexually dimorphic modulation of social and emotional behaviors

The results we have presented here add three additional elements to our knowledge of the molecular mechanisms regulating local circuit function in the mPFC and their contributions to gender specific social behaviors. A first principle established here is that local and remote control of mPFC circuitry by the same neuropeptide or neuromodulator can have different effects on complex, gender-specific social behaviors. This raises the possibility that the conditions for local release within the cortex differ from those required for release from afferents within the same structure. We have argued above, for example, that one likely mechanism controlling activation of CrhINs and local release of CRH is stimulation of the 5-HT_{3A}R by a subset of serotonergic fibers in the mPFC. Thus, while serotonergic innervation of CRH expressing neurons in the PVN has been documented **(Liposits et al., 1987)**, no expression of the ligand-gated type of serotonin receptor known to govern high frequency firing in response to serotonin is observed in the PVN. This may indicate that the "closed loop" between serotonin and CRF release that exists in the cerebral cortex but not in the hypothalamus is responsible for local release of CRF due to high frequency stimulation induced during a challenging situation (Chen et al., 2020).

A second concept revealed by these data is that the interplay between specific interneuron classes involves several mechanisms that control their reciprocal interactions and the consequent behaviors. Although we have previously demonstrated that OXT stimulation of OxtR-INs in the prefrontal cortex releases an antagonist to CRH in the mPFC (CRHBP), this mechanism is most likely to impact the CRH released from the PVN since both of these events modulate anxiety-related behaviors **(Li et al., 2016)**.

Here, we introduce CrhINs as a new element governing the interplay between OXT and CRH in the mPFC by demonstrating that CrhINs directly inhibit OxtR-INs **(Figure 2.12, 2.13)** thereby suppressing the release of the antagonist CRHBP within the mPFC. The third finding reported here is that postsynaptic responses of both L2/3 pyramidal cells and OxtR-INs in response to CrhIN optogenetic activation are elevated in male relative to female mPFC brain slice preparations **(Figure 2.12, 2.13)**.These data suggest that GABAergic and CRH signaling from CrhINs may play a significant role in the sociosexual dimorphic behaviors demonstrated here, further emphasizing the need to investigate the detailed molecular properties of cortical interneurons to understand neuromodulation in males and female social behaviors.

3.2 Future Directions and unsolved questions

The results from investigations into CrhIN activity and function contribute directly to our understanding of cell type diversity in the cerebral cortex and the inherent sexual dimorphisms at the electrophysiological and behavioral level. As compared to female CrhINs, activation of male CrhINs exhibit stronger PSCs in both OxtR-INs **(Figure 2.12, 2.13)** and L2/3 pyramidal cells (**Figure 2.17)**. In parallel, modulation of male mPFC CrhIN activity and CRH production influences novelty seeking **(Figure 2.28, 2.29)** and sociability seeking behaviors **(Figure 2.30)**, whereas again we observe no effect in females. The results point to a persistent sexually dimorphic nature wherein CrhIN activity is far more efficacious in males than in females.

To further demonstrate their sexually dimorphic nature at the electrophysiological level, we repeated 20hz optogenetic stimulation protocols **(Figure 2.20)** in female mice **(Figure 3.2)**. As compared to male CrhINs **(Figure 3.2A)**, female CrhIN LED induced APs do not exhibit the same action potential amplitude **(Figure 3.2E)**, and instead display immature APs following the first LED pulse. While 62% of L2/3 pyramidal cells responded in males **(Figure 3.2B, C, D)**, we observed negligible L2/3 PSC responses following 20hz LED stimulation in female L2/3 **(Figure 3.2F).**

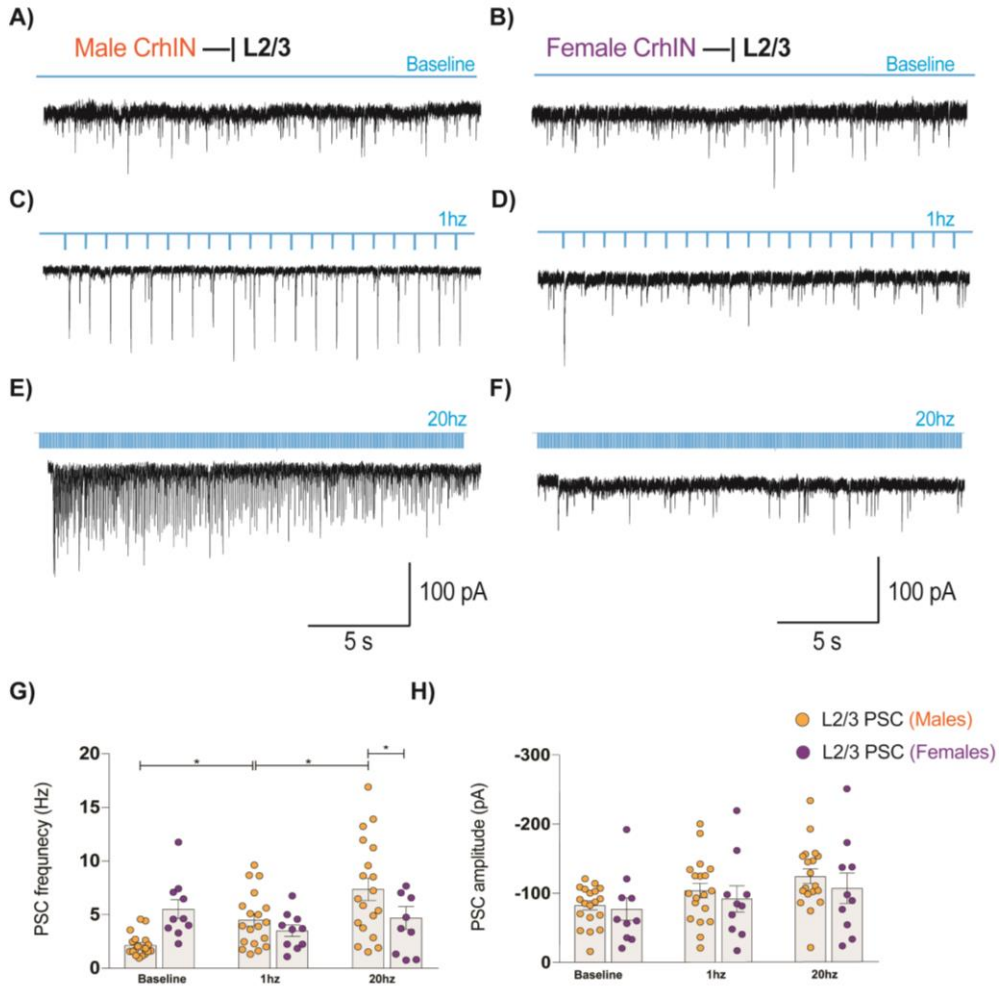

Figure 3.2. Sexually dimorphic firing properties and L2/3 PSCs.

a) Baseline sEPSC recording in male mPFC L2/3 pyramidal cell
b) Female baseline sEPSC recording in mPFC L2/3 pyramidal cell
c) Male CrhIN – L2/3 1hz PSC
d) Female CrhIN – L2/3 1hz PSC
e) Male CrhIN – L2/3 20hz PSC
f) Female CrhIN – L2/3 20hz PSC
g) Quantification of CrhIN – L2/3 PSC frequency between males and females
h) Quantification of CrhIN – L2/3 PSC amplitude between males and females

While the sexually dimorphic responses in L2/3 pyramidal cells to high frequency optogenetic stimulation are indeed striking **(Figure 3.2)**, they indicate that production or reception of CRH in cortex functions in a sexually dimorphic manner and is of greater impact in males than females. Importantly, CRHR1 are not expressed across all L2/3 pyramidal cells **(Figure 2.14, 2.15)** and we observed a 20hz optogenetic response in a subset of L2/3 pyramidal cells, termed responders **(Figure 3.3A, B)**, which account for 62% of L2/3 cells recorded in males **(Figure 3.3C, D)**.

To begin to unravel a mechanistic understanding surrounding the sexually dimorphic mechanisms characteristic of CrhINs, further investigations would be greatly aided by structuring their studies into two categories, presynaptic or postsynaptic mechanisms. Sexually dimorphic patterns across CrhIN function could be due to differences at the presynaptic level. This would suggest that female CrhINs release or contain less CRH protein as compared to males.

There exist at least two potential presynaptic mechanisms which could underlie the striking sexual dimorphisms observed at the electrophysiological level between males and females. First, it is thought that females have elevated circulating CRH levels in the extracellular space, as compared to males **(Li et al., 2016).** As such, female CRHR1 may already be saturated via elevated levels of circulating CRH, rendering a negligible L2/3 postsynaptic response following CRH release from cortical interneurons.

Future quantitative assessment analyzing CRH protein between male and female mPFC CrhINs would aid in this regard. However, given the well-established difficulties surrounding CRH protein antibody labeling, an alternative analysis should

review *CRH* mRNA puncta number between males and females as a proxy to CRH protein production. Second, we do observe that female CrhINs produce immature APs following 20hz LED stimulation **(Figure 3.3E)** and posit that these APs may not be sufficient to elevate presynaptic Ca^{2+} requirements for neuropeptide release. Third, as females are known to have elevated OXT levels, and since OxtR-INs release the CRH antagonist CRHBP **(Li et al., 2016),** it is likely that females have higher extracellular circulating and therefore unbound CRHBP which should dampen CRH reception in female mPFC. In parallel, reduced OXT levels in males ultimately enables more unbound CRH to act on CRHR1 present in L2/3 pyramidal cells.

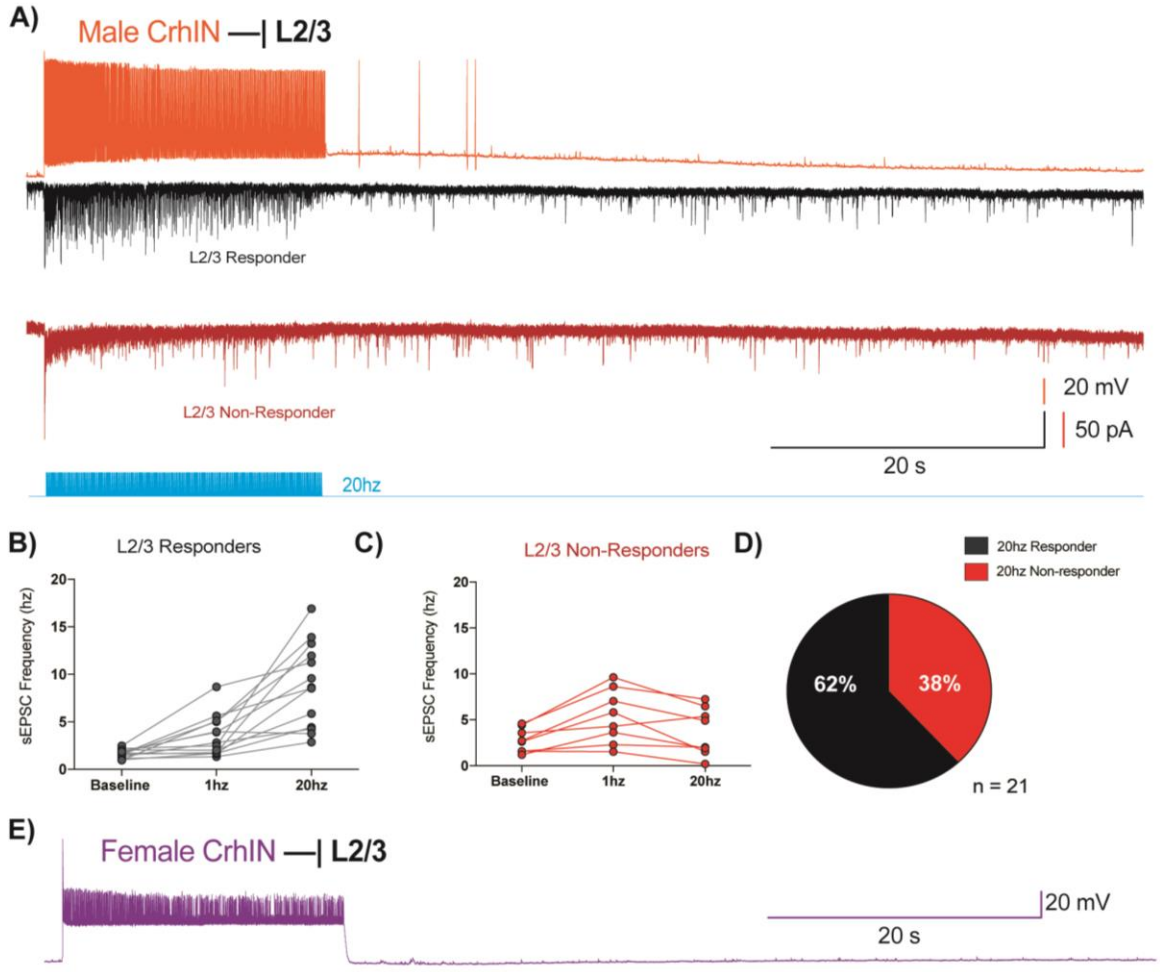

Figure 3.3. Response rates across L2/3 pyramidal cells in male mPFC following high frequency optogenetic stimulation of CrhINs.

a) Male mPFC CrhIN and L2/3 PSC traces following 20hz LED stimulation
b) PSC frequency between baseline, 1hz, and 20hz stimulation protocols in responding L2/3 cells
c) PSC frequency between baseline, 1hz, and 20hz stimulation protocols in non-responding L2/3 cells
d) Quantification of male L2/3 pyramidal cells across responders and non-responders
e) Female mPFC CrhIN current clamp trace following 20hz LED stimulation

Regarding postsynaptic mechanisms, female L2/3 pyramidal cells may express less CRHR1 protein, as compared to males, limiting CRH – CRHR1 signaling.

A quantitative assessment of L2/3 CRHR1 protein between males and females would unravel the underlying sexually dimorphic disparities observed with CrhIN activity in mPFC. While logical, these studies are hindered by lack of development of a specific and selective CRHR1 antibodies. To circumvent this, ISH studies could assess CRHR1 mRNA levels, although this is again made difficult by its relatively sparse expression at the mRNA level in mPFC **(Figure 2.14)**.

The obscured relationship between the molecular profiles of L2/3 pyramidal cells and their electrophysiological response to low and high frequency CrhIN activation would be greatly diminished by segregating cell type-specific postsynaptic responses with their transcriptional identities. The molecular signature within a subset of responding CRHR1 L2/3 pyramidal cells **(Figure 3.3B)** could help to explain the sexually dimorphic electrophysiological responses that may prove difficult to ascribe with bulk labeling approaches. To achieve this and circumvent issues of bulk profiling of heterogenous L2/3 pyramidal cell subpopulation, future studies should explore the rationale and feasibility of Patch-seq **(Cadwell et al., 2016),** a recently developed methodology that combines whole cell patch clamp electrophysiological recordings with single cell RNA-sequencing. With this approach, distinct molecular profiles could be collected from responder **(Figure 3.2B)** and non-responder **(Figure 3.2C)** male and female L2/3 pyramidal cells to isolate the molecular profile characteristic of L2/3 CRHR1 20hz-responsive pyramidal cells. These studies should provide insight into whether CRH-neuron postsynaptic

partners differentially express markers based on their presynaptic inputs, which if true, would add an additional layer of complexity between the sexually dimorphic patterns observed, specifically CrhIN inhibition of OxtR-IN, modulation of L2/3 pyramidal cell activity, and their influence over novelty seeking and sociability behavior.

CHAPTER 4. Appendix

4.1 Reagents

Table 4.5. *List of reagents used in experimentation.*

Reagents	Vendor	Catalogue #
Experimental Models: Organisms/Strains		
CRH-ires-CRE	Jackson Laboratory	12704
Crh$^{tm2.1Maj}$/*J* Crh-FLOX	Laboratory of Dr. Joseph Majzoub Jackson Laboratory	30110
VIP-ires-Flp	Jackson Laboratory	28578
Oxtr-CRE (ON82)	Laboratory of Dr. Nathaniel Heintz	N/A
C57BL/6J	Jackson Laboratory	664
Rosa26-flox-EGFP-L10a	Jackson Laboratory	22367
CRH-ires-FLP	Laboratory of Dr. Bernardo Sabatini	N/A
Pharmacologic Drugs		
Picrotoxin	Tocris	1128
CNQX disodium salt	Tocris	1045
NBI 27914 hydrochloride	Tocris	1591
CRF (6-33) (human, rat)	Bachem	4011473
Guanosine 5′-β-thio diphosphate trilithium salt	Sigma Aldrich	G7637
Clozapine N-oxide	Sigma Aldrich	C0832
Colchicine	Sigma Aldrich	64-86-8
Antibodies		
Rat x SST	Millipore	MAB354
Ms x PVALB	Millipore	MAB1572
Rb x VIP	Immunostar	20077
Rb x c-Fos	Cell Signaling	2250S
Chk x GFP	Abcam	ab13970
Rb x mCherry	Rockland	600-401-379
Ms x mCherry	Rockland	200-301-379
Commercial Assays		
RNAscope Multiplex Fluorescent Reagent Kit v2	Advanced Cell Diagnostics	323100

Mm-Crh	Advanced Cell Diagnostics	316091
Mm-Vip-C2	Advanced Cell Diagnostics	415961
Mm-Htr3a-C3	Advanced Cell Diagnostics	411141
Mm-Crhr1-C3	Advanced Cell Diagnostics	418011
TSA Fluorescein	Perkin Elmer	NEL701A001KT
TSA CY3	Perkin Elmer	NEL704A001KT
TSA CY5	Perkin Elmer	SAT705A001EA
Viruses		
AAV2.2-EF1a-DIO-hChR2(H134R)-mCherry	UNC Gene Therapy	
AAV2.2-EF1a-f DIO-hChR2(H134R)-EYFP	UNC Gene Therapy	
AAV1-CMV-Cre-GFP	UNC Gene Therapy	
AAV1-CMV-GFP	UNC Gene Therapy	
AAV2.2-DIO-mCherry	UNC Gene Therapy	
AAVDJ-fDIO-eYFP	UNC Gene Therapy	
AAV2/hSyn-DIO-mCherry	Addgene	
AAV2/hSyn-DIO-hM3Dq-mCherry	Addgene	

4.2 References

1) Acsady L, Görcs TJ, Freund TF (1996). Different populations of vasoactive intestinal polypeptide-immunoreactive interneurons are specialized to control pyramidal cells or interneurons in the hippocampus. Neuroscience 73:317–334.

2) Aldenhoff, J. B., Gruol, D. L., Rivier, J., Vale, W., & Siggins, G. R. (1983). Corticotropin releasing factor decreases postburst hyperpolarizations and excites hippocampal neurons. Science (New York, N.Y.), 221(4613), 875–877.

3) Arendt D, Musser JM, Baker CVH, Bergman A, Cepko C, Erwin DH, Pavlicev M, Schlosser G, Widder S, Laubichler MD, Wagner GP (2016). The origin and evolution of cell types. Nature 17:744–757.

4) Armbruster, B. N., Li, X., Pausch, M. H., Herlitze, S., & Roth, B. L. (2007). Evolving the lock to fit the key to create a family of G protein-coupled receptors potently activated by an inert ligand. Proceedings of the National Academy of Sciences of the United States of America, 104(12), 5163–5168.

5) Arrigoni, E., & Saper, C. B. (2014). What optogenetic stimulation is telling us (and failing to tell us) about fast neurotransmitters and neuromodulators in brain circuits for wake–sleep regulation. Current Opinion in Neurobiology, 29, 165–171.

6) Barbas H (2015). General Cortical and Special Prefrontal Connections: Principles from Structure to Function. Annu Rev Neurosci 38:269–289.

7) Bargmann C. I. (2012). Beyond the connectome: how neuromodulators shape neural circuits. BioEssays: news and reviews in molecular, cellular and developmental biology, 34(6), 458–465.

8) Basith, S., Cui, M., Macalino, S., Park, J., Clavio, N., Kang, S., & Choi, S. (2018). Exploring G Protein-Coupled Receptors (GPCRs) Ligand Space via Cheminformatics Approaches: Impact on Rational Drug Design. Frontiers in pharmacology, 9, 128.

9) Belgard, T. G., Marques, A. C., Oliver, P. L., Abaan, H. O., Sirey, T. M., Hoerder-Suabedissen, A., García-Moreno, F., Molnár, Z., Margulies, E. H., & Ponting, C. P. (2011). A transcriptomic atlas of mouse neocortical layers. Neuron, 71(4), 605–616.

10) Boyden ES, Zhang F, Bamberg E, Nagel G, Deisseroth K (2005). Millisecond-timescale, genetically targeted optical control of neural activity. Nat Neurosci 8:1263–1268.

11) Cadwell, C. R., Palasantza, A., Jiang, X., Berens, P., Deng, Q., Yilmaz, M., Reimer, J., Shen, S., Bethge, M., Tolias, K. F., Sandberg, R., & Tolias, A. S. (2016).

Electrophysiological, transcriptomic and morphologic profiling of single neurons using Patch-seq. Nature biotechnology, 34(2), 199–203.

12) Carter, M. E., Soden, M. E., Zweifel, L. S., & Palmiter, R. D. (2013). Genetic identification of a neural circuit that suppresses appetite. Nature, 503(7474), 111–114.

13) Cajal, S.R. (1888). Estructura del cerebelo. Gac. Med. Catalana *11*, 449–457.

14) Chaplin WF, John OP, Goldberg LR (1988). Conceptions of states and traits: dimensional attributes with ideals as prototypes. J Pers Soc Psychol 54:541–557.

15) Chun, L., Zhang, W. H., & Liu, J. F. (2012). Structure and ligand recognition of class C GPCRs. Acta pharmacologica Sinica, 33(3), 312–323.

16) Das A, Gilbert CD (1995). Long-range horizontal connections and their role in cortical reorganization revealed by optical recording of cat primary visual cortex. Nature 375:780–784.

17) Dascal N. (2001). Ion-channel regulation by G proteins. Trends in endocrinology and metabolism: TEM, 12(9), 391–398.

18) Derkach V, Surprenant A, North RA (1989). 5-HT3 receptors are membrane ion channels. Nature.

19) Dedic, N., Kühne, C., Gomes, K. S., Hartmann, J., Ressler, K. J., Schmidt, M. V., & Deussing, J. M. (2019). Deletion of CRH From GABAergic Forebrain Neurons Promotes Stress Resilience and Dampens Stress-Induced Changes in Neuronal Activity. Frontiers in neuroscience, 13, 986.

20) de Filippo, R., Rost, B. R., Stumpf, A., Cooper, C., Tukker, J. J., Harms, C., Beed, P., & Schmitz, D. (2021). Somatostatin interneurons activated by 5-HT2A receptor suppress slow oscillations in medial entorhinal cortex. eLife, 10, e66960.

21) Džaja, D., Hladnik, A., Bičanić, I., Baković, M., & Petanjek, Z. (2014). Neocortical calretinin neurons in primates: increase in proportion and microcircuitry structure. Frontiers in neuroanatomy, 8, 103.

22) Fish KN, Hoftman GD, Sheikh W, Kitchens M, Lewis DA (2013). Parvalbumin-containing chandelier and basket cell boutons have distinctive modes of maturation in monkey prefrontal cortex. J Neurosci 33:8352–8358.

23) Florey E, McLennan H (1959). The effects of Factor I and of gamma-aminobutyric acid on smooth muscle preparations. J Physiol 145:66–76.

24) Gallopin T, Geoffroy H, Rossier J, Lambolez B (2005). Cortical Sources of CRF, NKB, and CCK and Their Effects on Pyramidal Cells in the Neocortex. Cerebral Cortex 16:1440–1452.

25) Gobrogge, K., & Wang, Z. (2015). Neuropeptidergic regulation of pair-bonding and stress buffering: Lessons from voles. Hormones and behavior, 76, 91–105.

26) Goodfellow, N. M., Bailey, C. D., & Lambe, E. K. (2012). The native serotonin 5-HT(5A) receptor: electrophysiological characterization in rodent cortex and 5-HT(1A)-mediated compensatory plasticity in the knock-out mouse. The Journal of neuroscience : 32(17), 5804–5809.

27) Gong S, Doughty M, Harbaugh CR, Cummins A, Hatten ME, Heintz N, Gerfen CR (2007). Targeting Cre Recombinase to Specific Neuron Populations with Bacterial Artificial Chromosome Constructs. J Neuro 27:9817–9823.

28) Hannon, J., & Hoyer, D. (2008). Molecular biology of 5-HT receptors. Behavioural brain research, 195(1), 198–213.

29) Hauger RL, Risbrough V, Brauns O, Dautzenberg FM (2006). Corticotropin releasing factor (CRF) receptor signaling in the central nervous system: new molecular targets. CNS Neurol Disord Drug Targets 5:453–479.

30) He, M., Tucciarone, J., Lee, S., Nigro, M. J., Kim, Y., Levine, J. M., Kelly, S. M., Krugikov, I., Wu, P., Chen, Y., Gong, L., Hou, Y., Osten, P., Rudy, B., & Huang, Z. J. (2016). Strategies and Tools for Combinatorial Targeting of GABAergic Neurons in Mouse Cerebral Cortex. Neuron, 92(2), 555.

31) Heiman, M., Schaefer, A., Gong, S., Peterson, J.D., Day, M., Ramsey, K. E., et al. (2008). A Translational Profiling Approach for the Molecular Characterization of CNS Cell Types. *Cell*, *135*(4), 738–748.

32) Heinrichs SC, Koob GF (1992). Corticotropin-releasing factor modulates dietary preference in nutritionally and physically stressed rats. Psychopharmacology (Berl) 109:177–184.

33) Herman JP, Ostrander MM, Mueller NK, Figueiredo H (2005). Limbic system mechanisms of stress regulation: Hypothalamo-pituitary-adrenocortical axis. Progress in Neuro-Psychopharmacology and Biological Psychiatry 29:1201–1213.

34) Hillhouse EW, Grammatopoulos DK (2006). The Molecular Mechanisms Underlying the Regulation of the Biological Activity of Corticotropin-Releasing Hormone Receptors: Implications for Physiology and Pathophysiology. Endocrine Reviews 27:260–286.

35) Hofman MA (1988). Size and Shape of the Cerebral Cortex in Mammals. Brain Behav Evol 32:17–26.

36) Hooper, A., & Maguire, J. (2016). Characterization of a novel subtype of hippocampal interneurons that express corticotropin-releasing hormone. Hippocampus, 26(1), 41–53.

37) Hubel DH, Wiesel TN (1959). Receptive fields of single neurones in the cat's striate cortex. J Physiol 148:574–591.

38) Hughes, J., T. W. Smith, H. W. Kosterlitz, L. A. Foth Ergill, B. A. Morgan, And H. R. Morris (1975). Identification of two related pentapeptides from the brain with potent opiate agonist activity. Nature Lond. 258: 577-578.

39) Inda C, Santos Claro dos PA, Bonfiglio JJ, Senin SA, Maccarrone G, Turck CW, Silberstein S (2016). Different cAMP sources are critically involved in G protein-coupled receptor CRHR1 signaling. J Cell Biol 214:181–195.

40) Jiang, Z., Rajamanickam, S., & Justice, N. J. (2018). Local Corticotropin-Releasing Factor Signaling in the Hypothalamic Paraventricular Nucleus. The Journal of neuroscience : the official journal of the Society for Neuroscience, 38(8), 1874–1890.

41) Jo, M., & Jung, S. T. (2016). Engineering therapeutic antibodies targeting G-protein-coupled receptors. Experimental & molecular medicine, 48(2), e207.

42) Feldmeyer, D., Qi, G., Emmenegger, V., & Staiger, J. F. (2018). Inhibitory interneurons and their circuit motifs in the many layers of the barrel cortex. Neuroscience, 368, 132–151.

43) Füzesi, T., Daviu, N., Wamsteeker Cusulin, J. I., Bonin, R. P., & Bains, J. S. (2016). Hypothalamic CRH neurons orchestrate complex behaviours after stress. Nature communications, 7, 11937.

44) Geerling, J. C., Shin, J. W., Chimenti, P. C., & Loewy, A. D. (2010). Paraventricular hypothalamic nucleus: axonal projections to the brainstem. The Journal of comparative neurology, 518(9), 1460–1499.

45) Granger, A. J., Mulder, N., Saunders, A., & Sabatini, B. L. (2016). Cotransmission of acetylcholine and GABA. Neuropharmacology, 100, 40–46.

46) Jackson J, Ayzenshtat I, Karnani MM, Yuste R (2016). VIP+ interneurons control neocortical activity across brain states. J Neurophysiol 115:3008–3017.

47) Kawaguchi Y (1993). Correlation of physiological subgroupings of nonpyramidal cells with parvalbumin-and calbindinD28k-immunoreactive neurons in layer V of rat frontal cortex. J Neurophysiol. 70(1):387-96.

48)Kawaguchi Y, Kubota Y (1996). Physiological and morphological identification of somatostatin- or vasoactive intestinal polypeptide-containing cells among GABAergic cell subtypes in rat frontal cortex. J Neuro 16:2701–2715.

49)Kepecs, A., & Fishell, G. (2014). Interneuron cell types are fit to function. Nature, 505(7483), 318–326.

50)Kozielewicz, P., Turku, A., & Schulte, G. (2020). Molecular Pharmacology of Class F Receptor Activation. Molecular pharmacology, 97(2), 62–71.

51)Kupfermann I (1991). Functional studies of cotransmission. Physiological Reviews 71:683–732.

52)Lee S, Hjerling-Leffler J, Zagha E, Fishell G, Rudy B (2010). The Largest Group of Superficial Neocortical GABAergic Interneurons Expresses Ionotropic Serotonin Receptors. J Neuro 30:16796–16808.

53)Lee S, Kruglikov I, Huang ZJ, Fishell G, Rudy B (2013). A disinhibitory circuit mediates motor integration in the somatosensory cortex. Nature 16:1662–1670.

54)Leiser, S. C., Li, Y., Pehrson, A. L., Dale, E., Smagin, G., & Sanchez, C. (2015). Serotonergic Regulation of Prefrontal Cortical Circuitries Involved in Cognitive Processing: A Review of Individual 5-HT Receptor Mechanisms and Concerted Effects of 5-HT Receptors Exemplified by the Multimodal Antidepressant Vortioxetine. ACS chemical neuroscience, 6(7), 970–986.

55)Leone DP, Srinivasan K, Chen B, Alcamo E, McConnell SK (2008). The determination of projection neuron identity in the developing cerebral cortex. Current Opinion in Neurobiology 18:28–35.

56)Lim, L., Mi, D., Llorca, A., & Marín, O. (2018). Development and Functional Diversification of Cortical Interneurons. Neuron, 100(2), 294–313.

57)Liposits, Z., Paull, W. K., Wu, P., Jackson, I. M., & Lechan, R. M. (1987). Hypophysiotrophic thyrotropin releasing hormone (TRH) synthesizing neurons. Ultrastructure, adrenergic innervation and putative transmitter action. Histochemistry, 88(1), 1–10.

58)Letzkus JJ, Wolff SBE, Meyer EMM, Tovote P, Courtin J, Herry C, Lüthi A (2011). A disinhibitory microcircuit for associative fear learning in the auditory cortex. Nature 480:331–335.

59)Li K, Nakajima M, Ibañez-Tallon I, Heintz N (2016). A Cortical Circuit for Sexually Dimorphic Oxytocin- Dependent Anxiety Behaviors. Cell 167:60–66.e11.

60) Magee JC (2000). Dendritic integration of excitatory synaptic input. Nat Rev Neurosci 1:181–190.

61) Luo, C., Keown, C. L., Kurihara, L., Zhou, J., He, Y., Li, J., Castanon, R., Lucero, J., Nery, J. R., Sandoval, J. P., Bui, B., Sejnowski, T. J., Harkins, T. T., Mukamel, E. A., Behrens, M. M., & Ecker, J. R. (2017). Single-cell methylomes identify neuronal subtypes and regulatory elements in mammalian cortex. Science (New York, N.Y.), 357(6351), 600–604.

62) Mante V, Sussillo D, Shenoy KV, Newsome WT (2013). Context-dependent computation by recurrent dynamics in prefrontal cortex. Nature 503:78–84.

63) Marder, E., & Bucher, D. (2007). Understanding circuit dynamics using the stomatogastric nervous system of lobsters and crabs. Annual review of physiology, 69, 291–316.

64) Marcinkiewcz, C. A., Mazzone, C. M., D'Agostino, G., Halladay, L. R., Hardaway, J. A., DiBerto, J. F., Navarro, M., Burnham, N., Cristiano, C., Dorrier, C. E., Tipton, G. J., Ramakrishnan, C., Kozicz, T., Deisseroth, K., Thiele, T. E., McElligott, Z. A., Holmes, A., Heisler, L. K., & Kash, T. L. (2016). Serotonin engages an anxiety and fear-promoting circuit in the extended amygdala. Nature, 537(7618), 97–101.

65) McElligott, Z. A., Klug, J. R., Nobis, W. P., Patel, S., Grueter, B. A., Kash, T. L., & Winder, D. G. (2010). Distinct forms of Gq-receptor-dependent plasticity of excitatory transmission in the BNST are differentially affected by stress. Proceedings of the National Academy of Sciences of the United States of America, 107(5), 2271–2276.

66) Mellén, M., Ayata, P., & Heintz, N. (2017). 5-hydroxymethylcytosine accumulation in postmitotic neurons results in functional demethylation of expressed genes. Proceedings of the National Academy of Sciences of the United States of America, 114(37), E7812–E7821.

67) Meloni, E. G., Reedy, C. L., Cohen, B. M., & Carlezon, W. A., Jr (2008). Activation of raphe efferents to the medial prefrontal cortex by corticotropin-releasing factor: correlation with anxiety-like behavior. Biological psychiatry, 63(9), 832–839.

68) Miyoshi, G., & Fishell, G. (2011). GABAergic interneuron lineages selectively sort into specific cortical layers during early postnatal development. Cerebral cortex (New York, N.Y. : 1991), 21(4), 845–852.

69) Moy, S. S., Nadler, J. J., Perez, A., Barbaro, R. P., Johns, J. M., Magnuson, T. R., Piven, J., & Crawley, J. N. (2004). Sociability and preference for social novelty in five inbred strains: an approach to assess autistic-like behavior in mice. Genes, brain, and behavior, 3(5), 287–302.

70) Muschol, M., & Salzberg, B. M. (2000). Dependence of transient and residual calcium dynamics on action-potential patterning during neuropeptide secretion. The Journal of neuroscience : the official journal of the Society for Neuroscience, 20(18), 6773–6780.

71) Nakajima M, Görlich A, Heintz N (2014). Oxytocin Modulates Female Sociosexual Behavior through a Specific Class of Prefrontal Cortical Interneurons. Cell 159:295–305.

72) Nagel, G., Szellas, T., Huhn, W., Kateriya, S., Adeishvili, N., Berthold, P., Ollig, D., Hegemann, P., & Bamberg, E. (2003). Channelrhodopsin-2, a directly light-gated cation-selective membrane channel. Proceedings of the National Academy of Sciences of the United States of America, 100(24), 13940–13945.

73) Ivanova-Nikolova, T. T., & Breitwieser, G. E. (1997). Effector contributions to G beta gamma-mediated signaling as revealed by muscarinic potassium channel gating. The Journal of general physiology, 109(2), 245–253.

74) Oakley RH, Cidlowski JA (2013). The biology of the glucocorticoid receptor: New signaling mechanisms in health and disease. Journal of Allergy and Clinical Immunology 132:1033–1044.

75) Owen, S. F., Berke, J. D., & Kreitzer, A. C. (2018). Fast-Spiking Interneurons Supply Feedforward Control of Bursting, Calcium, and Plasticity for Efficient Learning. Cell, 172(4), 683–695.e15.

76) Palchaudhuri, M., & Flügge, G. (2005). 5-HT1A receptor expression in pyramidal neurons of cortical and limbic brain regions. Cell and tissue research, 321(2), 159–172.

77) Pandey, G. N., Rizavi, H. S., Bhaumik, R., & Ren, X. (2019). Increased protein and mRNA expression of corticotropin-releasing factor (CRF), decreased CRF receptors and CRF binding protein in specific postmortem brain areas of teenage suicide subjects. Psychoneuroendocrinology, 106, 233–243.

78) Partridge, J. G., Forcelli, P. A., Luo, R., Cashdan, J. M., Schulkin, J., Valentino, R. J., & Vicini, S. (2016). Stress increases GABAergic neurotransmission in CRF neurons of the central amygdala and bed nucleus stria terminalis. Neuropharmacology, 107, 239–250.

79) Pasternak, J. F., & Woolsey, T. A. (1975). On the "selectivity" of the Golgi-Cox method. The Journal of comparative neurology, 160(3), 307–312.

80) Peng, J., Long, B., Yuan, J., Peng, X., Ni, H., Li, X., Gong, H., Luo, Q., & Li, A. (2017). A Quantitative Analysis of the Distribution of CRH Neurons in Whole Mouse Brain. Frontiers in neuroanatomy, 11, 63.

81) Petilla Interneuron Nomenclature Group, Ascoli, G. A., Alonso-Nanclares, L., Anderson, S. A., Barrionuevo, G., Benavides-Piccione, R., Burkhalter, A., Buzsáki, G., Cauli, B., Defelipe, J., Fairén, A., Feldmeyer, D., Fishell, G., Fregnac, Y., Freund, T. F., Gardner, D., Gardner, E. P., Goldberg, J. H., Helmstaedter, M., Hestrin, S., Yuste, R. (2008). Petilla terminology: nomenclature of features of GABAergic interneurons of the cerebral cortex. Nature reviews. Neuroscience, 9(7), 557–568.

82) Pfeffer CK, Xue M, He M, Huang ZJ, Scanziani M (2013). Inhibition of inhibition in visual cortex: the logic of connections between molecularly distinct interneurons. Nature 16:1068–1076.

83) Pi H-J, Hangya B, Kvitsiani D, Sanders JI, Huang ZJ, Kepecs A (2013). Cortical interneurons that specialize in disinhibitory control. Nature 503:521–524.

84) Puig, M. V., Watakabe, A., Ushimaru, M., Yamamori, T., & Kawaguchi, Y. (2010). Serotonin modulates fast-spiking interneuron and synchronous activity in the rat prefrontal cortex through 5-HT1A and 5-HT2A receptors. The Journal of neuroscience : the official journal of the Society for Neuroscience, 30(6), 2211–2222.

85) Rudy B, Fishell G, Lee S, Hjerling-Leffler J (2010). Three groups of interneurons account for nearly 100% of neocortical GABAergic neurons McBain CJ, Fishell G, eds. Devel Neurobio 71:45–61.

86) Szabadics, J., Varga, C., Molnár, G., Oláh, S., Barzó, P., & Tamás, G. (2006). Excitatory effect of GABAergic axo-axonic cells in cortical microcircuits. Science (New York, N.Y.), 311(5758), 233–235.

87) Schöne, C., Apergis-Schoute, J., Sakurai, T., Adamantidis, A., & Burdakov, D. (2014). Coreleased Orexin and Glutamate Evoke Nonredundant Spike Outputs and Computations in Histamine Neurons. CellReports, 7(3), 697–704.

88) Sigel E, Steinmann ME (2012). Structure, Function, and Modulation of GABA A Receptors. J Biol Chem 287:40224–40231.

89) Smith, S. J., Sümbül, U., Graybuck, L. T., Collman, F., Seshamani, S., Gala, R., Gliko, O., Elabbady, L., Miller, J. A., Bakken, T. E., Rossier, J., Yao, Z., Lein, E., Zeng, H., Tasic, B., & Hawrylycz, M. (2019). Single-cell transcriptomic evidence for dense intracortical neuropeptide networks. eLife, 8, e47889.

90) Tabak, G., Keren-Raifman, T., Kahanovitch, U., & Dascal, N. (2019). Mutual action by Gγ and Gβ for optimal activation of GIRK channels in a channel subunit-specific manner. Scientific reports, 9(1), 508.

91) Tang, W. J., & Gilman, A. G. (1991). Type-specific regulation of adenylyl cyclase by G protein beta gamma subunits. Science (New York, N.Y.), 254(5037), 1500–1503.

92) Taniguchi H, He M, Wu P, Kim S, Paik R, Sugino K, Kvitsani D, Fu Y, Lu J, Lin Y, Miyoshi G, Shima Y, Fishell G, Nelson SB, Huang ZJ (2011). A Resource of Cre Driver Lines for Genetic Targeting of GABAergic Neurons in Cerebral Cortex. Neuron 71:995–1013.

93) Tasic, B., Yao, Z., Graybuck, L. T., Smith, K. A., Nguyen, T. N., Bertagnolli, D., Goldy, J., Garren, E., Economo, M. N., Viswanathan, S., Penn, O., Bakken, T., Menon, V., Miller, J., Fong, O., Hirokawa, K. E., Lathia, K., Rimorin, C., Tieu, M., Larsen, R., … Zeng, H. (2018). Shared and distinct transcriptomic cell types across neocortical areas. Nature, 563(7729), 72–78.

94) Tremblay, R., Lee, S., & Rudy, B. (2016). GABAergic Interneurons in the Neocortex: From Cellular Properties to Circuits. Neuron, 91(2), 260–292.

95) Tritsch NX, Ding JB, Sabatini BL (2012). Dopaminergic neurons inhibit striatal output through non-canonical release of GABA. Nature 490:262–266.

96) Tsai, H. C., Zhang, F., Adamantidis, A., Stuber, G. D., Bonci, A., de Lecea, L., & Deisseroth, K. (2009). Phasic firing in dopaminergic neurons is sufficient for behavioral conditioning. Science (New York, N.Y.), 324(5930), 1080–1084.

97) Tsao DY, Freiwald WA, Knutsen TA, Mandeville JB, Tootell RBH (2003). Faces and objects in macaque cerebral cortex. Nat Neurosci 6:989–995.

98) Uribe-Mariño, A., Gassen, N. C., Wiesbeck, M. F., Balsevich, G., Santarelli, S., Solfrank, B., Dournes, C., Fries, G. R., Masana, M., Labermeier, C., Wang, X. D., Hafner, K., Schmid, B., Rein, T., Chen, A., Deussing, J. M., & Schmidt, M. V. (2016). Prefrontal Cortex Corticotropin-Releasing Factor Receptor 1 Conveys Acute Stress-Induced Executive Dysfunction. Biological psychiatry, 80(10), 743–753.

99) Vale W, Spiess J, Rivier C, Rivier J (1982). Characterization of a 41-residue ovine hypothalamic peptide that stimulates secretion of corticotropin and β-endorphin. Obstetrical and Gynecological Survey 37:334.

100) van Aerde, K. I., & Feldmeyer, D. (2015). Morphological and physiological characterization of pyramidal neuron subtypes in rat medial prefrontal cortex. Cerebral cortex (New York, N.Y. : 1991), 25(3), 788–805.

101) Vassilatis, D. K., Hohmann, J. G., Zeng, H., Li, F., Ranchalis, J. E., Mortrud, M. T., Brown, A., Rodriguez, S. S., Weller, J. R., Wright, A. C., Bergmann, J. E., & Gaitanaris, G. A. (2003). The G protein-coupled receptor repertoires of human and mouse. Proceedings of the National Academy of Sciences of the United States of America, 100(8), 4903–4908.

102) Vertes RP, Fortin WJ, Crane AM (1999). Projections of the median raphe nucleus in the rat. J Comp Neurol 407:555–582.

103) Wang, L. A., Nguyen, D. H., & Mifflin, S. W. (2019). Corticotropin-releasing hormone projections from the paraventricular nucleus of the hypothalamus to the nucleus of the solitary tract increase blood pressure. Journal of neurophysiology, 121(2), 602–608.

104) Wang, Y., Hu, P., Shan, Q. et al. Single-cell morphological characterization of CRH neurons throughout the whole mouse brain. BMC Biol 19, 47 (2021).

105) Whitnall MH (1993). Regulation of the hypothalamic corticotropin-releasing hormone neurosecretory system. Progress in Neurobiology 40:573–629.

106) Willins, D. L., Deutch, A. Y., & Roth, B. L. (1997). Serotonin 5-HT2A receptors are expressed on pyramidal cells and interneurons in the rat cortex. Synapse (New York, N.Y.), 27(1), 79–82.

107) Wynn ML, Consul N, Merajver SD, Schnell S (2012). Logic-based models in systems biology: a predictive and parameter-free network analysis method. Integr Biol 4:1323–1329.

108) Yang XW, Model P, Heintz N (1997). Homologous recombination based modification in Esherichia coli and germline transmission in transgenic mice of a bacterial artificial chromsome. Nat Biotech 15:859–865.

109) Yuste R (2005). Origin and Classification of Neocortical Interneurons. 48:524–527.

110) Zhang R, Asai M, Mahoney CE, Joachim M, Shen Y, Gunner G, Majzoub JA (2017). Loss of hypothalamic corticotropin-releasing hormone markedly reduces anxiety behaviors in mice. Mol Psychiatry 22:733–744.

111) Zhang, S., Lv, F., Yuan, Y., Fan, C., Li, J., Sun, W., & Hu, J. (2019). Whole-Brain Mapping of Monosynaptic Afferent Inputs to Cortical CRH Neurons. Frontiers in neuroscience, 13, 565.

112) Zeisel, A., Hochgerner, H., Lönnerberg, P., Johnsson, A., Memic, F., van der Zwan, J., Häring, M., Braun, E., Borm, L. E., La Manno, G., Codeluppi, S., Furlan, A., Lee, K., Skene, N., Harris, K. D., Hjerling-Leffler, J., Arenas, E., Ernfors, P., Marklund, U., & Linnarsson, S. (2018). Molecular Architecture of the Mouse Nervous System. Cell, 174(4), 999–1014.e22.

113) Zemkova, H., Tomić, M., Kucka, M., Aguilera, G., & Stojilkovic, S. S. (2016). Spontaneous and CRH-Induced Excitability and Calcium Signaling in Mice

Corticotrophs Involves Sodium, Calcium, and Cation-Conducting Channels. Endocrinology, 157(4), 1576–1589.